Statistics of Extreme Wave Impacts on Ships

Green water (and slamming) studied with large experimental data sets

Boon, A.D.

DOI
10.4233/uuid:8effe160-aaaf-418c-ba89-f4009e2d7737

Publication date
2025

Document Version
Final published version

Citation (APA)
Boon, A. D. (2025). *Statistics of Extreme Wave Impacts on Ships: Green water (and slamming) studied with large experimental data sets*. [Dissertation (TU Delft), Delft University of Technology]. https://doi.org/10.4233/uuid:8effe160-aaaf-418c-ba89-f4009e2d7737

Important note
To cite this publication, please use the final published version (if applicable).
Please check the document version above.

Statistics of extreme wave impacts on ships

Green water (and slamming) studied with large experimental data sets

Anna Boon

Statistics of Extreme Wave Impacts on Ships

Green water (and slamming) studied with large experimental data sets

PROEFSCHRIFT

ter verkrijging van de graad van doctor aan de
Technische Universiteit Delft,
op gezag van de Rector Magnificus
prof.dr.ir. T.H.J.J. van der Hagen,
voorzitter van het College voor Promoties,
in het openbaar te verdedigen op
vrijdag 17 januari 2025 om 12:30 uur

DOOR

Anna Dymfna BOON

Dit proefschrift is goedgekeurd door de promotoren.

Samenstelling promotiecommissie bestaat uit:

Rector Magnificus		voorzitter
Prof. dr.	G.D. Weymouth	Technische Universiteit Delft, promotor
Dr. ir.	P.R. Wellens	Technische Universiteit Delft, promotor

onafhankelijke leden:

Prof. dr.	R. Pecnik	Technische Universiteit Delft
Dr. ir.	B. Hofland	Technische Universiteit Delft
Prof. dr.	R.M. van der Meer	Universiteit Twente
Dr. ir.	A. Tijsseling	Technische Universiteit Eindhoven
Dr.	D. Dessi	CNR ISAC, Italy
Prof. dr. ir.	B.J. Boersma	Technische Universiteit Delft, reservelid

This research was conducted as part of the project "Multi-fidelity Probabilistic Design Framework for Complex Marine Structures" (project number TWM.BL.019.007) of the research programme "Topsector Water & Maritime: the Blue route", which is (partly) financed by the Dutch Research Council (NWO), Stichting Bijlboegfonds, Damen, Command Materiel and IT (COMMIT) and Maritime Research Institute Netherlands (MARIN).

Cover: Data from Boon and Wellens [1]
Cover design in collaboration with Simon Pruijn
Printed by: Ipskamp
Typesetting: LaTeX

A catalogue record is available at the Delft University of Technology Library.

ISBN: 978-94-6366-976-4

Rozen verwelken en schepen vergaan,
dus lig niet te melken,
maar doe er wat aan.

- Drs. P

PREFACE

At the beginning of my PhD, I started by diving into literature about my research topic: extreme wave impacts. As I learned I shared my newfound knowledge with those around me. Most listened with polite interest, with a swift shift of subject after a question that showed their good manners. But not all. For some their head rose and eyes focused when they heard about the topic. These people had sailed the seas on sailboats or merchant vessels, and they started talking about their personal experiences with the wave impacts I was reading about.

They were talking about waves smacking against windows, soup bowls rolling over tables, the ship vibrating, waves towering over their head and the sound of steel straining and stretching. Their personal connection to the waves helped breathe life into the lifeless descriptions in academic work but was also puzzling. They kept repeating that the impact always happened on the third wave.

This 'third wave' was nowhere to be found in literature. Well, academic literature. Books and news articles do mention the third wave: *"You surely have heard of the saying that if a ship encounters three heavy waves, it will not make the third. [...] The bridge of our ship was already almost hanging in the water and we were just trying the untie the lifeboat when the third wave flowed onto deck and let the ship tremble like it was falling apart. I said: this rotten ship is done for" (translated from Dutch)* [2]. *"It was three waves, one after the other. The damage was done by the second and the third waves."* [3] *"White water broke over the bow with every second or third wave, reducing his speed to only two knots on his course for land."* [4] Even on nautical advice websites, the third wave is mentioned: *In this course the boat can slam, every third wave it will slam." (translated from Dutch)* [5]. *"Advice: Watch out for the third wave! [...] Sharp manoeuvres or sudden direction changes are best and easiest to do immediately after the third."* [6].

The stories about the third wave piqued my interest, but I was trying to be an academic, so I stuck to the academic literature and got to researching. The idea of the third wave, however, had gotten stuck in my head. During my experiments, I spent hours watching the model ship bobbing up and down, but in the continuous stream of waves, I never could identify that elusive third wave.

When the data was in and I started analyzing I kept looking, but none of the results showed that the third wave exists. I found that extreme wave impacts

occur randomly and that they can form dependent clusters, but these clusters are between two to six successive impacts. I looked at the waves and found that a negative pitch and positive wave coincide before water comes rushing onto the deck, but no cohesive counting method resulted in an impact on the third wave. You will find the results that the data supported in this thesis, but you will not find any mention of the third wave beyond this preface, as I never did find it.

Some sailors have looked into a vertical wall of green sea water towering high over their vessel before the wall crashed down on them and their ship. Learning that these impacts occur randomly is not comforting. The human inclination is to find patterns even if there are none, especially if fear is involved. The search for patterns results in the creation of myths. The third wave myth is not about physics; it is an attempt for those at the mercy of the seas to regain control over their fate.

Even though the third wave seems to be a myth, the existence of the myth still tells us something: that extreme wave impacts have not yet been concurred. Instead of trying to find the third wave, I made eliminating the need for myths my goal. By using evidence-based knowledge I want to create a safer maritime industry. This thesis bounds the steps I have made towards this greater goal on the topic of extreme wave impacts, and I hope it will serve as a stepping stone for those who want to follow.

Anna Boon
Delft, June 2024

SUMMARY

Extreme wave impacts can damage ships and pose a risk to those on board. An extreme wave impact can be green water: a wave impact on a ship's deck or superstructure, or slamming: a ship's underside slamming on a wave. To prevent serious accidents these green water and slamming impacts need to be minimized. Predicting the probability and impact pressures can make minimizing impacts possible. Extreme wave impacts are challenging to predict as they are multiphase, nonlinear, turbulent and rare. The rarity, complexity and variety of impacts have resulted in limited studies into the statistics of extreme wave impacts, causing questions about the probability, distributions and ranges in which impacts occur. To predict extreme wave impacts answers to these questions would be helpful.

The goal of this thesis is to study the statistics of extreme wave impacts. To fulfill this goal a large data set of extreme wave impacts is collected. A new testing facility is created to collect data by adding a wave maker to an existing recirculating tank. In the test facility water and waves flow past the model, allowing for long testing times. Three large experimental data sets with a ship with forward velocity in head waves are collected. The collected data is in total 246 hours of experimental data over 23 test cases, representing over 2766 hours of continuous sailing at full scale.

From the first experimental data set the probability of occurrence of green water and the expected maximum pressures during green water events are identified. The data set contains green water events in different sea states, forward speeds and drafts. Two proposed methods to estimate the probability of green water occurrence are compared. One method is based on the probability of water exceeding the deck and one on a ship's freeboard and the significant wave height, the former being in better agreement with the data, the latter being more practical for designers. The maximum pressures caused by green water are distributed according to the Fréchet distribution, also called extreme value distribution II. With the newly identified distribution, an equation to calculate the probability of a pressure limit being exceeded for a ship in operation is formulated. This first data set shows that the distribution of the time between green water occurrences is exponential, indicating that when green water occurs is independent of the time since the last occurrence.

The second set of experiments is aimed at identifying the influence of surge on green water and slamming. Long-running experiments with forward velocity and irregular waves are repeated with and without surge. Surge is found to increase the probability of green water events, but the impact pressures on deck and the probability of a green water event reaching the deck box decreases when the ship is free to surge. In this second data set green water and slamming events turn out to not occur independently as both event types cluster. The clusters occur for large probabilities of occurrence, which is why the first data set did not show these dependent clusters. Clusters are caused by large pitch motions. Larger pressures on deck are found for clustered events.

The conditions under which green water occurs and the relation between water exceeding the deck and green water are investigated. The relation is not direct and a difference between green water and exceedance that does not develop into a flow on deck is identified. A proposed prediction method follows from the difference between green water and exceedance. Pitch is identified as an important indicator for green water as green water events consistently occurred with large forward pitch motion, while exceedance also occurred with neutral pitch. A prediction method of probability is proposed that implements separate limits for the motions and wave elevation that occur simultaneously, thus including the phase difference between the motions and wave elevation.

Design variations with different drafts and freeboards at the bow are tested in the third set of tests. A large set of 3263 green water events in irregular waves with forward velocity is experimentally obtained for six different bow designs. The data demonstrates that both freeboard and draft at the bow affect the probability of green water. Increasing the draft at the bow increases the swell-up, reducing the effective freeboard and in turn, increasing the probability of green water. Increasing the freeboard results in a decrease in the probability of green water, as expected. However, the probability is not reduced equally for different green water impact pressures. The joint probability of green water occurrence and pressures shows that increasing the freeboard only decreases the probability of low-pressure events. Increasing the freeboard increases the probability of high-pressure events. These results highlight the importance of statistics when designing for green water.

The large experimental data sets have been combined with a machine learning method: SINDy. The models are trained to predict the acceleration of heave and pitch with the parameters heave, pitch, velocity of heave and pitch and the wave elevations along the hull. As a first step, a model is

trained on fictitious data. The data is based on empirical response amplitude operators. The resulting model represents a damped mass-spring system with external forcing. The identification of the damped mass-spring system with external forcing is sensitive to random noise in the input data. Models have also been trained on the experimental data available. The models trained on experimental data did not result in the expected damped mass-spring system with external forcing model. The likely cause is noise in the experimental data.

SAMENVATTING

Extreme golfklappen kunnen schepen beschadigen en een risico vormen voor de opvarenden. Een extreme golfklap kan groenwater zijn: een golfklap op het dek of de opbouw van een schip, of slamming: als een schip met zijn onderkant op een golf slaat. Om tragedies te voorkomen moeten groenwater en slamming tot een minimum worden beperkt. Het voorspellen van de kans en impactdruk kan het minimaliseren van golfklappen mogelijk maken. Extreme golfklappen zijn lastig te voorspellen, omdat ze dynamisch, meerfasig, niet-lineair, turbulent en zeldzaam zijn. De zeldzaamheid, complexiteit en variateit van de klappen hebben geresulteerd in beperkte studies naar de statistieken van extreme golfklappen, waardoor er vragen ontstaan over de kans, de statistische verdeling en situaties waarin golfklappen optreden. Om extreme golfklappen te voorspellen zijn antwoorden op deze vragen nodig.

Het doel van dit proefschrift is om de statistieken van extreme golfklappen te onderzoeken. Voor het behalen van dit doel is een grote dataset van extreme golfklappen vergaard. Om de gegevens te vergaren is een nieuwe testfaciliteit gecreëerd door een golfmaker op een bestaande recirculatietank te bouwen. In de testfaciliteit stromen water en golven langs het model waardoor lange testtijden mogelijk zijn. Grote experimentele datasets zijn verzameld voor een schip met voorwaartse snelheid in kopgolven. De experimentele metingen zijn 246 uur aan data voor 23 test variaties. Deze tijd komt neer op meer dan 2766 uur continu varen op ware grootte.

Met de eerste experimentele dataset zijn de waarschijnlijkheid van groenwater en de verwachte maximale druk tijdens groenwater geïdentificeerd. De dataset bevat groenwater in verschillende onregelmatige golven, voorwaartse snelheden en diepgangen. Twee voorgestelde methoden om de waarschijnlijkheid van groenwater te schatten worden vergeleken. Eén methode is gebaseerd op de waarschijnlijkheid dat water het dek overstijgt en één op het vrijboord van een schip en de significante golfhoogte. De eerste methode komt beter overeen met de gegevens, de tweede is praktischer voor ontwerpers. De maximale drukken veroorzaakt door groenwater volgen de Fréchet-verdeling, ook wel extreme-waardenverdeling II genoemd. Met de nieuw geïdentificeerde verdeling is een vergelijking geformuleerd om de waarschijnlijkheid van overschrijding van een druk voor een varend schip te

berekenen. Deze eerste dataset laat zien dat de verdeling van de tijd tussen groenwaterklappen exponentieel is, wat aangeeft dat wanneer groenwater optreedt onafhankelijk is van de tijd sinds het laatste klap.

De tweede reeks experimenten is gericht op het identificeren van de invloed van schrikken op groenwater en slamming. Langlopende experimenten met voorwaartse snelheid en onregelmatige golven zijn herhaald met en zonder dat het model vrij kan schrikken. Het blijkt dat schrikken de waarschijnlijkheid van groenwater vergroot, maar de drukken op het dek en de waarschijnlijkheid dat groenwater de opbouw op dek bereikt neemt af wanneer het schip vrij is om te schrikken. In deze tweede dataset blijken groenwater en slamming niet onafhankelijk voor te komen, aangezien beide typen gebeurtenissen clusteren. De clusters treden op bij grote waarschijnlijkheden van voorkomen, en daarom komen deze afhankelijke clusters niet voor in de eerste dataset. Clusters worden veroorzaakt door grote stampbewegingen. Bij geclusterde klappen is een grotere druk aan dek gemeten.

Onder welke omstandigheden groenwater ontstaat en de relatie tussen water dat het dek overschrijdt en groenwater is onderzocht. De relatie is niet direct en er is verschil tussen groenwater en overschrijding dat zich niet ontwikkelt tot stroming aan dek. Een voorgestelde voorspellingsmethode volgt uit het verschil tussen groenwater en overschrijding. De stampbeweging wordt geïdentificeerd als een belangrijke indicator voor groenwater, aangezien groenwater consequent plaatsvind bij grote voorwaartse stampbewegingen, terwijl overschrijding ook plaatsvond bij neutrale stampbewegingen. Er wordt een waarschijnlijkheidsvoorspellingsmethode voorgesteld die afzonderlijke limieten implementeert voor de bewegingen en golfhoogte die gelijktijdig optreden, en dus het faseverschil tussen de bewegingen en golfhoogte meeneemt.

Ontwerpvariaties met verschillende diepgangen en vrijboorden aan de boeg zijn getest in de derde reeks testen. Een grote dataset van 3263 groenwaterklappen in onregelmatige golven met voorwaartse snelheid vergelijkt zes verschillende boegontwerpen. Uit de gegevens blijkt dat zowel het vrijboord als de diepgang aan de boeg de kans op groenwater beïnvloeden. Het vergroten van de diepgang aan de boeg vergroot de zwelling van het water bij de boeg, waardoor het effectieve vrijboord afneemt en daarmee de kans op groenwater toeneemt. Het vergroten van het vrijboord leidt, zoals verwacht, tot een afname van de kans op groenwater. De waarschijnlijkheid wordt echter niet in gelijke mate verkleind voor verschillende groenwaterdrukken. De gezamenlijke waarschijnlijkheid van het optreden van groenwater en druk laat zien dat het vergroten van het vrijboord alleen maar de kans op lagedruk

klappen verkleint. Het vergroten van het vrijboord vergroot de kans op klappen die hoge drukken genereren. Deze resultaten benadrukken het belang van statistiek bij het ontwerpen voor groenwater.

De grote experimentele datasets zijn gecombineerd met een machine learning-methode: SINDy. De modellen zijn getraind om de versnelling van dompen en stampen te voorspellen met de parameters dompen, stampen, snelheid van dompen en stampen en de golfhoogten langs de romp. Als eerste stap is het model getraind op fictieve data. De data is gebaseerd op empirische responsamplitude-operatoren. Het resulterende model vertegenwoordigt een gedempt massaveersysteem met externe krachten. Of het gedempte massaveersysteem met externe krachten wordt geidentificeerd is afhankelijk van ruis in de invoerdata. Modellen zijn ook getraind op basis van beschikbare experimentele gegevens. De op experimentele gegevens getrainde modellen resulteerden niet in het verwachte gedempte massaveersysteem met extern krachten-model. De waarschijnlijke oorzaak is ruis in de experimentele data.

CONTENTS

SYMBOLS

Latin

A	Waterline area [m^2]
a	Added mass of ship model [kg]
c	Shape parameter Fréchet distribution[-]
C_B	Block coefficient of the ship [-]
c_s	Propagation velocity of waves [m/s]
D	Water depth [m]
d	Still water draft of the model at bow [m]
fb	Freeboard of ship at bow measured from waterline [m]
$f_{n,\theta}$	Natural pitch frequency [Hz]
GM_L	Longitudinal metacentric height [m]
g	Gravitational acceleration [m/s^2]
h	Difference in freeboard height [m]
H_{m0}	Significant wave height [m]
k	Wave number [1/m]
L_{pp}	Ship length between perpendiculars [m]
M	Mass of the ship model [kg]
m	Location parameter Fréchet distribution [Pa]
n	Number of impacts/events during test case [-]
n_w	Number of encountered waves [-]
p	Pressure [Pa]
$P_{box,max}$	Average maximum impact pressure on deck box [Pa]
$p_{box,max}$	Local maximum impact pressure on deck box [Pa]
p_{exc}	Pressure exceeded [Pa]
p_{lim}	Limit pressure [Pa]
P_{max}	Average maximum impact pressure on deck [Pa]
p_{max}	Local maximum impact pressure on deck [Pa]

$Pr(p_{exc}\|GW)$	Probability of pressure exceedance given green water occurred [s^{-1}]
$Pr(p_{exc} \cap GW)$	Probability of green water and pressure exceedance [s^{-1}]
$Pr(EX)$	Probability of relative wave elevation exceeding deck level [-]
$Pr(EX_{noGW})$	Probability of relative wave elevation exceeding deck level and not leading to green water [-]
$Pr(GW)$	Probability of green water [-] or [s^{-1}]
$Pr(GW_{box})$	Probability of green water reaching deck box [-] or [s^{-1}]
$Pr(GW_{EX} \cup EX_{noGW})$	Probability of the relative wave elevation exceeding deck level [-]
$Pr(SL)$	Probability of slamming [-] or [s^{-1}]
R	Sparsity promoting regularization SINDy
R_{RWE}	Variance of relative wave elevation [m^2]
$R_{R\dot{W}E}$	Variance of relative wave velocity [m^2/s^2]
RWE	Relative wave elevation [m]
$R\dot{W}E$	Relative wave velocity [m/s]
s	Skewness of distribution [-]
s_{op}	Spectral steepness [-]
st	Stroke amplitude of wavemaker [m]
su	Swell-up of water at bow of the ship [m]
T	Dynamic draft at the bow of model [m]
t_d	Impact duration [s]
t_e	Time of maximum measured relative wave elevation during impact or event [s]
T_{m02}	Mean wave period in sea state [s]
t_{min}	Minimum time between impacts [s]
T_p	Peak period [s]
t_r	Rise time of the pressure [s]
T_s	Motion period of wavemaker [s]
t_{test}	Testing duration [hours]
T_w	Wave period from the reference frame moving with current [s]

T_{z_e}	Zero-crossing encounter period of wave spectrum [s]
U	Modelled forward velocity of ship [m/s]
$\mathbf{U}$	Candidate parameters matrix SINDy
V	Local vertical flow velocity [m/s]
V_{Ochi}	Ochi criterion for relative wave velocity [m/s]
$\mathbf{W}$	Auxiliary coefficients SINDy [-]
$\mathbf{X}$	State matrix of system SINDy
x_b	Location of cross section [m]
x_{bow}	Distance from centre of gravity to bow [m]
x_{wm}	Distance from front of wavemaker [m]
z	Heave (vertical motion of ship) [m]

Greek

α	Scale parameter Fréchet distribution [-]
α_E	Half entrance angle of bow [rad]
ζ	Local wave elevation [m]
η	Wave elevation [m]
η_a	Wave amplitude [m]
Θ	Candidate functions SINDy
θ	Pitch (ships rotation around width direction) [rad]
κ	Threshold for sparsity promoting regularization [-]
λ	Mean time between impacts [s]
ν	Coefficient that determines regularization strength in optimization SINDy [-]
$\boldsymbol{\Xi}$	Coefficients in optimization SINDy [-]
ξ	Vertical location of ships bow [m]
ρ	Water density [kg/m^3]
ω	Wave frequency in the reference frame moving with the current [rad/s]
ω_e	Encounter wave frequency [rad/s]

ACRONYMS

CFD	Computational Fluid Dynamics
CoG	Centre of Gravity
DAQ	Data Acquisition system
EX	Measured exceedance event
EX_{noGW}	Measured exceedance event for which no green water occurred
fb+	With extended freeboard
fb-	Without extended freeboard
FPSO	Floating Production Storage and Offloading ship type
GW	Green Water
GW_{EX}	Green water with measured exceedance
GW_{no}	Green water without measured exceedance
IRF	Impulse Response Function
KS	Kolmogorov-Smirnov test
ML	Machine Learning
MPC	Model Predictive Control
OBS	Open Broadcaster Software
ODE	Ordinary Differential Equation
Q-Q plot	Quantile-Quantile plot
RMSE	Root Mean Square Error
SINDy	Sparse Identification of Nonlinear Dynamics
SL	Slamming

1

INTRODUCTION

Ships sail around, facilitating trade, installing infrastructure, and providing protection. The tasks these ships fulfil are important, as they are for instance the backbone of the world economy, facilitating over 80% of global trade [7], [8]. The ships sail through the waves on the ocean, causing the ship to move around. The waves and moving ship can collide. These collisions do not occur often but when they occur there are harmful consequences. Between 2011 and 2018 at least 210 impacts where waves damaged ships were reported in media, and a few instances resulted in the loss of lives [9].

Wave impacts can damage ships and pose a risk to those on board. These types of wave impacts are grouped in the category of 'extreme wave impacts'. 'Extreme' refers to the impacts being rare but having large consequences. There are different types of extreme wave impacts. The interaction of a ship with the waves can lead to 'green water': a continuous flow of water over the deck of a ship. The bottom side of a ship can also crash onto a wave, called 'slamming'.

To prevent serious accidents these green water and slamming impacts need to be minimized. To minimize extreme wave impacts in the design process accurate predictions of the maximum wave loads are needed. Ideally, the statistical distribution of the extreme loads can be predicted [10]. From the statistics design parameters like the most probable maximum can be determined. Extreme wave impacts are challenging to predict as they are dynamic, multiphase, nonlinear, turbulent and rare [11]–[13]. These aspects also make extreme wave impacts a challenging topic for research.

1.1 LITERATURE

A literature review of previous research into extreme wave impacts is created. The literature review focuses on research into green water and slamming impacts at the bow of a ship. The literature is discussed in the context of the main research methodologies: analytical models, numerical simulations and experimental modelling. The achievements and limitations of each method

with regards to extreme wave impacts are discussed. Before research methods is discussed, the background of the extreme wave impact problem is considered.

1.1.1 *Background*

Interactions between a ship and a wave can result in water on deck, called deck-wetness. Deck-wetness can be white water or green water. White water is a mixture of water and air like droplets, splash or spray [14], [15]. Green water is a continuous flow of water over the deck that can cause large impacts and damage to the bow, equipment or structure of the ship [16], [17]

Green water impacts consist of various stages: first, water exceeds deck level, followed by water flowing onto the deck. After this, a jet can develop from water over the sides of the bow meeting, and lastly, green water can impact on the superstructure [12]. All stages of green water turn out to be nonlinear and complex. The flow is dynamic, air can get entrapped in the water, and ship motions influence green water, but green water also influences ship motions [18].

Various types of green water impacts have been identified. Ariyarathne, Chang and Mercier [19] observed impulsive and non-impulsive impact types, which can be differentiated based on pressure rise time. Greco identifying different types of green water flows onto the deck: dam-break, plunging, plunging - dam-break and hammer-fist event types [15], [20]–[22]. For the dam-break type, water flows onto the deck, while for the plunging green water type, a wave first overturns, trapping air. The plunging - dam-break impact type is a combination of these two impacts, resulting in a flow with air entrapment [16]. The last impact type, the hammer-fist, is a block of water falling onto deck [15].

Slamming occurs when a ship impacts on a wave. Slamming has been defined as part of the ship coming out of the water, and then entering the water with a high velocity relative to the water [23]. Slamming can be keel or bottom slamming, with the lowest part of the ship being impacted. The bow flare or bow stem can also slam, meaning that the overhang of the bow slams on the water [24]. Slamming is characterized by an instantaneous high impact pressures during water entry [13]. During slamming, air can be trapped in between the water and the ship, creating an air cushion. When the air cushion collapses, cavitation and ventilation can occur, resulting in local hydroelastic effects [24]

After this initial local impact, the ship structure can vibrate, which is called whipping [25]. Whipping causes high accelerations throughout the hull,

contributing to vertical bending moments. Whipping can cause containers to come lose and fall overboard, but also results in fatigue of a ship hull, which can over time cause failure of the structure [13], [26]

Green water and slamming are similar as before impact, the water level relative to the ship exceeds a limit. With slamming, a part of the ship comes out of the water before the ship impacts on the water. For green water, water has to exceed deck level to flow onto the deck. For both green water and slamming the relative wave elevation (RWE) is thus an indicator. The relative wave elevation is commonly used in relation to green water [11], [18], [21], [23], [27]–[31]. For slamming the time derivative of RWE, relative wave velocity ($R\dot{W}E$), is also commonly used [32]–[36]. RWE can be calculated with

$$RWE = \zeta - \xi \,, \tag{1.1}$$

with ζ as the local wave elevation and ξ the vertical location of the ships bow. ζ can be calculated as

$$\zeta = \eta + su \tag{1.2}$$

with η representing the undisturbed wave elevation. su is the change in local water elevation due to local ship and water interaction. At the ship's bow these interactions are the wave reflecting of the ship, the ship motions creating radiated waves, and the forward motion of the ship generating waves [11], [12].

The vertical motion of the ship at the bow is calculated with

$$\xi = z + \tan(\theta) \cdot x_{bow} \tag{1.3}$$

where z is the motion of the ship in the vertical direction (heave), θ the rotation around the width direction of the ship (pitch) and x_{bow} the distance between the centre of gravity (CoG) and bow of the ship.

1.1.2 *Analytical models*

The relative wave elevation is an indicator for green water and slamming but does not describe the flow or impact. Analytical models to describe the flow and local pressures of extreme wave impacts have been proposed. The dam-break problem is a classical mathematical problem discussed by Stoker [37]. As certain green water impacts show a similarity to the dam-break flow, the dam-break model has been used to describe green water [18], [38]–[40]. As discussed in section 1.1.1, not all green water impacts are dam-break type impacts, and thus not all green water events can be treated as a dam-break event [16]. Even for the dam-break green water types, there are differences

between the dam-break model and the dam-break green water. The dam-break model assumes a two-dimensional problem where a large volume of water with no initial velocity flows over a horizontal, stationary deck. For green water, these assumptions do not hold as it is a three-dimensional dynamic impact type where water flows over a moving deck [17].

Researchers are working on improving the applicability of the dam-break model for green water [18], [40], [41]. In recent years Hernandez-Fontes has used high-speed camera's for detailed flow analysis for all green water impact types on a static box. From experimental work details of the flow and pressures are given for different impact types and a model for the propagation of water on deck is proposed [16], [42]–[45]. Chuang uses similar research techniques to investigate green water. The research gives improvements on the dam-break model so that pressures induced by green water can be predicted based on the exceedance level of water above deck [46], [47].

For slamming the first analytical model was proposed in 1932 by Wagner [48]. The initial model is for a two-dimensional wedge impacting on stationary water. The Wagner model has been extended [49]–[51], including for instance three-dimensionality. Even with the extension of the Wagner model, the full complexity of slamming cannot be modelled as for local impact air inclusion, bubbles and cavitation occurs [26]. Also, for slamming not only the local impact is relevant, but also global as a slam can cause whipping. Even mild slamming can cause a whipping response in a ship's hull [26]. For both local slamming and whipping hydroelastic effects have to be considered [52]. A theory on whipping to analyze the dynamic response of the hull is developed based on the assumption that events occur independently and with random intensity [53].

The discussed models are for flow and consequent impact, but an important aspect of extreme wave impacts is not considered: the rarity of impacts [54]. Analytical theory on the rarity of extreme wave impacts was developed over 50 years ago. Price and Bishop [29] proposed a predictive tool based on the assumption that extreme waves in a sea state are Rayleigh distributed [29], [55]. Assuming a linear ship response and no swell-up, the combination of waves and motions should lead to a Rayleigh distribution for the relative wave elevations. Combining the assumption of Rayleigh distributed relative wave elevations with the assumption that a relative wave elevation exceeding deck level equals green water, the probability of a green water impact (GW) can be calculated with

$$Pr(GW) = e^{-\frac{fb^2}{R_{RWE}}}, \tag{1.4}$$

where $Pr(GW)$ is the probability of green water, fb the freeboard level and R_{RWE} the variance in relative wave elevation. This equation assumes green

water impacts occur randomly and independently and that all components that make up the relative wave elevation are Gaussian distributed.

Ochi and Motter [23] proposed a similar equation to predict slamming (SL). The equation is based on the same assumptions of Rayleigh distributed waves and ship responses. The difference is that for slamming a component is added for the probability of the bow first coming out of the water before it re-enters with a relative wave velocity above the Ochi criterion (V_{Ochi}) [23]

$$Pr(SL) = e^{-\left(\frac{d^2}{R_{RWE}} + \frac{V_{Ochi}^2}{R_{\dot{RWE}}}\right)} . \tag{1.5}$$

d is the still water draft of the ship and $R_{\dot{RWE}}$ the variance in relative wave velocity.

Further work on extreme wave impacts finds that empirical results deviate from predictions based on equations 1.4 and 1.5. For green water nonlinearity in the waves and ship response and asymmetry in the relative wave elevation distribution causes deviations from the distribution [12], [14], [27], [28]. The largest green water impacts are observed in steep waves or wave groups where nonlinear effects are important, and the assumption of linearity does not apply [56]. Also, equation 1.4 assumes that all instances where water exceeds deck level lead to green water, but water exceedance does not always result in the impact associated with green water.

For slamming an initial comparison to experiments suggests that equation 1.5 can predict the probability of slamming to some extent [23], [57]. However, full-scale measurements of a sailing ship over the course of three years found that the Poisson distribution deviates from the measurements [58]. After these results, the fundamental assumption that slamming impacts are independent has been criticized. Research has shown that slamming events occur dependently in the form of clusters [25], [59]–[61]. Experimental evidence of clustering of slamming has been shown and a need to account for clustering when modelling impacts is found [25], [59], [62].

In conclusion, analytical models lead to predictive equations for both probability and pressures. However, the assumptions on which these analytical models are based are only applicable in a limited range. For green water, only one of the green water types is modelled by the proposed model. For slamming only the local effects are considered while generally neglecting the most harmful whipping effect. Problems with analytical probability models are shown through a limited agreement between empirical measurements and analytical predictions. The deviations show that analytical reasoning is not enough for an accurate predictive tool.

1.1.3 *Numerical simulations*

Numerical simulations are a common tool to obtain predictions needed in ship design. Active work is conducted on simulation schemes for extreme wave impacts. Extreme wave impacts are violent, multiphase, nonlinear, turbulent and rare. These aspects create difficulties in simulating impacts, as few simplifications can be made and a large span of spatial and temporal scales have to be modelled [13]. The complexity makes extreme wave impacts costly to simulate accurately with the tools available [63].

Simulations are being made more efficient by combining numerical schemes [17], [26], [64]–[70]. Even through coupling of different solvers, CFD cannot yet be used to predict the pressures due to extreme wave impacts because the computational time is orders of magnitudes longer than the actual events [13].

Not only work on improving the efficiency of the numerical schemes is being conducted, but also on the accuracy of simulations. More physical aspects relevant to extreme wave impacts are implemented. For instance, schemes to account for entrained air are proposed [71], [72]. Also, nonlinear wave body interaction schemes are proposed [22], [73], [74]. To account for hydroelastic effects fluid dynamic solvers are coupled with finite element methods [52]. Even with all the work on simulating extreme wave impacts, numerical techniques are not yet capable of addressing the complexity and computational cost.

1.1.4 *Combined analytical and numerical models*

The above sections show that analytical models have limited applicability and simulations are costly and cannot model the full complexity of extreme wave impacts. Even though these problems exist, extreme wave impacts on a ship have to be predicted to be able to minimize the impacts.

In recent years methods which combine analytical and numerical models for the predictions of extreme wave impacts are being developed. One of the proposed methods is to combine machine learning with the traditional imperfect numerical or analytical models to predict extreme wave impacts [75], [76]. Another option is to use low-fidelity predictions like an analytical model to identify when an impact might occur, called ‘screening’. The impacts found with screening will then be modelled with a high-fidelity model, like simulations, to make time-efficient predictions for the most probable maximum green water impact [77]. Other work proposes that a known rareness is combined with time and frequency simulations to predict extreme events [78].

Most of these methods work by either assuming a known probability or indicator. For extreme wave impacts the relative wave elevation is often used as an indicator and is assumed to follow the Rayleigh distribution. However, as discussed in 1.1.1 the assumptions under which these results are true are only applicable in a narrow range of situations. An important step in extreme wave impact research is to identify a more widely applicable indicator and find the actual probability distributions for the occurrence of events and pressures of extreme wave impacts.

1.1.5 *Experimental modelling*

For research into extreme wave impacts experimental data is vital [47], [77]. Quite some research into green water has been conducted experimentally. Experiments have their own limitations forcing researchers to simplify their setup. A common simplification is using a static box as a replacement for the ship, neglecting the ship shape and motions [15], [19], [20], [27], [41], [44], [45], [79]–[85]. In experiments where a ship is considered, forward velocity is often neglected as a Floating Production Storage and Offloading (FPSO) ship model is used [18], [20], [28], [56], [82], [86]–[89]. Other simplifications are using regular waves [15], [22], [44], [45], [67], [79], [80], [82], [86], [87], [90]–[93], or a single 'rogue' wave [19], [20], [83], [85], [94]. Also for slamming experimental setups have been simplified to hone in on aspects of interest. Instead of simplifying the ship to a static box, slamming research simplifies the ship to a wedge shape falling into static water [71], [95]–[99]. Regular wave experiments with a ship model are also conducted for slamming [32], [100], [101].

All the above-mentioned experiments are for scaled models, but extreme wave impacts on a full-scale sailing ship have also been measured [24], [34], [53], [57], [58], [62], [102]–[104]. The complexity of impacts means that methods to extrapolate model scale results of the local flow and impact to full scale are not yet developed [13], [26], [105]. The full-scale measurements are thus particularly interesting as no scaling is applied. A downside of full-scale experiments is that environmental conditions are not accurately measured. Another problem is the rarity of extreme wave impacts. The rarity means that even with measurements that last the complete lifetime of the ship, insufficient data is collected to analyze the statistics of extreme wave impacts [26].

The discussed experiments resulted in various insights, but their contribution to the understanding of the statistics of extreme wave impacts is limited. Throughout extreme wave impact research, the rarity of impacts has been an important but complicating aspect. One problematic limitation in experi-

mentally researching the rarity of extreme wave impacts is the finite length of test facilities. When modelling forward velocity the model needs to move with respect to the water. As large water basins used for testing have a finite length, the testing times are brief. If the rarity of extreme wave impacts is modelled correctly in these tanks it can be that no extreme wave impacts occur during an experimental campaign, which can be considered a problem when researching extreme wave impacts.

A solution is to reduce the rarity of extreme wave impacts through the testing conditions and test setup. Even with increased probability experiments need long testing times. Another solution that does model the rarity of extreme wave impacts correctly is to neglect forward velocity [28], [56], [89], [91]. Because of wave reflections testing times are still limited. Also, forward velocity influences extreme wave impacts and neglecting forward velocity neglects these effects. Experimental research that implemented these solutions still concludes that more experimental data is needed to identify the probability distributions of extreme wave impacts [18], [23], [25], [90], [106]. A study by Veer and Boorsma [89] for an FPSO without forward velocity included 248 green water events and used the data to identify types of green water flows. Work by Essen and Seyffert [77] included enough data to empirically evaluate the amount of data needed for converged green water statistics. The results show that long testing times are needed.

1.2 RESEARCH GAP

The work discussed has created insight into extreme wave impacts and is making steps towards modelling and predicting these impacts. One of the main problems of extreme wave impacts is still the statistical properties of impacts. The combined rarity, complexity and variety of impacts have resulted in limited empirical investigation of the statistics. Questions about the statistics, probability, distributions and ranges in which impacts occur are unanswered. Answers to these questions are needed to be able to minimize extreme wave impacts. Further knowledge of the statistics is thus called for.

1.3 RESEARCH OBJECTIVE

The goal of this thesis is to determine the statistics of extreme wave impacts. The scope is limited to a sailing ship in head seas as extreme wave impacts are largest in head seas [30], [92]. The focus is on green water over the bow of the ship, with keel slamming at the bow considered through the Ochi criterion [23].

1.4 RESEARCH METHOD

To study the statistics of extreme wave impacts a representative large data set is needed. From a large data set the distributions of pressures and occurrence, the dependencies of the probabilities and the range of situations in which impacts can occur will become known. The goal of this thesis is to collect this large data set and use it to identify the actual statistics of extreme wave impacts.

To obtain a large data set for extreme wave impacts a novel experimental test facility is developed. The test facility should allow for continuous testing as a ship model is kept stationary while water and waves flow past the model. To that end an existing facility is equipped with a wave maker and a wave spending beach. Three sets of experiments were conducted in this test facility. The first test campaign focused on identifying the probabilistic distribution of impacts and pressures. The second was aimed at identifying the influence of surge on green water and slamming and the last set of experiments tested different design variations.

1.5 STRUCTURE OF THE THESIS

The test facility and data acquisition are described in chapter 2. Using the collected data the statistics of extreme wave impacts are researched. The first results, in chapter 3, show the probability distributions of green water. Chapter 4 discusses the probability of occurrence for green water and slamming, as well as the effect of surge on green water and slamming. Chapter 5 exemplifies the importance of using probabilistic distributions when comparing ship designs. Chapter 6 discusses the range of motions and waves that can lead to green water impacts. Lastly, chapter 7 investigates the possibility of developing a predictive model for extreme wave impacts with interpretative machine learning.

2

TEST FACILITY

The primary objective of this thesis is to collect a large data set and use it to research extreme wave impacts. As discussed in the introduction, studying extreme wave impacts is challenging because of their rarity and their complexity, as the tests need to be high fidelity and long running. Experiments are the most viable research option. To model the rarity of the impacts correctly and have enough measurements to get insight into the statistics, long testing times are needed. Traditional towing tank facilities have limitations in testing times because when forward velocity is modelled the model will move through the tank. This forward motion will inevitably result in the end of the tank being reached, ending the test run. Compensating this time limitation with many tests is unrealistic because of the time and labor intensity.

To overcome the limitations of towing tanks a facility that does allow for long testing times is created: the wave-current tank, shown in figure 2.1. The long testing times with modelled forward velocity are made possible by keeping the model stationary while the water and waves flow past the model. To generate the waves needed for extreme wave impact research a wavemaker is placed at the beginning of the test section. The waves are dissipated at the back of the test section using a beach.

While the tank itself is an older piece of equipment, the addition of the wavemaker and beach has been specifically implemented for the research in the thesis. As these additions are recent developments, the test facility underwent multiple tests before conducting the extreme wave impact experiments. The dimensions of the facility are shown in table 2.1 and the results of testing the wave generation and dissipation as well as the flow in the tank are presented in the following sections.

2.1 FLOW IN TANK

The tank is a piece of equipment that was already available at Delft University of Technology. In the bottom of a tank a turbine generates water flow. The water flows from this bottom section through flow guiders which create a

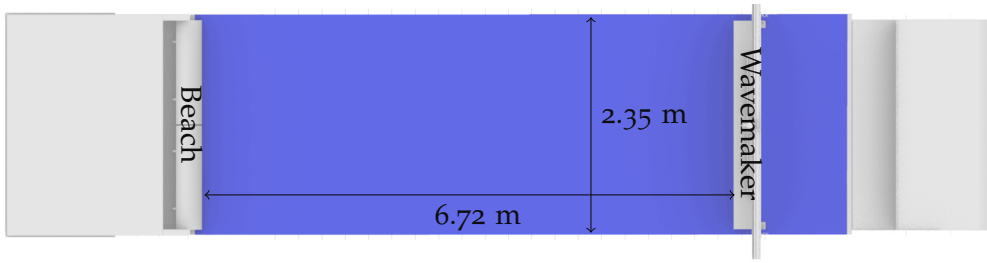

(a) Top view

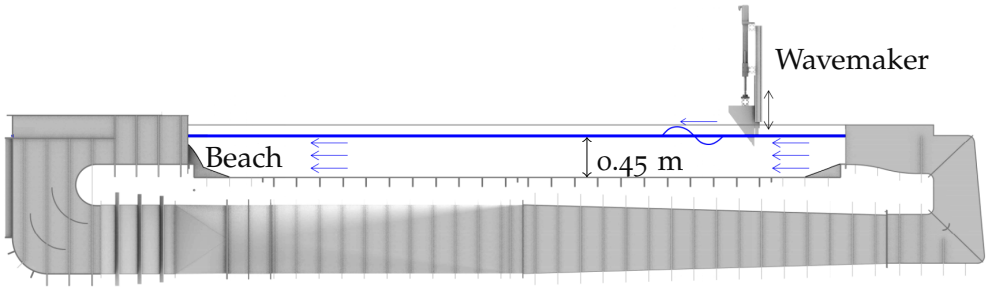

(b) Side view

Figure 2.1: Schematic of the flumetank with the location of the added wavemaker and beach indicated

Table 2.1: Dimensions of test facility used for experiments

Length test section	7.4 m
Width test section	2.35 m
Water depth in test section	0.45 m
Distance from beach to wavemaker	7.05 m
Height wedge wavemaker	0.47 m
Angle bottom wedge wavemaker	37 degrees
Draft wedge wavemaker	0.125 m
Length beach	0.65 m
Height beach	0.45 m

uniform flow into the top where the test section is located. The test section is 7.4 meters by 2.35 meters and a maximum depth of 0.5 meters. The water depth is measured in stationary water with a measuring tape at various locations throughout the tank. Flow velocities up to 0.5 m/s can be generated in the tank.

As stated the tank has special guiders to generate uniform flow. Additional tests were conducted to check flow uniformity. These tests were conducted because, as will be explained in section 2.2, the wavemaker is placed in the flow, and thus the wavemaker affects the velocity profile in the tank. The flow velocity was measured with a Valeport Braystoke open channel flowmeter. The measurement device is placed at various locations and the average measurement over 4 minutes is used. The results are shown in figures 2.2 and 2.3. x_{wm} is the distance from the front of the wavemaker.

The flow profile shows that the wavemaker affects the flow profile near the wavemaker. Close to the wavemaker near the free surface the wake of the wavemaker causes the flow to reverse. At 5.3 meters from the wavemaker, the flow has been restored to uniform flow. Figure 2.3 shows similarly that close to the wavemaker the wake of the wavemaker affects the flow velocities. At a distance of above 1.8 meters from the wavemaker, uniform flow seems to be restored in the middle of the tank.

2.2 GENERATING WAVES

To generate the waves needed for extreme wave impact experiments, a wedge shaped-plunging type wavemaker is added to the tank. This wavemaker type is chosen because the wavemaker has to operate after the inflow location and should not obstruct this inflow, as flow in the tank is necessary to model forward velocity. The dimensions of the wavemaker were designed using the theoretical models of Madsen [107], Wu [108] and Lowell and Irani [109]. The wavemaker has a draft of 0.125 meters, an angle of 37 deg and a total height and width of 0.47 m and 0.30 m. The wavemaker can make waves with a length between 0.05 and 3 meters and at a maximum flow velocity of 0.5 m/s. The theoretical models show that evanescent waves will also be created which can be measured up to 1.5 meters from the wavemaker. The wavemaker is moved by an electric linear servomotor (Festo EMMT-AS-80-M-HS-RSB) controlled by the servo controller (CMMT-AS-C3-11A-P3-EP-S1). The motions of the wavemaker are guided by linear guides in the middle and at the side of the tank.

The wavemaker operates in water with current velocity, making the transfer ratio from the wavemaker motion amplitude to the wave amplitude dependent

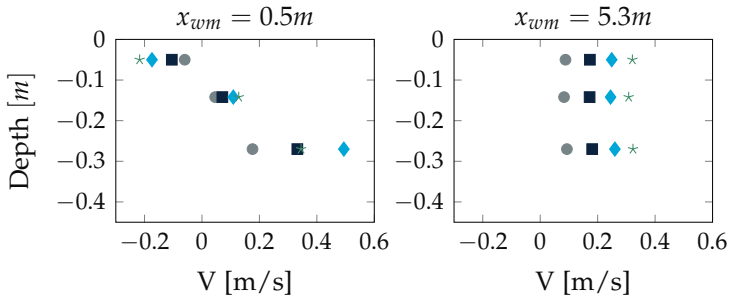

Figure 2.2: Flow velocities in flumetank with wavemaker in water measured at 1.18 m from side of tank at several vertical and horizontal positions in length and depth direction

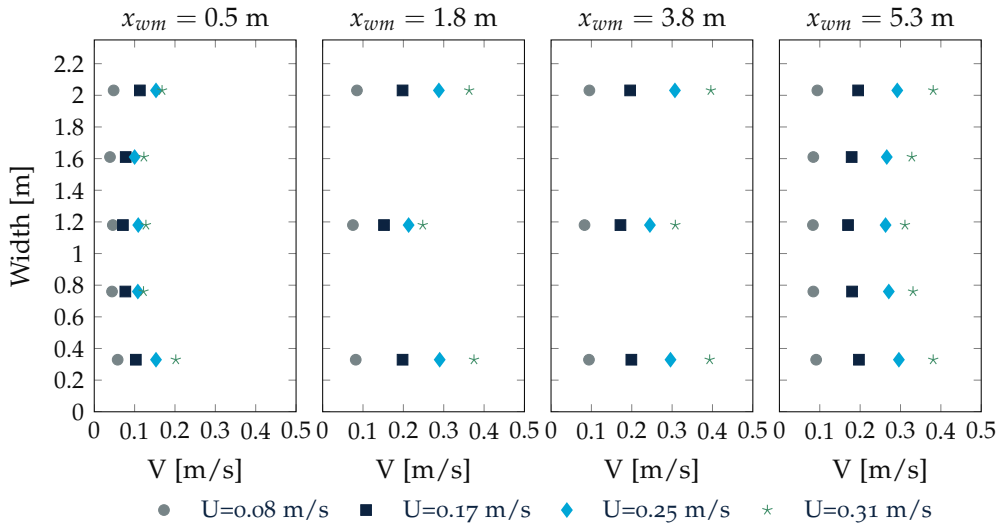

Figure 2.3: Flow velocities in flumetank with wavemaker in water measured at a depth of 0.13 m from the waterline in various horizontal positions

on the current velocity. Regular wave tests at various current velocities were conducted to obtain the transfer ratios. The transfer ratios are shown in figure 2.5

An effect of the wavemaker operating in the water current is that the Doppler effect has to be accounted for. To account for the Doppler effect the frequency of wavemaker motion has to be increased relative to the intended frequency for the still water sea state. The increase for each wave frequency can be calculated with

$$T_w = T_s \cdot \frac{c_s}{c_s + U} \tag{2.1}$$

where T_w is the wave period from the reference frame moving with the current, T_s is the motion period of the wavemaker, c_s is the propagation velocity of the waves and U is the flow velocity.

Another aspect of placing the wavemaker after the water inflow is that a wake is created on the side of the wavemaker where the waves are generated, as discussed in section 2.1. The wake results in backward flow locally near the water surface in front of the wavemaker. This flow reversal results in short waves with a velocity below the backflow to not pass into the main test section. The wake also means that the waves are steeper locally in front of the wavemaker than they will be once they flow into the main test section, and thus the steepness of the waves is limited by the wake of the wavemaker. The regular wave tests show that the wake also causes some variations in the smaller generated waves, probably due to the eddies in the wake of the wavemaker. For the larger waves, the wavemaker generates repeatable waves, also shown in the variation of transfer ratio in figure 2.5. As the research conducted in the test facility focuses on the statistics and uses irregular waves, the variations found in the wave generation are acceptable.

2.3 DISSIPATING WAVES

After the waves and current have flowed past the model, the waves have to be dissipated. It is crucial to minimize wave reflections as reflecting waves will move into the test section, resulting in unknown following waves interfering with the experiments. To minimize wave reflections a beach is designed and placed at the end of the test section to dissipate the waves.

The beach design is based on literature [110]–[112]. One of the primary design considerations was to ensure that the beach does not obstruct the flow of water towards the outflow location. A 1 mm thick stainless steel plate with 5 mm wide square perforation with a total perforation rate of 45% is chosen for the beach. The plate was bent into a half parabola with a height of 0.45 m and a width of 0.65 meters. A picture of the beach is shown in figure 2.6

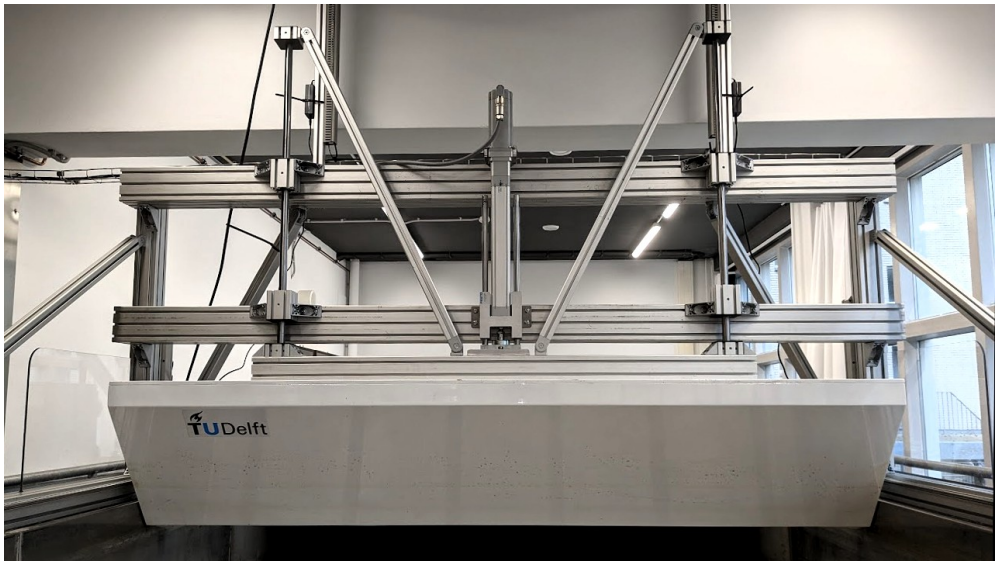

Figure 2.4: Wavemaker that generates waves at the start of the test section

Tests were conducted to verify that wave reflections were minimized. The incident and reflected wave amplitude were measured separately by using regular wave trains of a time length shorter than the time it takes the first wave to travel from the wavemaker to the beach and back to the wave probe. As a result, the incoming and reflected waves were not simultaneously at the wave probe. The reflection coefficient is defined as the reflected wave amplitude divided by the incident wave amplitude of those measurements. The tests were repeated for various flow velocities, wave periods and amplitudes.

The tests show that the beach has a high transmission ratio, meeting the low blocking condition needed to not hinder water flow towards the outflow location. The results are shown in figure 2.7. As a result of the high transmission ratio the reflection coefficient for 0 m/s flow condition is nearly 0.8 for long waves, indicating that the waves are almost completely reflected. The time between the incoming and reflected waves shows that the measured reflection is from the waves reflecting off the wall behind the outflow location, and no measurable wave reflections came from the beach. With increasing flow velocity the reflection coefficient decreases, as shown in figure 2.7. For shorter waves, the reflection coefficients seem to increase but this is a result of keeping the wave steepness constant, resulting in the noise in measurements becoming larger relative to the wave height for shorter waves.

The reflection tests show that reflections decrease with increased flow velocity. The tests also show that waves travel through the beach, reach the outflow location, and reach the back wall behind it. At the back wall, the

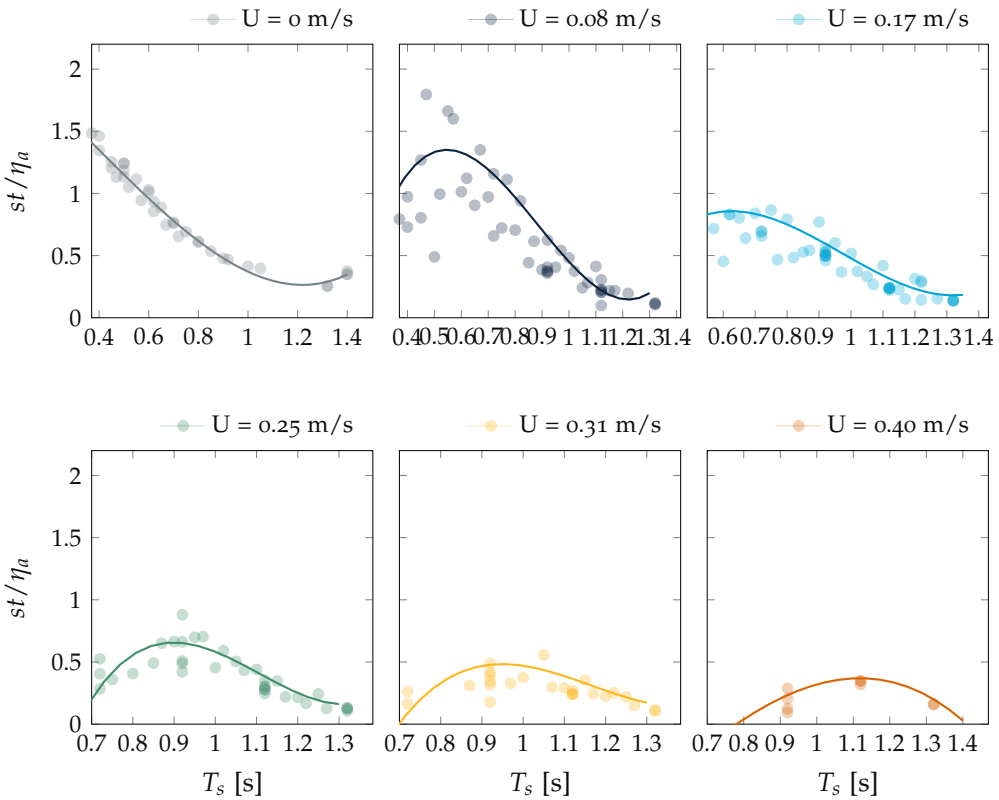

Figure 2.5: Transfer ratio of wavemaker motion amplitude (st) to wave amplitude (η_a) for different flow velocities. The marks indicate the measured transfer ratio. The solid line is a fitted 3rd order curve that is used in the experimental campaigns to design the wave spectra

Figure 2.6: Beach that was designed to dissipate waves at the end of the test section

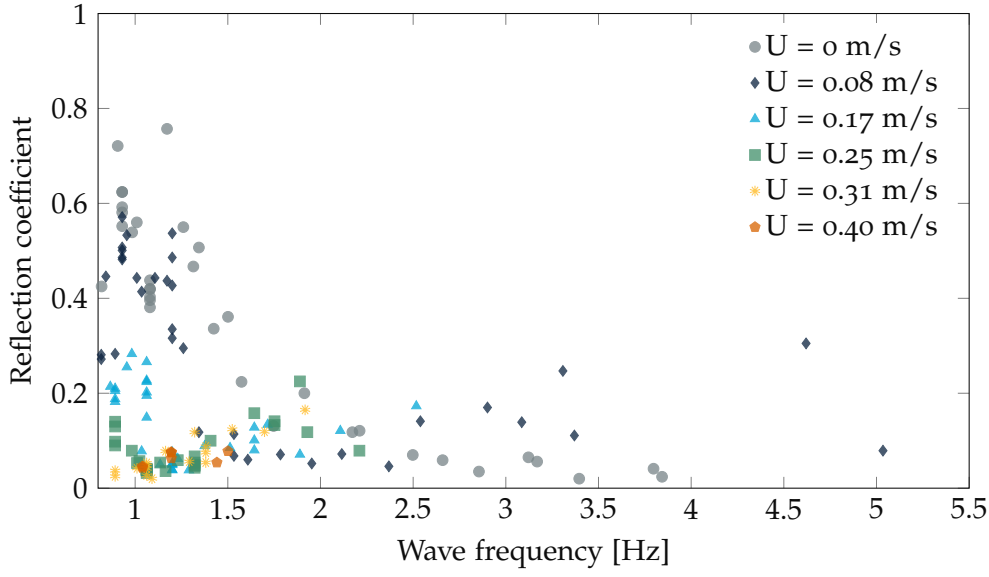

Figure 2.7: Reflection coefficients in the wave-current tank

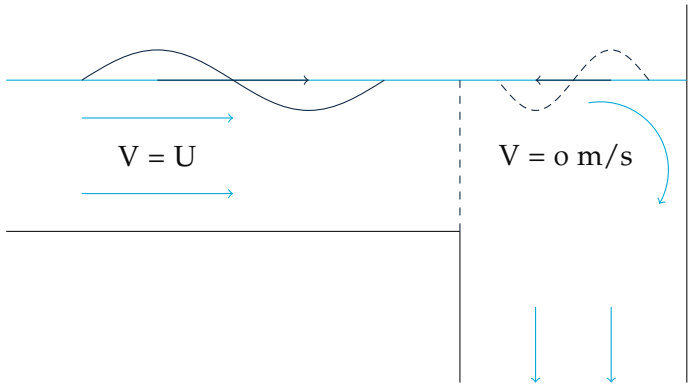

Figure 2.8: Area at the outflow of the wave-current tank (left side figure 2.1) that influences the reflection coefficients. Local horizontal velocity indicated as V

waves get reflected and the waves travel back through the outflow location, through the beach, and into the test section. This process is schematically shown in figure 2.8. During this process the waves are shortened as at the outflow location the average local horizontal flow velocity (V) is zero. The waves thus transfer from a medium with horizontal velocity to one without, shortening the waves. As the waves are shortened the wave velocity reduces. After reflecting on the back wall they will encounter the current velocity in the opposite direction of their travelling velocity. The shortened waves can have a propagating velocity under the current velocity, rendering them unable to travel against the current, leading to a reflection coefficient of zero. For which frequencies wave reflection will be zero due to the current velocity can be calculated with:

$$U > \frac{\frac{g}{\omega}\tanh(kD) - U}{\tanh(kD)^2} \tag{2.2}$$

ω is the wave frequency in the reference frame moving with the current, g is the gravitational acceleration, k is the wave number and D is the water depth. Shallow water effects in the test section are accounted for. The outflow is over a meter deep, and thus deep water waves are assumed in this section. For the lowest tested flow velocity (0.08 m/s) the shortest wave period that gets reflected is 0.54 s and for the highest tested flow velocity, the shortest wave that is reflected is 0.72 s.

The waves that can be reflected as they have a high enough velocity shorten again when moving from the outflow location against the current into the test section. As a result, the waves become steep and unstable. The steeper shortened waves are more effectively dissipated by the beach compared to

the waves at their original length without current. The shortened wave passes through the beach on their return to the test section and encounters incoming waves, also increasing the dissipation of the reflected waves. As a result, current flow also reduces the reflection of all wave frequencies, explaining the low reflection coefficients shown in figure 2.7.

The testing of the wave-current tank shows experiments with irregular waves and limited wave reflections are possible in the facility. The wavemaker can generate a range of different waves, allowing for the modelling of an irregular wave spectrum. The beach and outflow conditions limit the wave reflections at forward velocity. To limit wave reflections experiments are conducted at forward velocities of at least 0.2 m/s to ensure low reflection coefficients.

2.4 DATA ACQUISITION

The original tank did not have a data acquisition system. As the experiments are designed to continuously run for up to forty hours a system that acquires the data automatically is made. Not only does the data acquisition need to operate reliably without supervision, but the system should also be able to handle large quantities of data as the measurement frequency has to be high enough to capture the dynamic impacts.

To handle the acquisition and storage of data, a data acquisition system was designed and built specifically for the experiments. The design of the data acquisition system is schematically shown in figure 2.9. The DAQ NI USB-6211 was used to acquire data and convert the signal from analogue to digital. For experimental setups with more than 16 signals, a DAQ NI-6009 was used additionally. To handle the acquisition of all data except the visual footage a LabVIEW program is created which perpetually creates new files to save data within a certain time interval and moves the old files to offsite storage. Using separate files ensures that the (working) memory of the computer is not exceeded and the files are of a manageable size. The LabVIEW program was built such that no data was lost when one file was closed and a new file opened. The raw data is stored in TDMS files, which are structured binary files and thus require low memory.

During the experiments, video footage is obtained and saved using the open-source software 'Open Broadcaster Software' (OBS). This video footage, together with the measurements, could be viewed live during the experiments on the streaming website www.Twitch.com, allowing for offsite real-time supervision of the experiments. All footage, taken at 30 Hz, is also saved for later review.

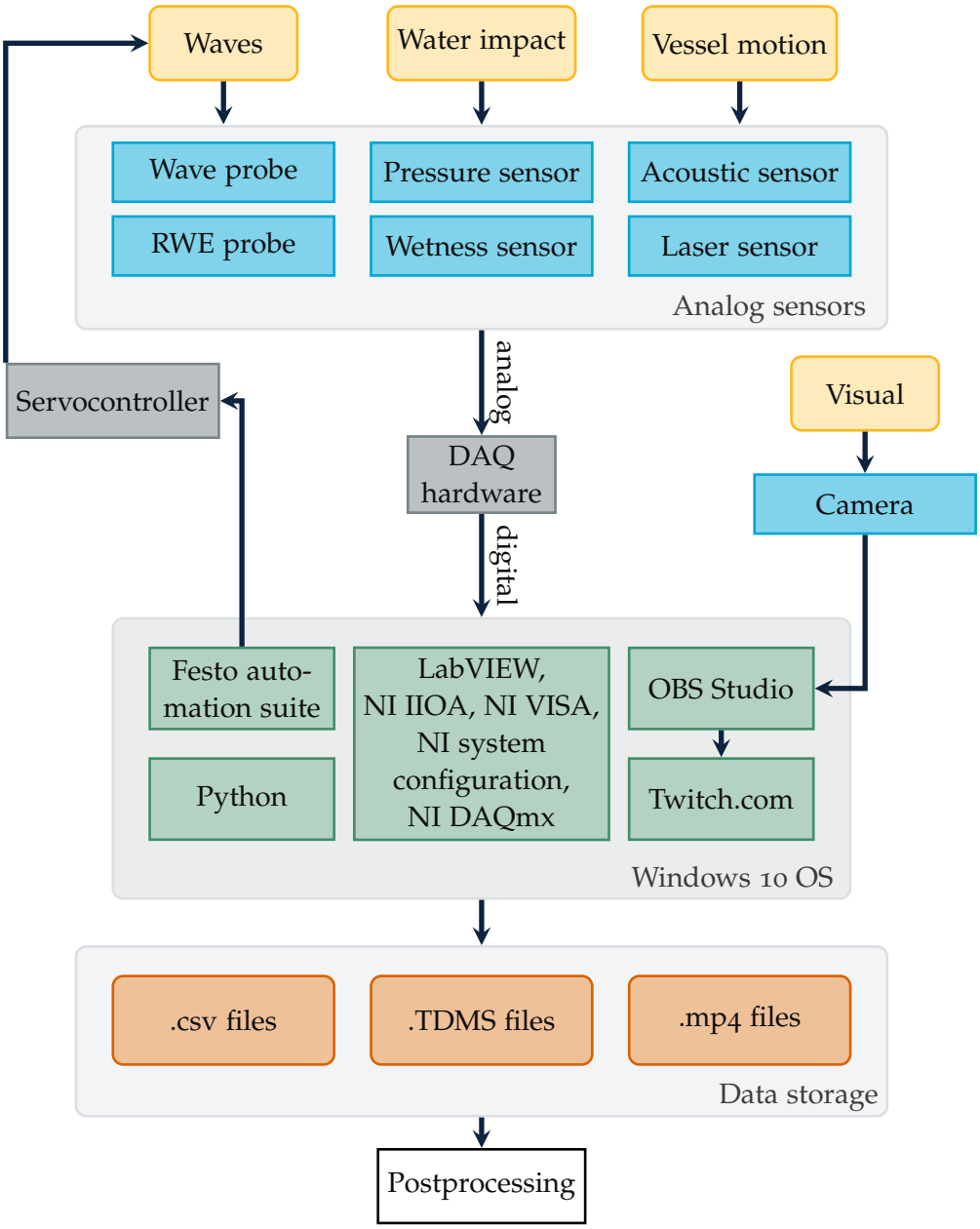

Figure 2.9: Schematic of the data acquisition system made for the long-running experiments and operating system for wave generation

The building of the mechanical part of the wavemaker was described before, but the software system to move the wavemaker also had to be made. The system was built such that a high frequency resolution sea state is generated offline, including the translation of the needed wavemaker motions based on the empirically determined transfer functions. The motions of the wavemaker as a list of amplitudes are then transformed into an analogue signal of amplitudes for the servomotor to navigate the wavemaker to, as is shown in schematic 2.9.

3

PROBABILITY AND DISTRIBUTION OF GREEN WATER IMPACTS AND PRESSURES

This chapter is based on:

[113] A. D. Boon and P. R. Wellens, 'Probability and distribution of green water events and pressures', *Ocean Engineering*, 2022. DOI: 10.1016/j.oceaneng.2022.112429

3.1 INTRODUCTION

Knowing how often green water impacts occur during a ship's lifetime is helpful for ship design. In literature, the probability of water exceeding the deck or deck wetness has been used as an analogy for the probability of green water. The exceedance probability is often obtained from setups with mainly fixed, ship-like models in irregular waves [12], [28], [91]. Probabilities of exceedance have also been found based on simplified setups with a static box above water without forward speed [27], [81]. All these methods depend on the probability of a wave exceeding the deck, while exceedance impacts are not always green water impacts, as white water and spray impacts also occur, but do not induce the large pressures and subsequent damage [20]. The probability of green water occurrence for a ship with forward velocity, in the strict definition that it leads to large pressures, has, to the authors' knowledge, not yet been quantified.

Besides the occurrence of green water, also the expected pressures caused by green water impacts are needed to design for green water. For the pressures much research focuses on the pressure and pressure development during an impact, using static box shapes in regular or breaking waves [19], [44], [45], [80]–[83]. From a design perspective, however, the distribution of the maximum pressures over a range of green water impacts is of interest as this would give the expected pressures on a ship during a green water impact. Hamoudi and Varyani [55] give significant loads for a sailing ship model in

irregular waves but do not show the distribution or other statistics. Ogawa [91] gives a calculation method to find the probability of a mean deck load being exceeded using a relation between exceedance level and load. The resulting method is based on the probability density function of the relative water height, not the actual distribution of the loads. Soares and Pascoal [28] fitted a distribution to the water height maxima, which is related to pressures [12], [91], but stated that more work is needed. Research by Fonseca and Soares [92] gives the pressures on a ship model in large irregular waves but concludes that due to the limited amount of data, no definitive relations could be derived. A statistical investigation with a large data set of pressures on deck thus remains to be performed. Specifically, a large data set of green water impacts on a sailing ship with forward speed in irregular waves is needed to find the actual statistical distribution of the pressures induced by green water impacts for a ship in operation.

The main objective of this chapter is therefore to propose a method to quantify, first, the probability of occurrence of green water with significant pressures and, second, the expected maximum pressures during a ship's lifetime by finding the pressures' probability distribution. For this, a large amount of green water impacts on a ship in realistic sailing conditions is needed. Because green water impacts are rare in realistic sailing conditions, obtaining such a data set is challenging as large testing times are required. Towing tanks used normally have limited length, and thus limited testing time when including forward speed. To get around these limitations, the test facility discussed in chapter 2 is used. In this wave-current tank, the model is kept stationary while the water flows, removing the time limitation and allowing for 40-hour-long sea states at forward speed. This chapter describes the experimental setup, the data collection and processing, the fitting of distributions, estimation methods for the probability of green water occurrence, and how to determine the probability of a limit pressure being exceeded during the lifetime of a ship with a method beneficial for design purposes.

3.2 EXPERIMENTS

A large data set of green water impacts was collected to find the probability of green water occurrence and statistical distributions of the pressure following green water impacts. The experiments model a ship in irregular waves, with free heave and pitch, forward speed and different sea states. Head waves are used as they lead to the most severe green water impacts [79]. The data set includes the occurrence of green water, as well as the pressures during the

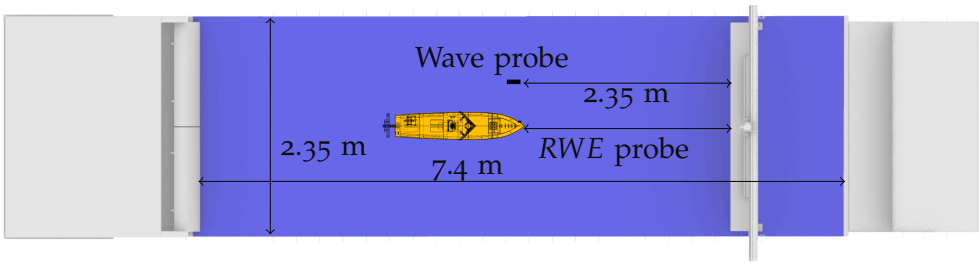

Figure 3.1: Top view of the test setup in the wave-current tank

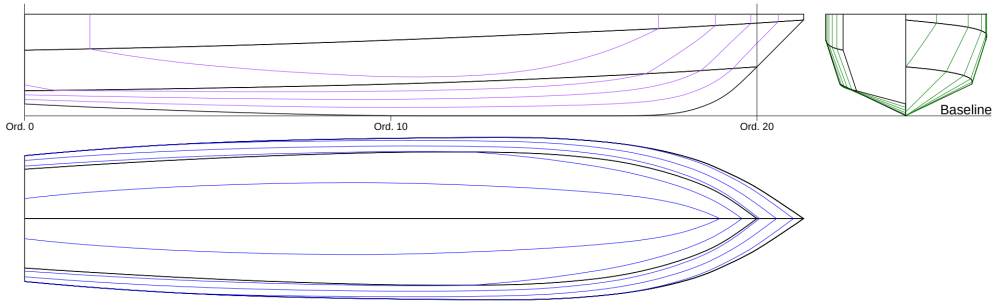

Figure 3.2: Lines plan of the used ship model

green water impacts on the deck and deck box that models a structure. The used test facility is described in chapter 2. A schematic of the test setup in the tank is shown in figure 2.1.

3.2.1 *Test conditions*

Eleven long-running tests were conducted with 174 hours of testing time in total. Different wave spectra, modelled forward velocities and drafts were tested.

Statistically representative sea states were generated by creating 40-hour long wave files with a high frequency resolution below 0.05 mHz. Wave spectra with different energy distributions were created, as the measured spectra translated to an earth-fixed frame in figure 3.3 show. The earth-fixed frame of reference is the frame of reference moving with the current. The transfer function between wavemaker and wave changed for different modelled forward speeds. Thus the spectra tested for different modelled forward velocities were similar but not identical, as shown in figure 3.4.

Properties of conducted tests are shown in table 3.2. Here, T_p is the peak frequency in the earth-fixed frame of reference, H_{m0} the spectral significant wave height, T_{z_e} the zero-crossing encounter period of the spectra, which

Table 3.1: Dimensions and parameters of the used model

Length between perpendiculars	1.50 m
Breadth moulded	0.330 m
Depth moulded	0.207 m
Draft	0.105 / 0.117 / 0.126 m
Total mass	41.0 / 46.0 / 51.0 kg
Vertical centre of gravity	0.161 m
Longitudinal centre of gravity	0.703 m
Radius of gyration in pitch	0.366 m
Natural heave frequency	1.12 / 1.11 / 1.10 Hz
Natural pitch frequency	1.64 / 1.64 / 1.64 Hz
Deck box (length x width x height)	0.150 x 0.180 x 0.090 m
Distance to deck box from stem	0.300 m
Location RWE probe from stem	0.04 m

depends on U. The experiments continued for different testing durations, indicated with t_{test}. n_{GW} is the number of green water impacts that occurred during a test and $Pr(GW)$ is the probability of green water per encountered wave. The number of encountered waves (n_w) was estimated with T_{z_e} and t_{test}.

With the chosen test conditions limitations are introduced. The tested wave spectra are all within a limited range of peak periods and significant wave heights, which will limit the applicability of the results. The applicability of the results is also limited to the used ship model. As the wave spectra tested for different modelled forward velocities are similar but not identical, no direct comparison can be made for different forward velocities.

3.2.1.1 *Full scale comparison*

To confirm that the numbers in table 3.2 model realistic situations, a Froude scaling factor of 125 is assumed based on the ship model likeness to naval vessels of about 190 meters long like the Austin-class, but without a bulb [114]. The total testing time shown in table 3.2 would translate to about 1945 continuous sailing hours. According to the scaling factor of 125, the water depth is 54 meters, the peak periods vary between 9.2 and 11.7 seconds and the significant wave heights between 3 and 5.3 meters. These are rough (5) to very rough (6) sea states according to the Douglas sea scale. These sea states cover a small but relevant part of the scatter diagram of possible sea states. The

Table 3.2: Test cases

Case	T_p **[s]**	H_{m0} **[m]**	T_{z_e} **[s]**	U **[m/s]**	d **[m]**	t_{test} **[hours]**	n_{GW}	$Pr(GW)$
1	0.95	0.035	0.67	0.25	0.117	8	9	0.00021
1a	0.97	0.034	0.67	0.28	0.117	8	7	0.00016
1b	0.93	0.038	0.65	0.21	0.117	8	20	0.00045
1c	0.97	0.024	0.67	0.28	0.117	8	0	0
2	1.05	0.032	0.68	0.25	0.117	40	2	0.00001
3	1.05	0.038	0.68	0.25	0.117	40	34	0.00016
4	0.91	0.040	0.61	0.25	0.117	40	199	0.00084
4a	0.82	0.042	0.62	0.21	0.117	2	9	0.00083
5	0.95	0.042	0.67	0.25	0.117	14	91	0.00119
4 D_+	0.91	0.040	0.61	0.25	0.105	3	6	0.00034
4 D_-	0.91	0.040	0.61	0.25	0.126	3	32	0.00181
Total						174	409	

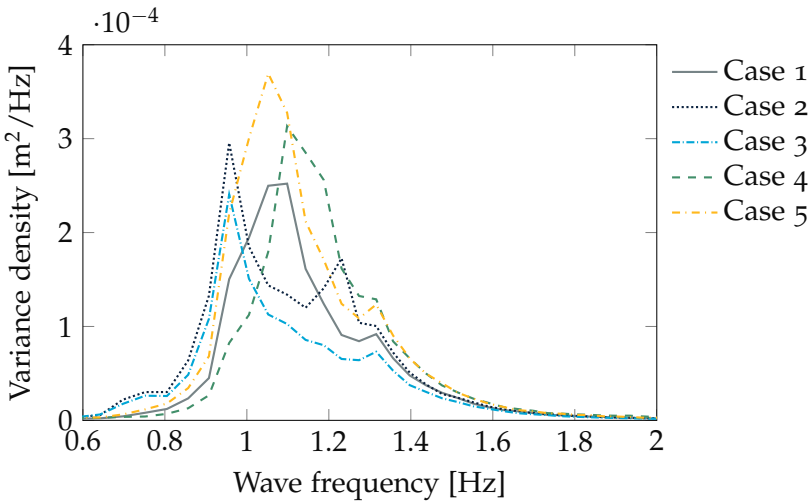

Figure 3.3: Wave spectra for earth-fixed frame of reference with different energy distributions for experiments with a modelled forward speed of 0.25 m/s

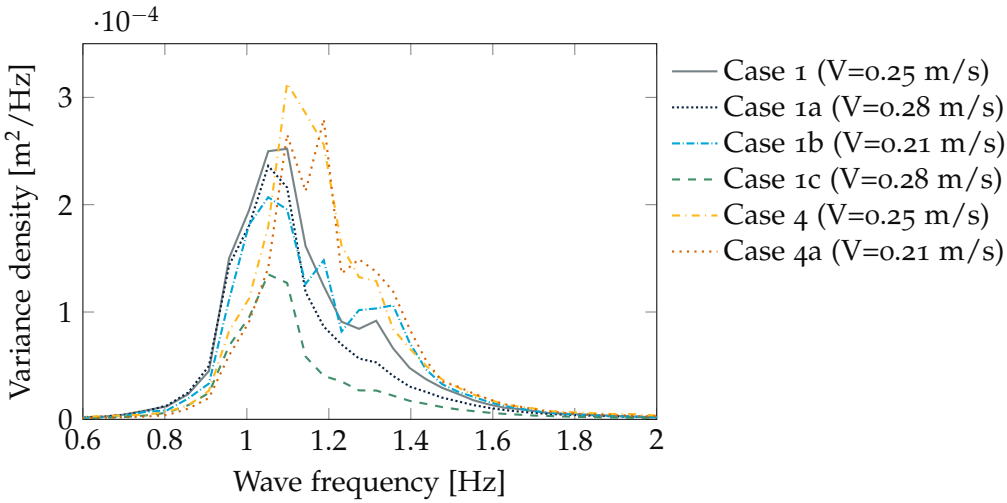

Figure 3.4: Wave spectra for earth-fixed frame of reference with two types of energy distributions for experiments with different modelled forward speeds and a draft of 0.117 m

sailing speed is between 4.6 and 6.1 knots, which is low but representative of a ship sailing through rough seas. Using scaled experiments introduces limits in the applicability of the pressure results since density, viscosity and surface tension are not accounted for when using Froude scaling [83]. A scaling factor of 125 is in line with scaling factors in other green water research with values of 100 [82], [83], [87], 125 [84], [86] and 169 [19].

3.2.2 *Data acquisition*

To measure the impacts of interest on the deck and deck box, five pressure sensors were placed on the deck and three on the deck box as shown in figure 3.5. The pressure sensors are GE druck PDCR 42 type sensors with a range up to 350 kPa. Two deck pressure sensors, number 2 and 5 in figure 3.5, broke during the experiments and their data was not used. The net frequency of 50 Hz induced noise into the pressure signal so the signal was filtered with a 2^{nd} order low pass filter at 45 Hz. To be able to identify when an impact occurred, wetness sensors were placed next to the front four deck pressure sensors. The wetness sensors consist of small probes on deck measuring changes in the electrical resistance, giving as a result of their limited height a binary wet or not signal. The motions of the vessel were measured using Panasonic HG-C1400 laser distance sensors. One was placed next to the hinge in the centre of gravity to measure heave, and the second 0.682 m from the first to

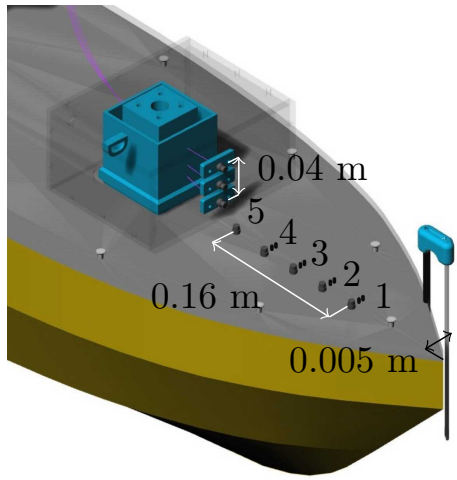

Figure 3.5: Bow of the ship model with locations of sensors. The pressure sensors are on the starboard side and the wetness sensors are on the port side of the ship model

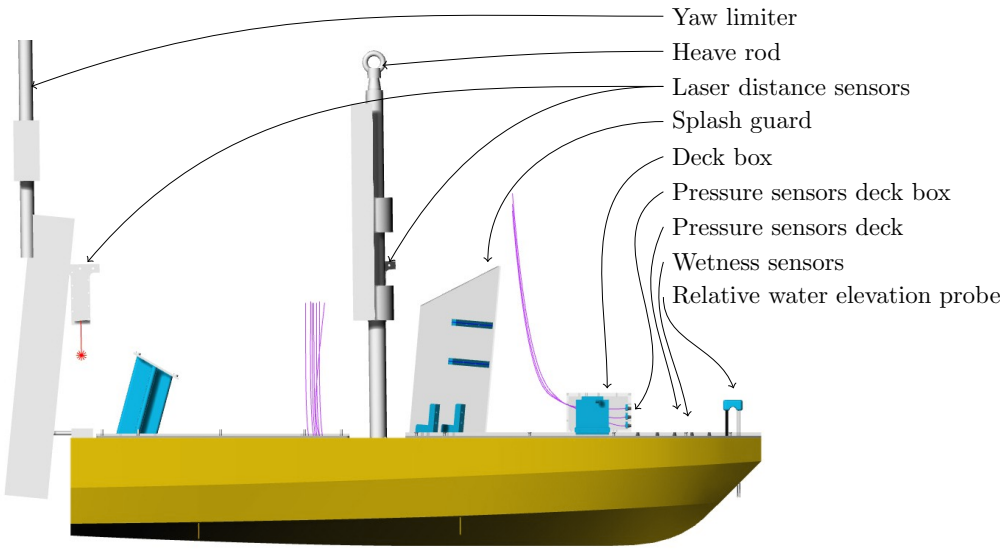

Figure 3.6: Side view of test setup

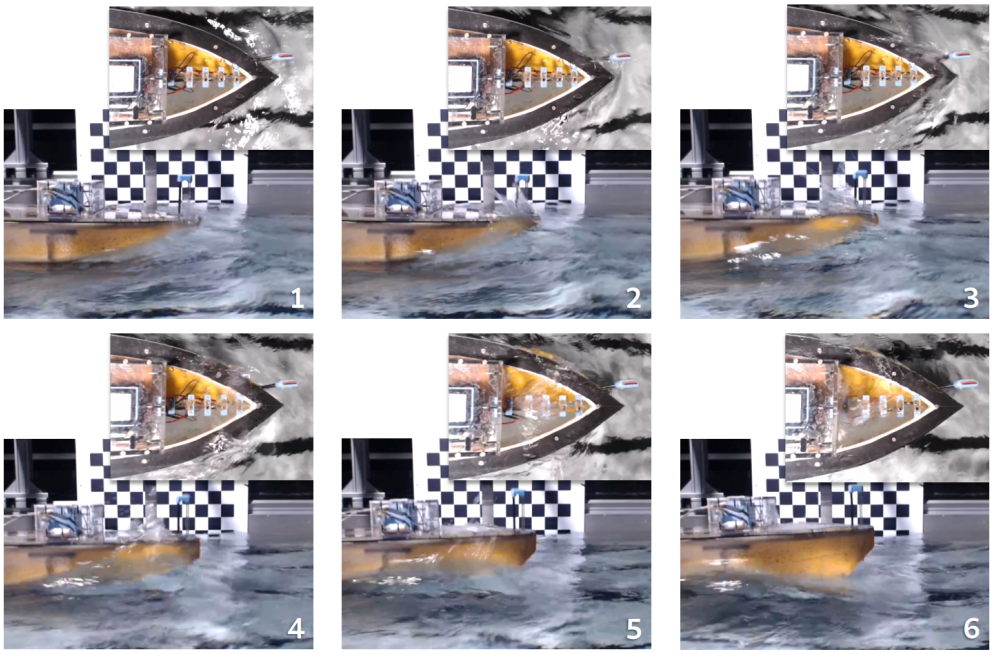

Figure 3.7: Example of video footage to monitor the long-running experiments. Images numbered 1 to 6 in chronological order showing a 0.2 second period with a green water impact

the aft of the vessel to measure pitch. A load cell was placed in the hinge to measure overall resistance, as well as in the deck box to measure the force of a large impact. The overall setup is shown in figure 3.6. A resistance type wave probe was placed 1.15 m port of the vessel, and 0.64 m from the side of the tank. The wave probe was at the same location in the lengthwise direction of the tank as the resistance type RWE probe at 2.35 m from the closest point of the wavemaker. The RWE probe was attached at the port side of the bow of the model 0.05 m from the centre and 0.04 m behind the stem.

The experiments were automated to allow them to be long-running and continuous for up to 40 hours. To allow for the large amounts of data to also automatically be saved a new data acquisition system was needed. Two DAQ devices (NI 6009 and NI 6211) were used to control the wavemaker and save data. The data sampling rate was 1000 Hz as peak pressures act for times of about 1 millisecond [115]. As the experiments were automated, no live in-person supervision of the data was performed. A system was set up using www.Twitch.tv which allowed for live offsite supervision and which automatically saved all footage for later review. Footage of both the top and the side of the bow of the vessel was taken in sync at 30 Hz. Images of the footage during a green water impact are shown in figure 3.7.

3.2.3 *Impact identification*

Green water impacts are identified using wetness sensors and visual identification. Green water impacts in the present study are defined as a flow of water on deck that reaches at least the most forward wetness or pressure sensor, located 0.012 m behind the stem of the bow. This definition only excludes spray-like impacts, which induce pressures lower than the pressure found during green water impacts. The data and visual footage of each impact were checked to ensure the quality of the data. Pressure sensor data from one impact from case 4 was deemed unusable due to an impact against the tank during the extreme wave impact which induced noise in all the pressure sensors.

Most impacts did not reach the deck box. Impacts that did reach the box are sorted based on the maximum pressure found on the box. 41 impacts were included in the deck box impact data set.

Exceedance events are defined as the RWE probe measuring a water level above deck height for at least 0.01 seconds.

3.3 RESULTS

Before analyzing the results, their relation to results from previous research is found. Both the pressure and the impact durations are considered and compared to results from Ariyarathne, Chang and Mercier [19], Hernández-Fontes, Hernández, Mendoza *et al.* [43], Cuomo, Allsop, Bruce *et al.* [116] and Hattori, Arami and Yui [117] and Song, Chang, Ariyarathne *et al.* [83].

The relation between rise time of the pressure (t_r) and maximum pressure on deck (p_{max}) is known to be $p_{max} = a{t_r}^b$. Figure 3.8 shows a pressure trace with t_r and t_d indicated, which were calculated with the zero-crossing times before and after the peak and the time at which the peak value was measured. Figure 3.9 shows for one impact from each tested case the pressure time traces of the deck pressure sensors. The coefficients a and b have been empirically determined for coastal structures [116]–[118] and green water on ships [19], [83]. For the present study the relation between t_r and p_{max} is shown in figure 3.10. The spread in the figure is similar to the spread in the figures found in Cuomo, Allsop, Bruce *et al.* [116] and Hattori, Arami and Yui [117] and Song, Chang, Ariyarathne *et al.* [83]. The parameters for the best fit with b limited to values found in literature are a = 17.3 and b = -0.6. Note that the parameters are dimensional thus scale will influence the results. The fits from Song, Chang, Ariyarathne *et al.* [83] and Ariyarathne, Chang and Mercier [19] with scaling factors of 100 and 169 are shown.

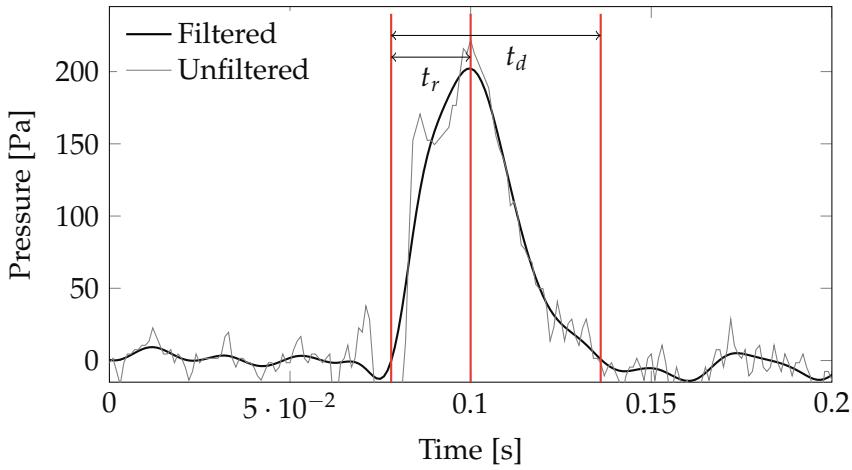

Figure 3.8: Pressure trace of green water impact on pressure sensor 1 in case 4 with rise time t_r and duration time t_d indicated

Second, the pressure development quantified by the relation between t_r and impact duration t_d is compared. Previous research considered consecutive green water impacts on a fixed structure, caused by regular waves finds for t_r/t_d a spread of data between 0.18 and 0.64 over 120 impacts [43]. The range of t_r/t_d found in the present study is shown in figure 3.11. The present work includes a larger range of impacts, with most impacts within the expected 0.18 to 0.64 range. Impacts in the present study were smaller, with smaller peak pressures, compared to the impacts in Hernández-Fontes, Hernández, Mendoza *et al.* [43], leading to a smaller t_r/t_d because of the inverse relationship between the rise time and pressure peak. Overall the shown data agrees with the spread found by Hernández-Fontes, Hernández, Mendoza *et al.* [43].

Summarizing, the data from the present study is in accordance with previous research, with a larger spread in impacts and number of impacts. More low pressures, indicating lower fluid velocities, are present in the data set in the present study. Previous research focused on the physics or categorization of individual green water impacts, for which a large enough impact is necessary for analysis. This goal is in contrast with the present study which focuses on the distribution of all sizes of green water impacts.

3.3.1 *Distributions of impact occurrence*

The distribution of the occurrence of green water impacts over time has been identified for each tested case with more than 10 green water impacts, which were cases 1b, 3, 4, 4 D_ and 5. The time between the occurrence of green

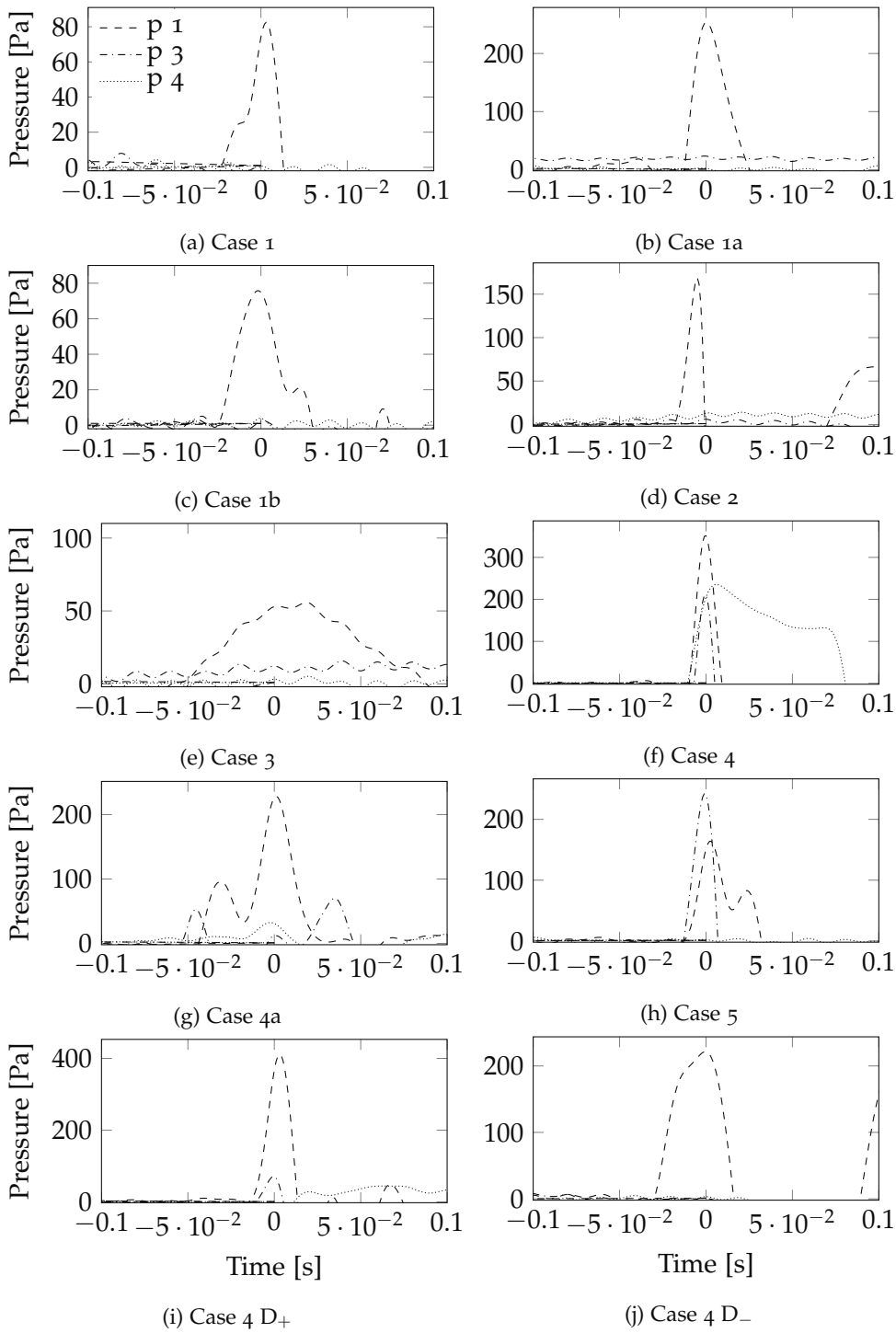

(a) Case 1

(b) Case 1a

(c) Case 1b

(d) Case 2

(e) Case 3

(f) Case 4

(g) Case 4a

(h) Case 5

(i) Case 4 D_+

(j) Case 4 D_-

Figure 3.9: Pressure signals on deck pressure sensors for one impact from each test case. The data is time-shifted so the pressure peak occurs at 0 for each sensor

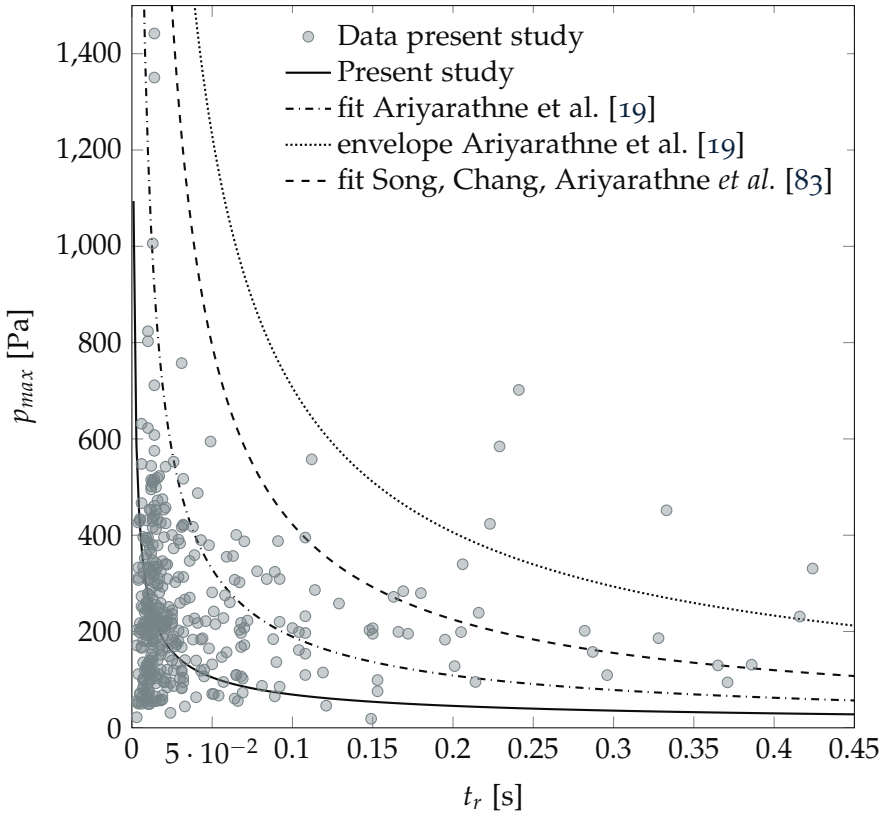

Figure 3.10: Relation t_r and p_{max} with best fit and previous found correlations shown, the results from the present study show lower rise times compared to previous research

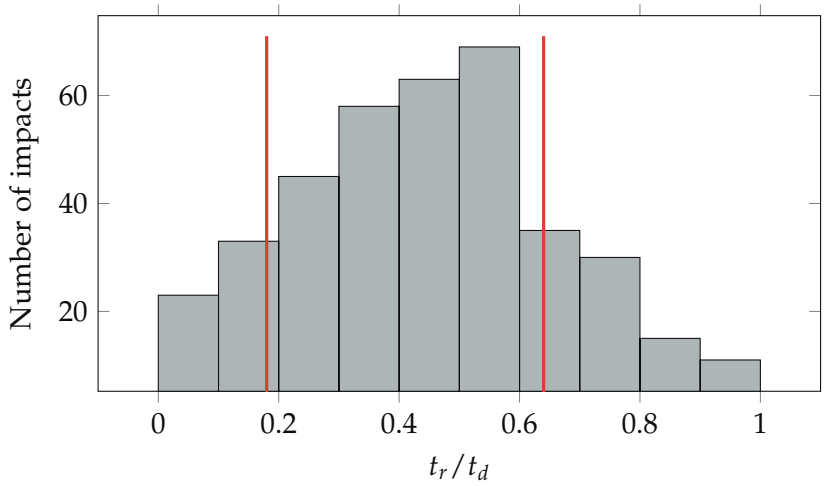

Figure 3.11: Histogram of t_r/t_d showing overall agreement with $0.18 < t_r/t_d < 0.64$ found by Hernández-Fontes, Hernández, Mendoza *et al.* [43]. A larger range of impacts is found for the present study

water impacts is used to base distributions on. For each case distributions are fitted through the set of times between impacts. The distributions were the Gumbel, Fréchet, Weibull, chi, chi-squared, Rayleigh, Cauchy, exponential, exponential power, power law, gamma, normal, log-normal, and uniform distribution. By using the least-squares method on the data in 100 bins the best fit is found for each case.

The best-fitting distribution for the times between impacts was overall the exponential distribution. For some cases the gamma distribution gave a better fit, but this was for cases with fewer impacts. The exponential distribution is a special case of the gamma distribution and has one free parameter fewer to fit with compared to the gamma distribution. The extra parameter means that for data with more variance than the sample mean (as is the case for smaller data sets) the gamma distribution has an extra parameter to force a better fit. The time between impacts is concluded to be exponentially distributed.

The exponential distribution is in line with green water impacts occurring continuously and independently at a constant average rate. Thus, the time when a green water impact occurs is independent of the time since the last impact. The results of the distribution for case 4, the case with the most green water impacts, are shown in figure 3.12a with the experimental data visualized in 35 bins. A quantile-quantile plot (Q-Q plot) for case 4 is shown in figure 3.12b. The Q-Q plot visualizes outliers and overall deviations from the distribution with a diagonal line indicating a perfect fit [119]. The plot

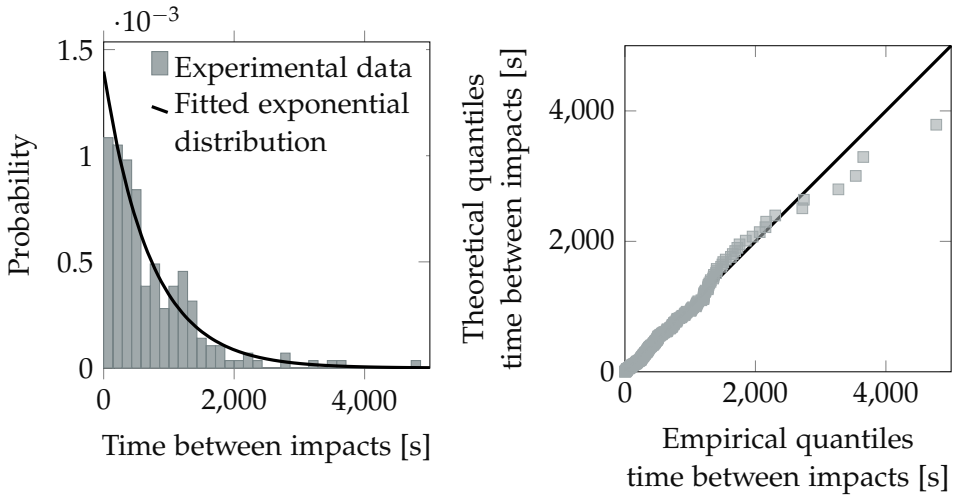

(a) Histogram of experimental data and the fitted exponential distribution

(b) Q-Q plot showing the distribution fits the data well

Figure 3.12: Time between green water impacts for case 4 and the fitted exponential distribution

shows some outliers but a general agreement with the distribution. This is the conclusion for other cases as well.

For further verification, an exponential distribution was fitted for all the cases. The parameters of the fitted exponential distributions are shown in table 3.3. In this table, λ is the mean time between impacts.

A goodness-of-fit test was conducted for the fitted distributions using the Kolmogorov-Smirnov (KS) test. The test uses the maximum difference between an empirical and hypothetical cumulative distribution and gives a p-value [120]. A limit of 0.05 is set for the p-value, meaning that for p-values below 0.05, the distribution is concluded to not represent the data. The results for the goodness-of-fit test are shown in table 3.3. All p-values are well above 0.05. The exponential fit can thus represent the empirical data of the time between green water impacts.

Besides the green water impacts also the distribution for the time between exceedance impacts is identified and is also found to be exponentially distributed. The results of the fit and the KS goodness-of-fit test are also shown in table 3.3. As again all values are above 0.05 the exponential fit is also a suitable distribution for the distribution of the time between exceedance impacts.

Table 3.3: Parameters of fitted exponential distribution for time between green water and exceedance impacts and p-values from Kolmogorov-Smirnov goodness-of-fit test

	Green water occurrence			Deck exceedence occurrence		
	Parameters [s]		**p-value**	**Parameters [s]**		**p-value**
Case	Location	λ_{GW}		Location	λ_{EX}	
1	162	3200	0.76	129	1065	0.69
1a	286	4114	0.37	34.6	2119	0.64
1b	151	1440	0.77	2.26	710	0.12
1c	-	-	-	-	-	-
2	1857	72000	0.50	1402	48000	0.12
3	64.0	4235	0.88	63.2	2321	0.65
4	1.00	724	0.48	1.45	439	0.26
4a	182	732	0.93	2.90	210	0.51
5	3.00	564	0.50	1.41	296	0.41
4 D$_+$	185	1800	0.74	3.58	477	0.73
4 D$_-$	6.00	338	0.74	1.43	171	0.59

Table 3.4: Parameters of fitted Fréchet distribution, p-value from Kolmogorov-Smirnov test and skeweness of data and distribution for p_{max}, $p_{box,max}$, P_{max} and $P_{box,max}$

	Parameters			**KS-test**	**Skeweness**	
Case 4	shape	location	scale	p-value	s_{data}	s_{distr}
p_{max}	6.57	-511	663	0.361	0.427	11.6
$p_{box,max}$	0.417	31.2	11.5	0.066	-	-
P_{max}	3.40	-84.5	164	0.059	0.496	2.56
$P_{box,max}$	0.503	18.5	7.15	0.159	-	-
Case 5	shape	location	scale	p-value	s_{data}	s_{distr}
p_{max}	8.06	-243	447	0.062	0.881	2.18
$p_{box,max}$	0.496	30.9	6.34	0.888	-	-
P_{max}	10.1	-264	371	0.440	0.670	1.90
$P_{box,max}$	0.531	20.2	2.13	0.961	-	-

3.3.2 *Distributions of pressures*

To analyze the pressures on the deck and deck box the measured pressures are captured in parameters p_{max}, $p_{box,max}$, P_{max} and $P_{box,max}$. The local maximum pressure on deck p_{max} is the maximum pressure measured by one of the sensors during a green water impact. The maximum local pressure on the deck box is $p_{box,max}$. The mean maximum pressure P_{max} is the maximum pressure measured per impact per deck sensor, averaged over all the deck sensors. $P_{box,max}$ is the mean maximum pressure on the deck box.

The pressures are thought to depend on the sea state, as Soares and Pascoal [28] found larger mean relative water height maxima for larger H_{m0}. As the relative water heights are known to relate to the maximum pressure [12], [91], different pressures are expected for different cases. Cases 4 and 5, with more than 50 green water impacts each, are used for further statistical analysis.

The same method is used to find the distributions of pressures as is used to find the distribution of occurrence of impacts in paragraph 3.3.1. With this method, the sum least-square error applied over the data binned in 100 bins showed the Fréchet distribution, also known as the inverse Weibull distribution, to be the best fit. Figure 3.13, for case 4, shows the fit and the experimental data visualized in 35 bins. When one takes the maximum of a set of variables, which is done for p_{max} and $p_{box,max}$, the distribution of the overall data will always become an extreme value distribution [121]. This

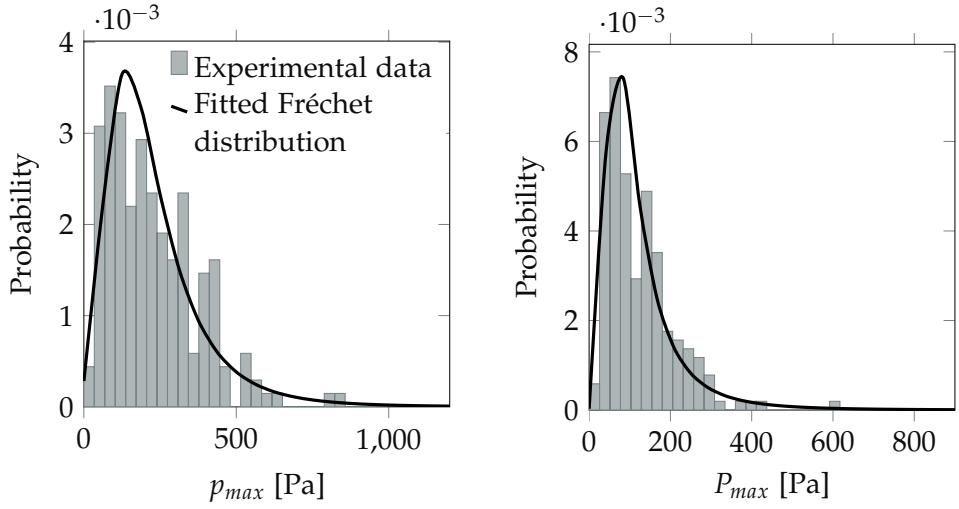

(a) p_{max} and the fitted Fréchet distribution (b) P_{max} and the fitted Fréchet distribution

Figure 3.13: Histograms of experimental data of case 4 with the fitted Fréchet distribution

fact is in line with the Fréchet distribution fitting the results as the Fréchet distribution is the generalized extreme value distribution type II.

The pressures on both the deck and deck box for both cases 4 and 5 are concluded to be distributed according to the Fréchet distribution. To further the confidence in the fit of the Fréchet distribution again the KS goodness-of-fit test was conducted. The results are shown in table 3.4. All p-values are larger than the acceptance limit of 0.05, also when fitting a Fréchet distribution for P_{max} and p_{max} for the other cases than 4 and 5 with more than 10 green water impacts. The size of the deck box data set is considered too limited, as discussed in paragraph 3.2.3, consisting of 23 impacts for case 4 and of 9 impacts for case 5. The skewness of the pressures on the deck box is therefore not reported in table 3.4 (dashes are shown instead) and the deck box pressures are not included in further analysis.

The highest pressures that occur are of most interest from an engineering perspective as they cause the largest damages. The representation of those highest pressures by the fitted distribution is thus investigated. To visually inspect how well the Fréchet distribution fits the extreme cases, Q-Q plots are shown in figure 3.14. For case 4 the fitted distribution overestimates the larger pressures for both P_{max} and p_{max}. For case 5 the two highest values for p_{max} deviate from the distribution, causing the largest P_{max} to also deviate from the distribution. The deviation from the distribution further away from the mean of the distribution can be quantified using the skewness (s). Higher

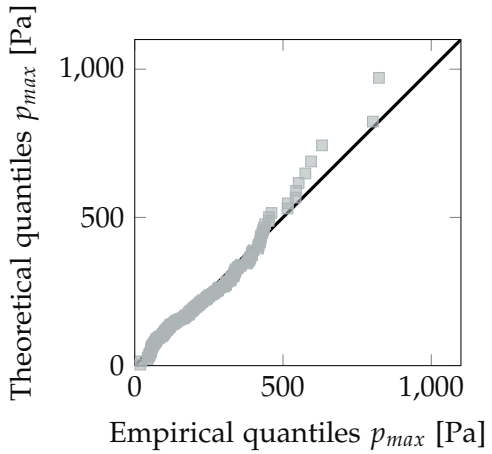

(a) Q-Q plot for p_{max} of case 4

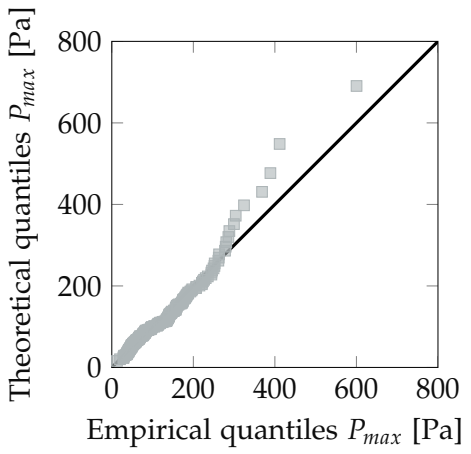

(b) Q-Q plot for P_{max} of case 4

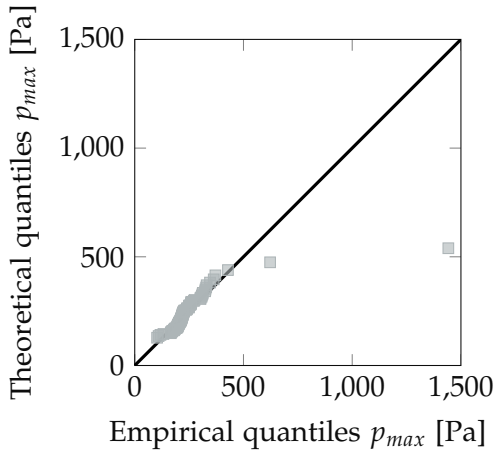

(c) Q-Q plot for p_{max} of case 5

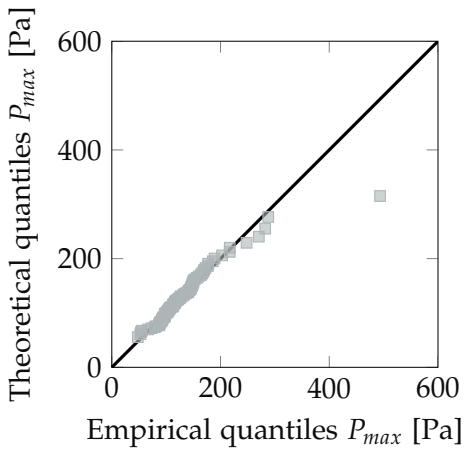

(d) Q-Q plot for P_{max} of case 5

Figure 3.14: Q-Q plots showing the quality of fit of the Fréchet to P_{max} and p_{max} for cases 4 and 5. The lines indicate the fitted theoretical distribution and the squares the experimental data

values of skewness indicate more values further away from the mean. The values for the skewness are shown in table 3.4. All values show a skeweness larger than 0, indicating a skew to values above the mean. The skew of the theoretical distribution is for both cases for both p_{max} and P_{max} larger than the skew of the empirical data. The fitted Fréchet distribution thus estimates more pressure above the mean pressure compared to the number of measured values, meaning that the Fréchet distribution gives a conservative estimation for pressures above the mean pressure.

3.3.3 *Calculating probability pressure exceedance*

In the previous paragraphs, first, the probability of green water occurring and second the distributions of the pressures are obtained. The probability of impacts is calculated as

$$Pr(GW) = \frac{n_{GW}}{n_w} = \frac{\frac{t}{\lambda_{GW}}}{\frac{t}{T_{z_e}}} = \frac{T_{z_e}}{\lambda_{GW}}. \tag{3.1}$$

With the newly found distribution of the pressures, the probability of a certain limit pressure (p_{lim}) being exceeded during an impact can be calculated with the cumulative distribution function of the Fréchet distribution

$$Pr(p_{max} > p_{lim}) = 1 - exp(-\frac{p_{lim} - m}{c})^{\alpha}, \tag{3.2}$$

in which m is the location parameter, c the shape parameter and α the scale parameter. The empirically found values for these parameters are given in table 3.4.

Combining equation 3.1 and 3.2 and using compound probability theory gives us

$$\begin{aligned} Pr(p > p_{lim}) &= 1 - (1 - Pr(p_{max} > p_{lim}))^{n_{GW}} \\ &= 1 - (exp(-\frac{p_{lim} - m}{c})^{\alpha})^{\frac{t}{\lambda_{GW}}}. \end{aligned} \tag{3.3}$$

This equation gives the probability of a pressure on deck being exceeded during a ship's operation. In this equation, n_w is the number of waves encountered during a ship's operation. As we will see below, the probability of green water occurring depends mostly on the sea state, draft and forward speed. For the pressure distribution a dependency on the sea state is known (paragraph 3.3.2).

The probability of a limit pressure being exceeded for a certain sailing time, sea state, draft and forward speed can now be calculated with equation 3.3.

Note that the average probability of green water occurrence (λ_{GW} or $Pr(GW)$) is independent of the distribution.

As the Fréchet distribution is conservative for the large pressures (paragraph 3.3.2), the probability calculated with equation 3.3 is also conservative for large pressures. This is assuming that the probability of green water occurrence is accurately or conservatively estimated.

3.3.3.1 *Relation between the probability of green water and exceedance*

In our experiments deck exceedance is not always measured when green water impacts occur, and exceedance does not always lead to green water, see figure 3.15. The figure shows green water occurring for a measured relative water elevation lower than the deck. Also, figure 3.15 shows that not all exceedances lead to green water, as is the case for exceedances below 0.015 m. This does not mean that for those exceedances no water comes on deck, as deck wetness with small amounts of water can still occur in the form of, for instance, spray, but this deck wetness does not meet the definition of green water used in this study (paragraph 3.2.3).

A relation between $Pr(GW)$ and the probability of an exceedance event occurring ($Pr(EX)$) is valuable as $Pr(EX)$ is easier to obtain compared to $Pr(GW)$, with various methods to estimate $Pr(EX)$ available in literature [12], [27], [28], [55], [91]. $Pr(EX)$ is calculated by dividing the number of individual exceedance impacts measured with the RWE probe by n_w. The average time between exceedance and green water impacts per case is given in table 3.3. The relation between $Pr(EX)$ and $Pr(GW)$ is shown in figure 3.16. The dotted lines in the figure indicate the 95% confidence interval. The 95% confidence interval is approximated based on the exponential distribution of the impacts over time using the method described by Ross [122], which underestimates the confidence interval for fewer than 15 impacts [123]. The confidence interval depends on the number of impacts, which explains the differences.

A linear relation between $Pr(EX)$ and $Pr(GW)$ is fitted for, quantified with $Pr(GW) = \frac{Pr(EX)}{2.17}$. The relation holds for the different wave spectra, forward speeds and drafts tested. The deviations from the relation like case 4 show that the relation does not capture the intricacy of the different physics for exceedance and green water impacts or the influencing factors.

3.3.3.2 *Relation between $Pr(GW)$ and H_{m0}*

Finding a relation between $Pr(GW)$ and parameters from the environmental conditions would simplify solving equation 3.3 from an engineering perspective. $Pr(GW)$ depends on the wave spectrum, draft and forward speed (table

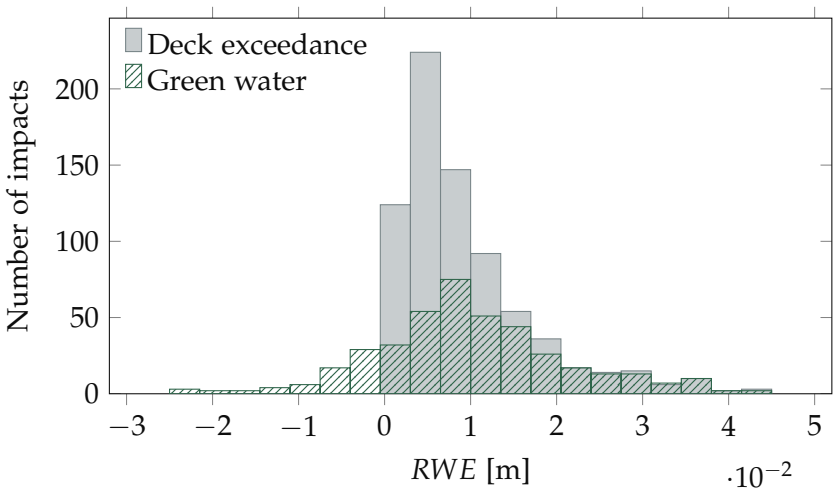

Figure 3.15: Difference between green water impacts and deck exceedance impacts shown using the relative water elevation

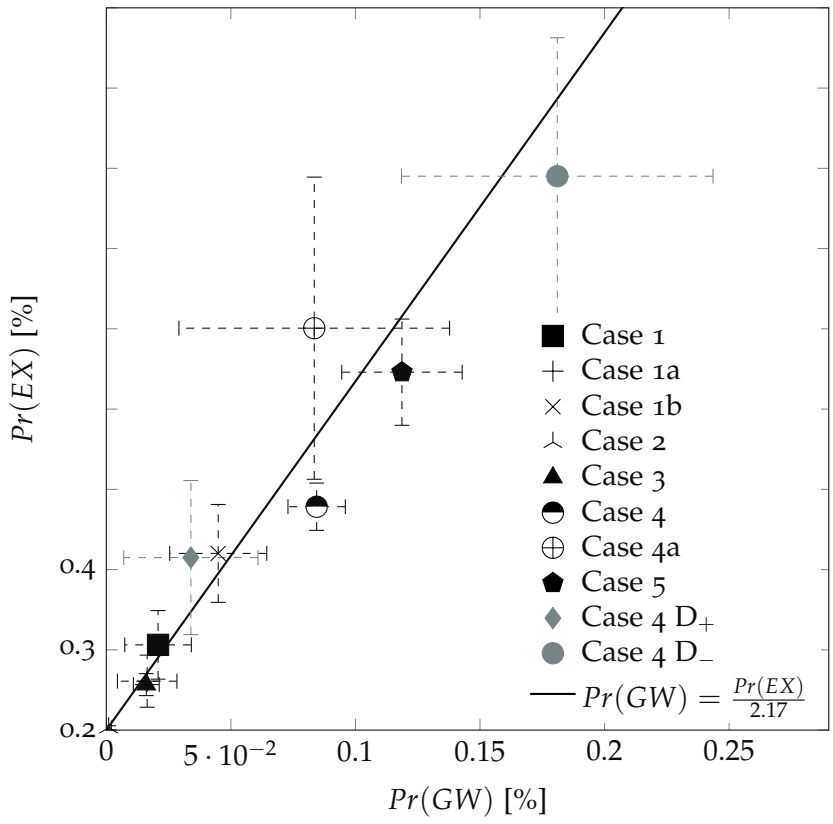

Figure 3.16: Relation between $Pr(GW)$ and $Pr(EX)$ with identified linear relation shown. Dashed lines indicate 95% confidence interval

3.2). $Pr(GW)$ of all tested cases is visualized for various significant wave heights in figure 3.17.

A correlation between H_{m0} and $Pr(GW)$ is found. To quantify the correlation, we use work by Koosheh, Etemad-Shahidi, Cartwright *et al.* [124] and Franco, Gerloni and Meer [125] and Besley [126], showing a correlation for the probability of wave overtopping for coastal structures. Their formulation includes the relative freeboard crest distance in coastal context and H_{m0}. The relative freeboard crest distance can be translated to the freeboard when considering a ship and the probability of overtopping to the probability of green water. Implementing the translations creates:

$$Pr(GW) = e^{-(C\frac{fb}{H_{m0}})^2} = e^{-(1.19\frac{fb}{H_{m0}})^2}, \tag{3.4}$$

with fb being the still water freeboard at the bow and C a parameter to be fitted for. The relation including the freeboard is in line with Greco [21] and Hamoudi and Varyani [55] who showed that the freeboard has the largest influence on green water. The form of the relation is also in line with equations found for the probability of deck wetness based on the Rayleigh distribution [29], [91].

With the least-squares method fitting the relation to H_{m0} and $Pr(GW)$ for cases with fb = 0.091 m C is found to be 1.19, in line with previous research which found values between 1.098 and 1.4 [124]–[126]. The fit is also visualized in figure 3.17, as well as the fit for the different drafts, with fb = 0.103 m and fb = 0.082 m, shown for the relevant range of H_{m0}. Overall the fit represents the data.

Forward speed is not included in the relation. In the present study a decrease in forward speed from 0.28 m/s to 0.21 m/s for cases 1a (U=0.28 m/s), 1b (U=0.21 m/s) and 1c (U=0.28 m/s) is found to coincide with an increase in $Pr(GW)$. The relation is not consistent as $Pr(GW)$ does not always increase when the ship's forward speed decreases. For case 4a (U = 0.21 m/s) a similar $Pr(GW)$ was found as for case 4 (U = 0.25 m/s). For case 1 (U=0.25 m/s) and case 1a (U=0.28 m/s) also similar $Pr(GW)$ were found. The differences in $Pr(GW)$ for cases 1a, 1b and 1c are best explained by differences in the wave spectra, as discussed in 3.2.1. A relation with forward speed could thus not be demonstrated with our present data. Future studies will require increased emphasis on forward speed to allow for a relational formulation of $Pr(GW)$ with H_{m0}, fb and U.

3.3.3.3 *Comparing the two estimation methods for $Pr(GW)$*

In paragraph 3.3.3.1 and 3.3.3.2 two methods are proposed for estimating $Pr(GW)$: one based on $Pr(EX)$ and one based on H_{m0}. The methods are

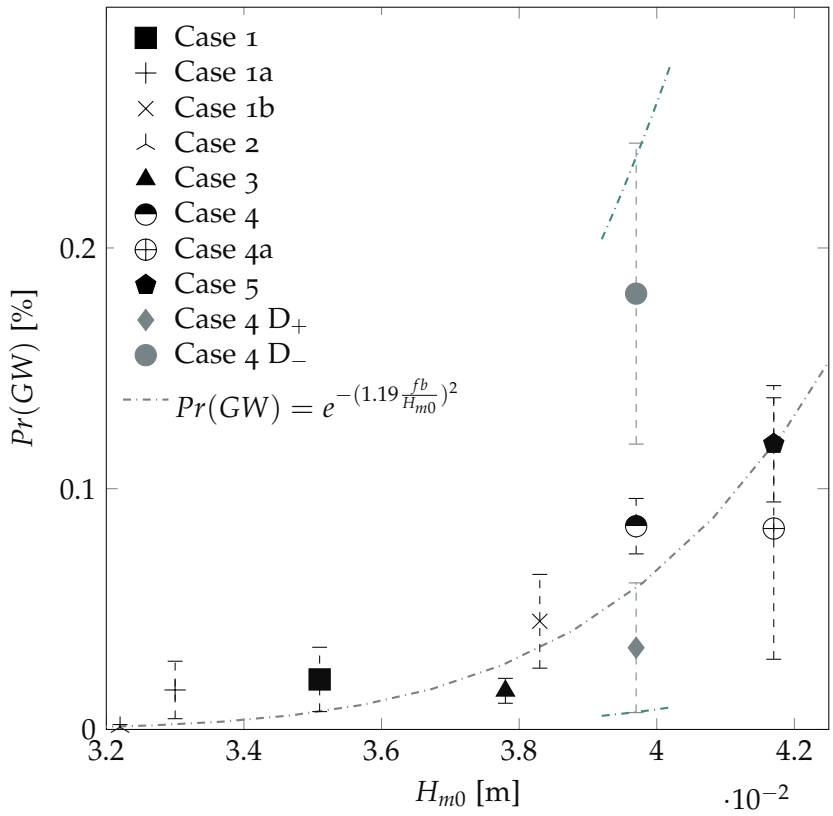

Figure 3.17: $Pr(GW)$ as a function of H_{m0} shown for all cases, as well as the fitted relation based on Koosheh, Etemad-Shahidi, Cartwright *et al.* [124] (dash-dotted). Grey indicates different drafts and shorter lines of fit are the fits for those different drafts. Dashed lines indicate 95% confidence interval

Table 3.5: Comparing the methods for estimating $Pr(GW)$ proposed in the previous paragraphs

	Experiments	$Pr(GW) = \frac{Pr(EX)}{2.17}$		$Pr(GW) = e^{-(1.19\frac{fb}{H_{m0}})^2}$	
	$Pr(GW)$	$Pr(GW)$	error [%]	$Pr(GW)$	error [%]
1	0.00021	0.00026	23	0.00034	62
1a	0.00016	0.00015	-7.8	0.00017	4.4
1b	0.00045	0.00052	15	0.00121	169
1c	0	0.00002	-	0	-
2	0.00001	0.00001	38	0.00007	686
3	0.00016	0.00014	-13	0.00101	530
4	0.00084	0.00044	-48	0.00193	128
4a	0.00083	0.00087	2.4	0.00346	306
5	0.00119	0.00104	-12	0.00346	191
4 D$_+$	0.00034	0.00036	7.5	0.00899	2547
4 D$_-$	0.00181	0.00086	-53	0.00053	-71

compared based on the error between the actual and estimated $Pr(GW)$ in table 3.5.

The method based on $Pr(EX)$ performs better than the method based on H_{m0}. However, the results of the method based on $Pr(EX)$ depend on how well $Pr(EX)$ is estimated. The values shown in table 3.5 are based on the true value of $Pr(EX)$ and the relation is also fitted for, thus resulting in the most optimal results. The estimation method for $Pr(GW)$ based on H_{m0} uses a few input parameters which will be known when engineering a vessel, making it a practical method, but errors are larger than those of the method based on $Pr(EX)$.

3.4 CONCLUSIONS

A method is proposed to quantify the probability of green water and the expected pressures following a green water impact during a ship's operation by finding their distributions. By conducting experiments in a wave-current tank a large green water data set representing 1945 hours of continuous sailing at full scale is obtained. In the experiments the wave spectrum, forward speed and draft were varied.

The distribution of the maximum pressures is identified as the Fréchet distribution, an extreme value distribution. A difference in skew between the theoretical distribution and the data indicates that the Fréchet distribution gives conservative estimations for large pressures. The time between the occurrence of green water is exponentially distributed for all different tested cases, indicating that when a green water impact occurs is independent of the time since the last impact. The same is true for deck exceedance impacts.

An equation is formulated to calculate the probability of a limit pressure being exceeded during a ship's operation. The sailing time, probability of green water and parameters of the Fréchet distribution for maximum pressures are taken as input.

Two methods to calculate the probability of green water occurring are presented. The first method uses the linear relation between the probability of deck exceedance and the probability of green water. The second method calculates the probability of green water occurrence based on the freeboard and significant wave height. The first method gives estimations that are closer to the experimental data while the second is more practical from an engineering perspective.

4

THE EFFECT OF SURGE ON EXTREME WAVE IMPACTS AND AN INSIGHT INTO CLUSTERING

This chapter is based on:

[127] A. D. Boon and P. R. Wellens, 'The effect of surge on extreme wave impacts and an insight into clustering', *Journal of Ship Research*, 2024. DOI: 10.5957/JOSR.07230022

4.1 INTRODUCTION

To be able to design for extreme wave impacts the pressures they induce and how often they occur have to be known. Green water and slamming are complex and their occurrence and impacts depend on parameters like the ships geometry, forward velocity, motions and waves [18], [20], [23]. As green water and slamming are complex problems the probability and pressures of impacts are normally found by modelling a ship, either experimentally or with CFD simulations. In modelling the problem is simplified by limiting the parameters and reducing the degrees of freedom to save costs and make the modelling possible.

Most experimental extreme wave loading research reduces the degrees of freedom by restricting surge [20], [22], [28], [67], [87], [92], [93], [101], [128], [129]. Exceptions are research with full-scale ships [104], [130] and free running experiments [32], [90], [100]. However, the role of surge on extreme wave loading impacts is not specifically investigated in these full-scale and free running studies. Literature shows that both green water and slamming impacts occur when a large forward pitch motion occurs out of phase with a wave [56], [62]. The phase difference between the pitch and waves will be influenced by surge. Surge is thus expected to influence green water and slamming. The goal of this chapter is to identify what the influence of surge is on green water and slamming impacts.

4.2 METHODOLOGY

To research extreme wave loading impacts, which do not occur often, long testing times are needed. Data for a sailing ship in head waves free to heave, pitch and, for half the cases, surge was collected for six different test conditions over a total of 42 hours of experimental data. The data can be downloaded from doi.org/10.4121/15f0d739-b84c-48f3-879a-68c08f068ab3 [1].

4.2.1 *Experiments*

The model experiments were carried out at the wave-current tank described in chapter 2. A 3D printed S175 model without forecastle at a Froude scaling of 1:130 was used for the experiments. The model was made smooth and watertight with multiple rounds of sanding and epoxy. The dimensions are given in table 4.1. The vertical centre of gravity and radius of gyration was found with swing tests and the natural periods with free-decay tests. The ship model was placed 2.79 m from the wavemaker and 0.93 m from the side of the tank.

The suspension of the model allowed for free heave, pitch and surge motion as is shown in figure 4.1. The model was suspended through a hinge in the centre of gravity. Two vertical linear guides, called the heave rods, were attached to this hinge, allowing for pitch and heave but limiting sway. The two vertical linear guides went through the surge carriage. This surge carriage was mounted to horizontal rails, allowing for the model to surge with limited resistance. In this setup, the mass of the pitching system (mass model) differs from the mass of the heaving system (mass model + mass heave rods), which again differs from the mass of the surging system (mass model + mass heave rods + mass surge carriage). The difference in mass for the surging and pitching system is not representative for real-worlds scenario's. The sway motions were not perfectly restricted and some motion with a maximum of 0.5 degrees was allowed. Soft springs with a spring stiffness of 3 N/m were attached to each side of the surge carriage to ensure in the free-to-surge cases the model would not move off the surge rail. The spring stiffness was chosen so that the natural surge period was at least ten times the wave encounter frequency. To restrict surge motions the surge carriage could be clamped so surge was restricted but the model was still free to heave and pitch.

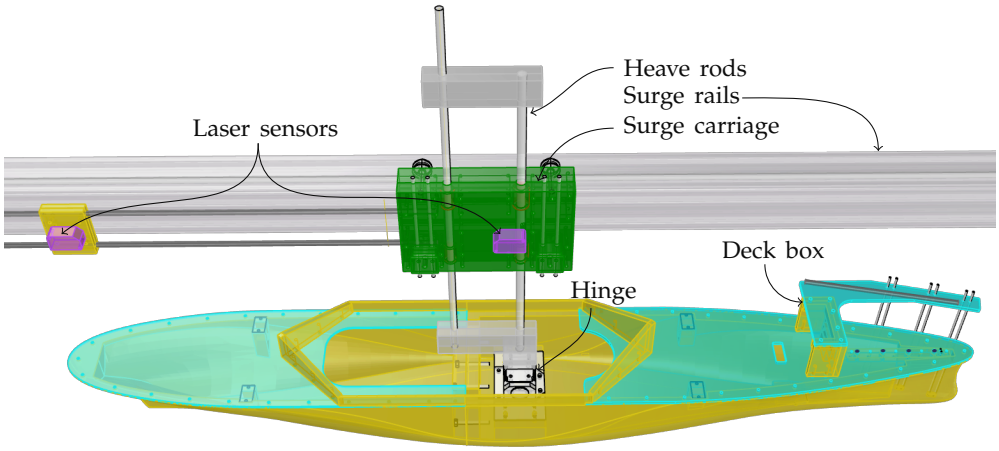

Figure 4.1: Test setup

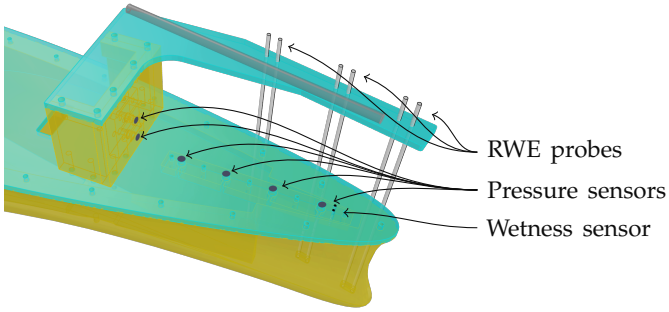

Figure 4.2: Measuring equipment on bow

4.2.2 *Measurement equipment*

Various measuring devices were placed in the setup through which data was acquired at 1000 Hz. Figure 4.2 shows the location of the measuring equipment on the bow. Three resistance type relative wave elevation (RWE) probes were used. The distance between the probes is 0.06 m and their orientation is vertical at 0.01 m to the side of the deck. To measure the pressure six GE druck PDCR 42 type sensors with a range of up to 350 kPa are used. Four were placed on the centre line of the model on the deck with 0.04 m between them and two were placed on the deck box at a height of 0.01 and 0.03 m. The signal from the 3rd pressure sensor (0.14 m from the stem) was noisy and thus not used. The heave and pitch of the vessel were measured using Panasonic HG-C1400 laser distance sensors at the centre of bouyancy and 0.645 m to the back of the vessel. Both sensors were attached to the surge carriage. The

Table 4.1: Dimensions and parameters of the used model

Length between perpendiculars	1.346 m
Breadth moulded	0.195 m
Draft	0.076 m
Freeboard (fb)	0.047 m
Mass model	8.76 kg
Mass heave rods	2.26 kg
Mass surge carriage	1.14 kg
Vertical centre of gravity	0.067 m
Vertical centre of buoyancy	0.040 m
Longitudinal centre of buoyancy	0.653 m
The radius of gyration in pitch	0.359 m
Trim angle	0 degrees
Natural heave period in water	0.767 s
Natural pitch period in water	0.625 s
Natural surge period in water	11 s
Dimensions deck box (length x width x height)	0.048x0.10x0.075 m
Distance to deck box from stem	0.22 m
Location RWE probe 1 from stem	0.025 m
Location pressure sensor 1 from stem	0.06 m

surge was measured with the Honeywell 940-R4Y-RD-ICO acoustic sensor measuring the horizontal location of the surge carriage. A load-cell was placed between the hinge and the heave rod to measure the resistance. A wetness sensor was placed 0.005 m before the front pressure sensor to measure water on deck but during the experiments water stayed around this sensor after impacts so the data was not used. A resistance type waveprobe was placed at 0.863 m from the side of the tank and 2.79 m from the wave maker. All data was filtered with a 3rd order low pass filter at 40 Hz to remove the noise from the electrical net.

Two webcams were used to acquire footage of all experiments, one placed to the side of the setup and one above the setup. All data, footage, 3D print files and laser cut files are available on doi.org/10.4121/15f0d739-b84c-48f3-879a-68c08f068ab3 [1].

Table 4.2: Wave spectra at model scale

T_p **[s]**	H_{m0} **[m]**	s_{op} **[-]**	U **[m/s]**	Froude number **[-]**	t_{test} **[hours]**
0.972	0.048	0.042	0.25	0.07	7
0.972	0.041	0.037	0.25	0.07	7
0.972	0.033	0.030	0.25	0.07	7

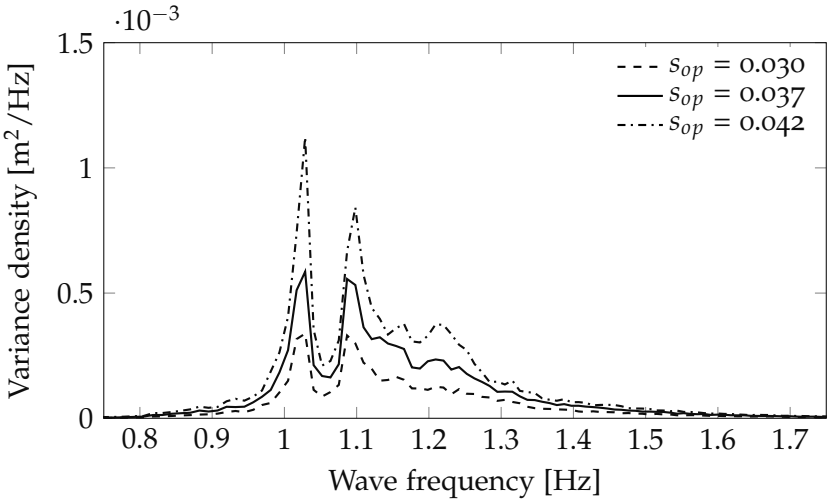

Figure 4.3: Wave spectra with the different spectral steepnesses

4.2.3 *Test conditions*

The tests were conducted in six different test conditions: with and without surge and with different spectral steepness (s_{op}) of 0.030, 0.037 and 0.042. The spectral steepness is calculated as $s_{op} = 2\pi \frac{H_{m0}}{g \cdot T_{m_{02}}^2}$ where H_{m0} is the significant wave height, $T_{m_{02}}$ the mean wave period and g is the gravitational acceleration. Most incidents with extreme wave impacts on ships occur for $s_{op} > 0.035$ so the values around this spectral steepness were tested [131]. Representations of the sea states were generated with the wavemaker following a 7-hour long continuous wave file. The wave files were created by calculating the amplitudes of the wave components in the sea state, with a frequency resolution below 0.1 mHz to prevent repetition in the desired time span, and adding these wave components together with a random phase. Figure 4.3 shows the energy distribution of the wave spectra used and table 4.2 gives the main parameters of the wave spectra.

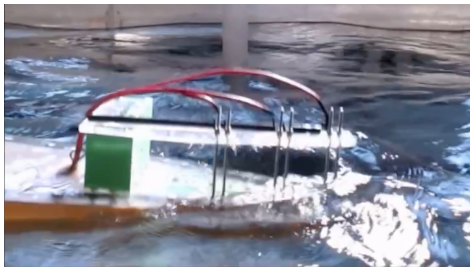

(a) Before green water: water exceeds deck level

(b) Before slamming: water exceeds deck level

(c) During green water: water impacts on deck

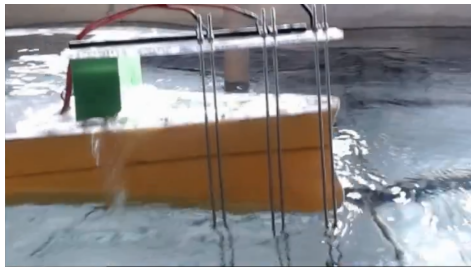

(d) Before slamming: keel out of water

(e) During green water: water impacts on deck box

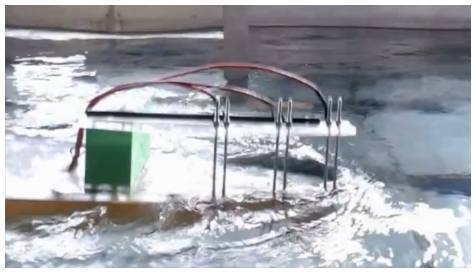

(f) After slamming: water exceeds deck level

Figure 4.4: Stills from a green water impact on left side (figures a, c and e) and slamming impact on right side (figures b, d and f). Chronological order from top to bottom

4.2.4 *Impact identification*

For slamming bottom slamming impacts were considered, where the ship impacts on the water. Slamming impacts were identified using the Ochi slamming kinematic criterion [23]. The criterion consists of: 1) the bow is out of the water (the measured relative wave elevation is lower than the draft) and 2) the relative velocity is above the limit value. The limit value is 0.33 m/s at the scale of the experiments. A total of 83 slamming impacts were found. No slamming impacts were found for $s_{op} = 0.030$.

For green water, where water impacts on the ship, a distinction between deck impacts and deck box impacts was made. During a green water impact the water always impacts on deck, but for only some green water impacts did the water also flow far enough to impact on the deck box. Two criteria are used for green water identification. The first criterion is that a pressure larger than 50 Pa was measured on the most forward pressure sensor. The second criterion is that the impact coincided with a continuous flow of water on deck. The second criterion was ensured by visually checking all the initially identified green water impacts. To identify the deck box impacts a lower limit value of 20 Pa on the bottom pressure sensor on the deck box was used. In total 4703 green water impacts are identified, of which 1543 impacts also impacted the deck box.

4.3 RESULTS

With the experiments, a large data set of extreme wave loading impacts is obtained for a ship model with forward velocity in irregular waves, with and without surge. The effect of surge on the probability of impacts and the pressures is analyzed. As the effect of surge is of interest, the surge is quantified in table 4.3 for context. This table shows the standard deviation of the surge throughout the experiments, as well as the average surge measured during green water and slamming impacts. The surge motions during green water and slamming impacts in table 4.3 are between 3.6 and 1.9 times smaller than the extreme surge motions reported in Dhavalikar and Negi [132] for the S175 ship in a similar sea state.

4.3.1 *Probabilities and pressures*

The probability of green water on deck is shown in figure 4.5a. In this figure $Pr(GW)$ indicates the probability of green water on deck, $Pr(GWbox)$ the probability of green water that caused an impact on the deck box and $Pr(SL)$

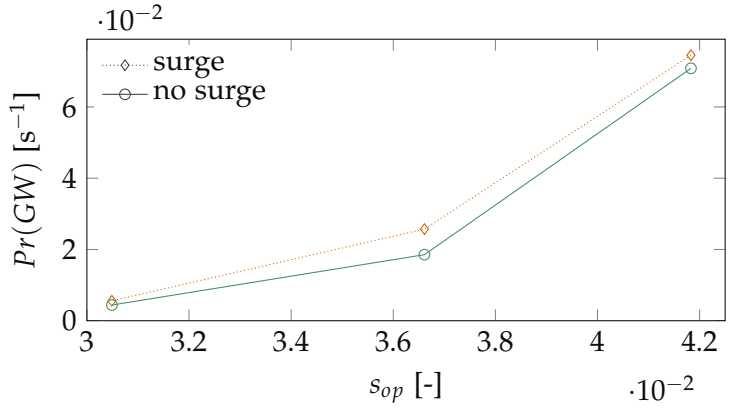

(a) Surge increases the probability of green water impacts ($Pr(GW)$)

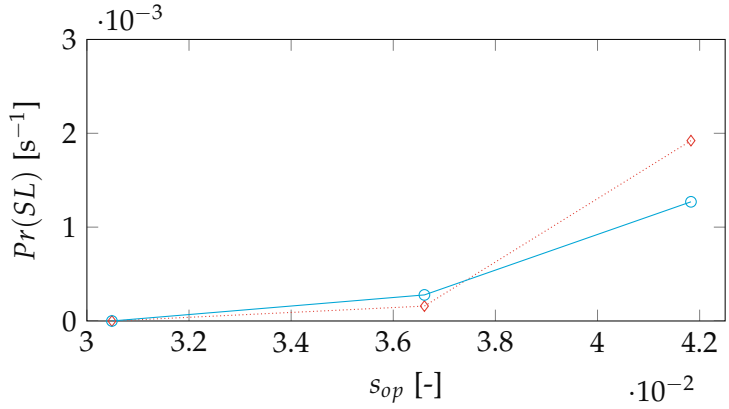

(b) The influence of surge on the probability of slamming ($Pr(SL)$) is not consistent for different spectral steepnesses (s_{op})

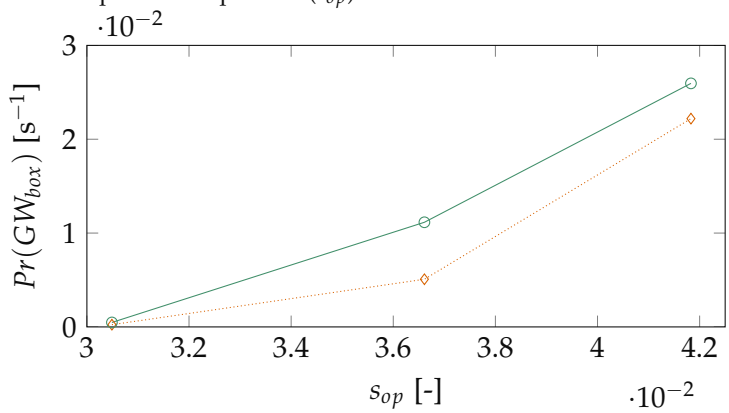

(c) Surge reduces the probability of impact on the deck box ($Pr(GWbox)$)

Figure 4.5: Effect of surge on the probability of green water and slamming

Table 4.3: Surge motions

s_{op} [-]	Standard deviation [m]	Average during green water [m]	Average during slamming [m]
0.042	0.0036	0.020	-
0.037	0.0041	0.020	0.019
0.030	0.0048	0.021	0.023

the probability of slamming. The definitions of the event types are given in section 4.2.4.

The probability of green water is higher for cases where the model can surge compared to no-surge cases. An effect of the surge on the probability of green water was expected as surge will change the phase between pitch and wave. Apparently, the phase shift introduced by surge increases the number of green water impacts. No clear conclusions can be made for the influence of surge on the probability of slamming impacts, shown in figure 4.5b. However, for the largest spectral steepness, the probability of slamming is also larger for surge cases compared to no-surge cases.

The reverse is true for deck box impacts: the probability of impacts on the deck box is larger if the model is restricted in surge, shown in figure 4.5c. The water has to travel over the bow to the deck box for green water to impact the deck box. The larger probability of deck box impacts for no-surge cases thus indicates that large impacts are more likely when the model is restricted in surge. A possible reason is that part of the energy of the water at the bow is transferred to decrease the forward velocity of the ship through surge, resulting in less energy in the impacting water and water not travelling as far over the bow when the model can surge.

If green water impacts are indeed larger for the no-surge cases because the surge motion absorbs energy, larger pressures should occur for the no-surge cases compared to surge cases. Figure 4.6a shows that restricting surge indeed leads on average to large impact pressures for deck impacts. The impacts are larger on deck for both the maximum pressure measured on deck during an impact (p_{max}) as for the median of the maximum pressures measured by each pressure sensor on deck (P_{max}) for the no-surge case.

However, figure 4.6b shows the reverse for the pressures on the deck box: the pressures on the deck box are larger when the model is free to surge. On average the peak impact pressure on the deck box occurred 0.32 seconds after the peak impact on the deck was measured. With the time difference, a theory was that 0.32 seconds after the initial impact the model starts surging

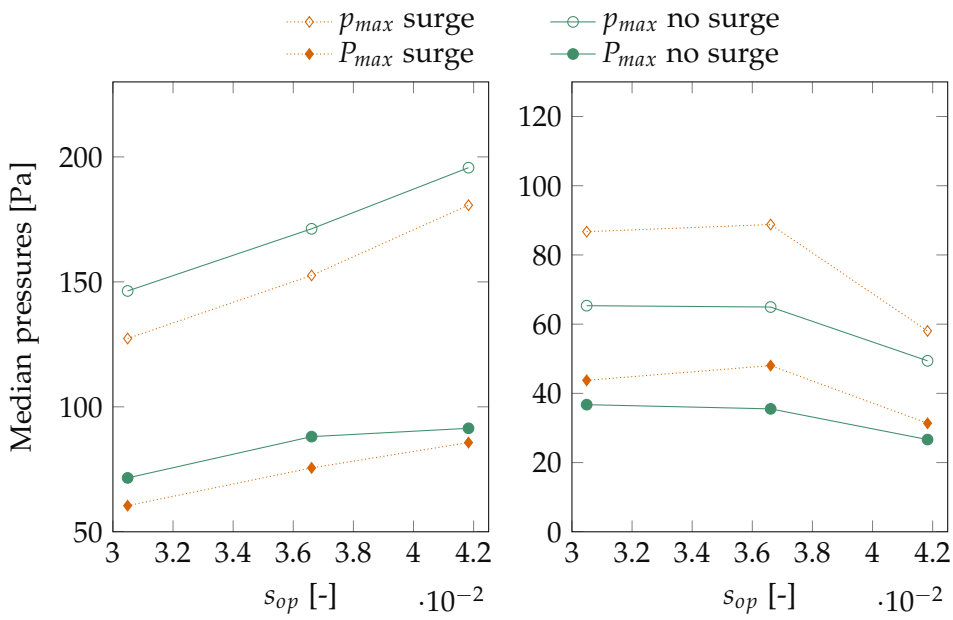

(a) Deck pressures

(b) Deck box pressures

Figure 4.6: Larger maximum (p_{max}) and median (P_{max}) impact pressures on deck were measured for restricted surge compared to cases where the model was free to surge. Similar impact pressures on the deck box were found with and without surge

forward on the wave, causing a large relative velocity to the water, increasing the pressure on the deck box. However, no surge velocities were found large enough to cause the difference in impact pressures shown in figure 4.6b. Further research is required to explain the larger impact pressures on the deck box for surge cases compared to no-surge cases.

Figures 4.5 and 4.6 show that all the probabilities and pressures increase with an increase in spectral steepness, except for the deck box impact pressures. The increase in the probability of slamming and green water and pressures during these impacts is expected as a larger spectral steepness at a constant peak period and spectral shape indicates more energy in the spectrum. The median deck box pressures are constant up to s_{op} =0.037 and then decrease for s_{op} =0.042. For s_{op} =0.042 the probability of impacts occurring is large, meaning they follow each other up quickly. A possible cause for the decrease in deck box pressures is the interaction of impacts with water on deck from the previous impact.

Table 4.4: The fitted Fréchet and exponential distribution are quantified with the shape, scale and location parameters. The quality of fit of the distributions to the data is tested, with p-value > 0.05 as the limit value. The p-values show that the Fréchet distribution fits the pressures, but the exponential distribution does not fit the time between events

			surge			no surge		
		s_{op}	0.030	0.037	0.042	0.030	0.037	0.042
Green water Deck	p_{max}	**p-value**	**0.53**	**0.33**	**0.48**	**0.95**	**0.34**	**0.11**
		shape	9.04	2.10	3.76	3.65	1.38	3.83
		scale	435	150	289	211	129	285
		location	-328	-25.8	-134	-88.4	10.6	-115
	P_{max}	**p-value**	**0.60**	**0.81**	**0.78**	**0.81**	**0.09**	**0.26**
		shape	5.99	1.80	3.25	2.59	1.27	3.39
		scale	131	67.6	123	67.0	61.8	125
		location	-82.7	-67.9	-50.5	-96.5	8.13	-46.9
	λ	**p-value**	**0.01**	$\mathbf{9e^{-30}}$	$\mathbf{4e^{-137}}$	**0.02**	$\mathbf{3e^{-23}}$	$\mathbf{2e^{-174}}$
		location	0.57	0.60	0.58	0.31	0.48	0.55
		scale	177	38.1	15.0	207	55.0	13.6
Green water Box	p_{max}	**p-value**	**0.98**	**0.57**	**0.69**	**0.85**	**0.35**	**0.57**
		shape	1.18	1.46	1.39	1.10	0.90	1.57
		scale	57.6	70.2	37.1	47.3	31.0	30.1
		location	0.49	-3.33	8.20	5.35	15.0	9.64
	P_{max}	**p-value**	**0.98**	**0.79**	**0.74**	**0.89**	**0.50**	**0.36**
		shape	1.02	1.42	1.34	1.11	1.07	1.51
		scale	22.5	36.5	19.1	24.1	21.9	15.6
		location	6.21	-0.97	5.74	4.49	5.71	6.48
	λ	**p-value**	**0.78**	$\mathbf{2e^{-6}}$	$\mathbf{3e^{-25}}$	**0.32**	$\mathbf{1e^{-5}}$	$\mathbf{1e^{-41}}$
		location	2387	0.64	0.62	575	0.61	0.58
		scale	4179	224	51.1	2546	153	37.9
Slamming	λ	**p-value**	**-**	**0.80**	**0.02**	**-**	**0.61**	**0.19**
		location	-	3980	0.70	-	270	0.67
		scale	-	1433	510	-	2480	745

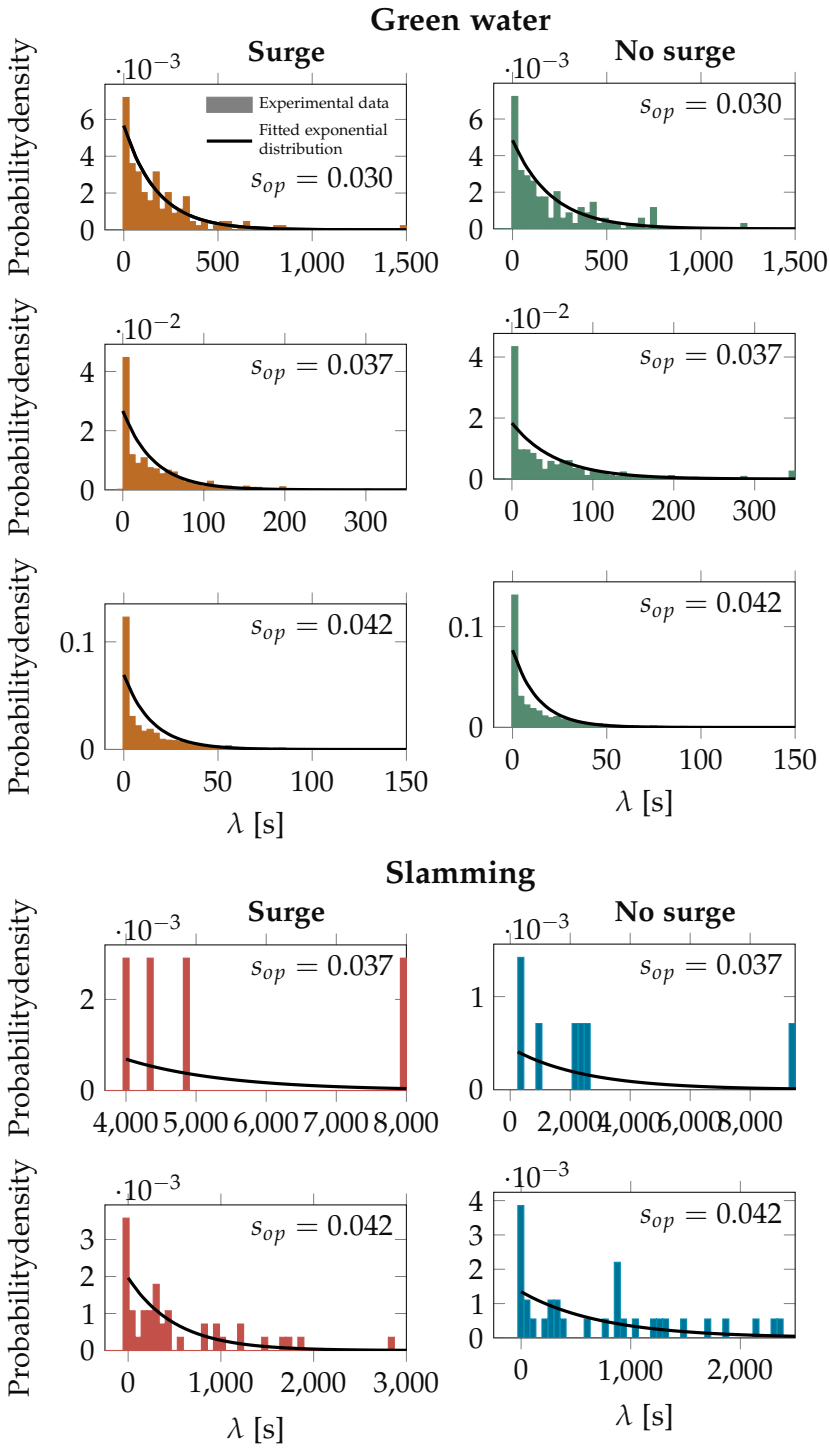

Figure 4.7: Density histograms of time between events (λ) show zero-inflation caused by clustering. The fitted exponential distribution does not fit the data due to the zero-inflation

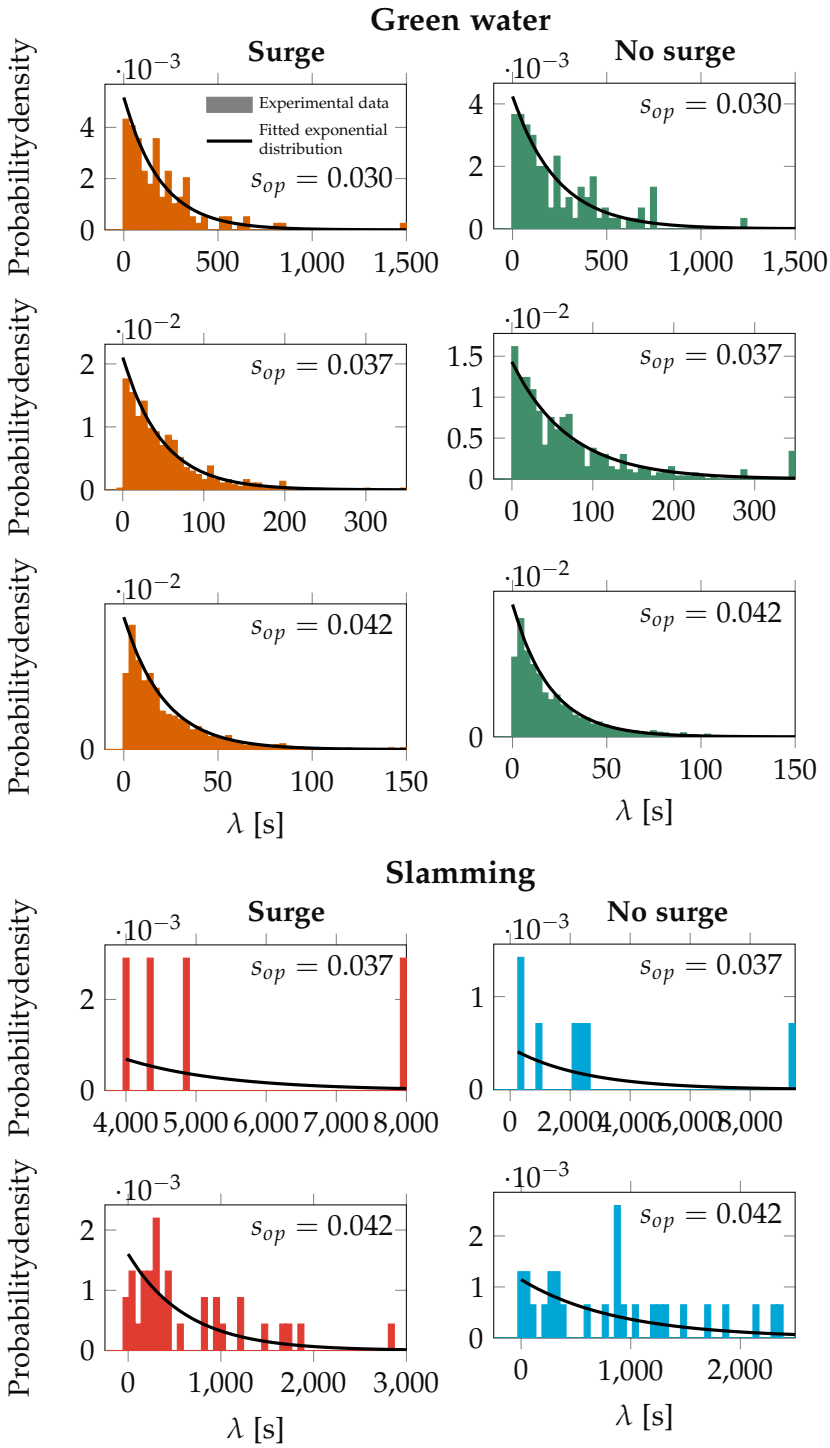

Figure 4.8: Density histograms of time between events (λ) with clustering removed. With the clusters removed the fitted exponential distribution does fit the data

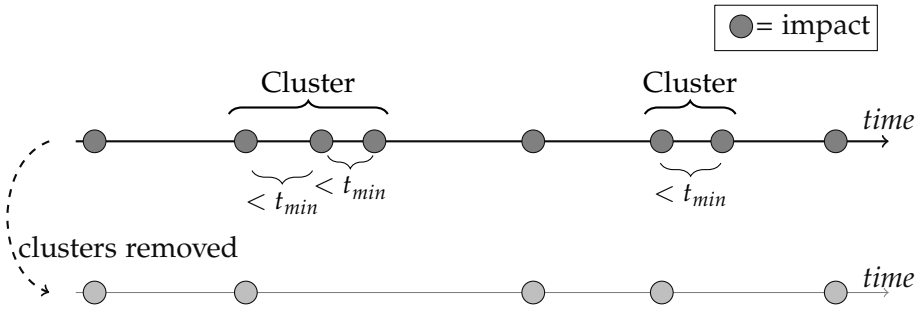

Figure 4.9: Identification of clusters by using t_{min} which is based on the natural pitch frequency

4.3.2 *Statistical distributions*

After looking at the median of the pressures and probabilities per case in the previous paragraph the overall statistical distributions are looked at. Previous literature shows that for green water impacts the pressures are Fréchet distributed [113]. For slamming and green water the time between impacts (λ) has been shown to be exponentially distributed [23], [53], [106], [113].

The applicability of the distributions from the literature on the new data is checked. To be able to check, first the Fréchet and exponential distributions are fitted to the data of the different tests using least squares to find the optimal parameters. The quality of fit for the fitted distribution is then checked using the Kolmogorov-Smirnov test. If the p-value of the Kolmogorov-Smirnov test is above a limit value, the statistical distribution can describe the data. The limit of 0.05 is chosen, but the less strict limit of 0.01 is also commonly used. The results are shown in table 4.4. The Fréchet distribution fits the distribution of the pressures for the deck and deck box impacts.

The exponential distribution does not fit the new data. For none of the cases does the exponential distribution fit the distribution of time between green water deck impacts, and the exponential distribution does not fit the times between green water deck box impacts and slamming impacts for the large probability cases. Boon and Wellens [113] did show that the times between green water impacts follows the exponential distribution and thus concluded that impacts occur randomly and independently. So is the previous chapter wrong or is there a problem with the experimental data? To visually inspect why the impacts do not follow the exponential distribution, the distributions of the time between impacts are plotted in figure 4.7 for green water deck and slamming impacts.

The figures show an excess of the minimum value for all the cases for which the exponential distribution does not fit. Data sets that are expected to be independent and random but have an excess of the minimum value are zero-inflated [133]. Zero-inflated data can be a result of combining two distributions, like an exponential distribution and a distribution that generates the minimum value. The minimum value, in our case the shortest time between impacts, is captured in the location parameter shown in table 4.4. Zero-inflation occurs mostly for a time between impacts of 0.48 to 0.7 seconds. This range matches the natural period of the pitch.

In slamming literature a possible physical phenomenon that can generate the minimum value is found: clustering [25], [59], [60]. For clustering grouping of impacts causes multiple impacts to occur after one another, resulting in a mechanism in the system that causes the assumption of impacts occurring independently to be invalid.

To test if clustering is the cause of the zero-inflation for green water and slamming, the impacts that follow an impact are removed from the data. Removing the clusters should remove the distribution that generates the minimum value from the set and leave us with the originally expected exponential distribution.

4.3.3 *Clusters*

Clusters are removed from the data set by ignoring impacts that occur within the minimum time (t_{min}), visualized in figure 4.9. t_{min} is set to be larger than the natural pitch period (0.625 s), as zero-inflation was found to occur around this period. t_{min} is also chosen larger than the peak wave encounter period (0.81 s) as for slamming and green water literature shows that impacts occur when a large forward pitch motion occurs out of phase with a wave [56], [62]. t_{min} is set at 1 second.

With the clusters removed from the data the exponential distribution is now found to fit the data. The fit of the data with the clusters removed is shown in table 4.5 and visualized in figure 4.8. The exception is the steepest spectral steepness as the p-value is below 0.05. The probability of impacts occurring is large for these cases ($Pr(GW) > 0.06s^{-1}$), thus eliminating impacts that follow each other also eliminates impacts that are independent and occur close together. Figure 4.8 indeed shows a decrease in the data at the lowest value, showing that the low p-value is caused by eliminating impacts that independently follow each other. For slamming with and without surge no clustering occurred for $s_{op} = 0.037$, thus slamming impacts only start cluster-

Table 4.5: After removing clusters from data evaluating the quality of fit of the fitted exponential distribution. The exponential distribution is quantified with the location and scale parameter

			surge			no surge		
		s_{op}	0.030	0.037	0.042	0.030	0.037	0.042
Green water	λ	**p-value**	**0.89**	**0.83**	**0.01**	**0.96**	**0.09**	**$4e^{-4}$**
Deck		location	1.50	1.35	1.37	1.08	1.04	1.36
		scale	195	48.9	21.7	237	70.9	20.1
Green water	λ	**p-value**	**0.78**	**0.50**	**0.20**	**0.32**	**0.05**	**0.08**
Box		location	2387	2.27	1.36	575	1.47	1.37
		scale	54179	277	66.5	2546	178	51.1
Slamming	λ	**p-value**	**-**	**0.80**	**0.65**	**-**	**0.61**	**0.42**
		location	-	3980	1.59	-	270	2.33
		scale	-	1433	626	-	2480	877

ing for $Pr(SL) > 1.6e^{-4}s^{-1}$. Even above $Pr(SL) > 1.6e^{-4}s^{-1}$ the clustering for slamming impacts is limited, as the p-value is 0.02.

In the new data green water impacts are found to cluster, but Boon and Wellens [113] did not find clustering of green water impacts. For slamming not all cases are found to cluster, while most slamming literature did find clustering [25], [59], [60]. In our data slamming impacts only cluster above a certain probability of occurrence, so possibly green water impacts also only start clustering above a certain probability of occurrence. Figure 4.10 compares the work in this chapter to the literature. Note that all the work in figure 4.10 was for different ships in different sea states and different forward velocities, thus the exact values of when clustering starts can vary. In the figure, the grey tones indicate the areas in which clustering occurs based on the quality of fit before clusters are removed from the data, quantified by the p-values in table 4.4. The used p-value limit of 0.05 is a strict limit, as a p-value above 0.01 is also often considered acceptable and as such cases with a p-value between 0.01 and 0.05 are placed in a transition region.

Figure 4.10 shows that even though the previous and present work do not agree on whether impacts cluster, neither is wrong, they just investigate different ranges. For the low range of probability of occurrence tested in Boon and Wellens [113] indeed, no clustering is expected, while for the high probability of occurrence in Dessi and Ciappi [25] clustering is expected. Exceptions are Ochi and Motter [23] and Ferro and Mansour [106] which do

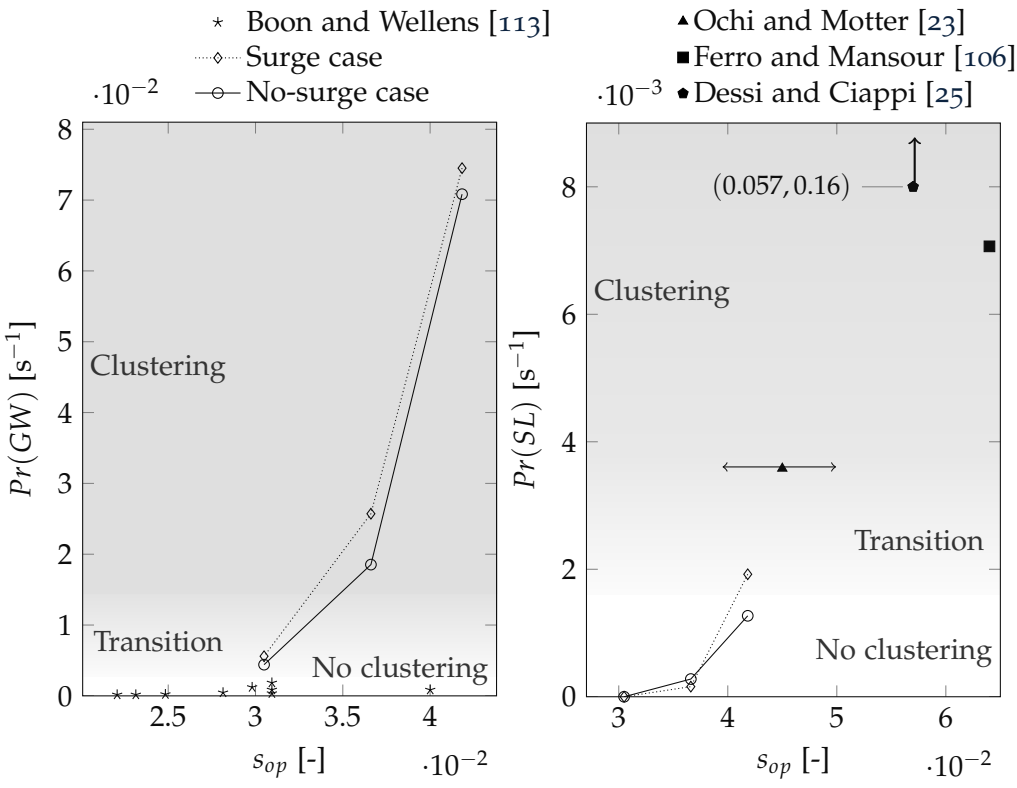

(a) Green water

(b) Slamming

Figure 4.10: The probability of green water and slamming from both the present experiments as well as literature set out. Gray background visualizes the range where zero-inflation occurs and thus when clustering occurs

not mention clustering. The distributions shown in their work do show zero-inflation, as is expected from figure 4.10. For Ochi and Motter [23] no spectral steepness is known but was estimated based on the Beaufort 9 condition.

4.3.3.1 *Difference between clusters and single impacts*

After identifying clustering and when impacts cluster, the next step is to look into what the influence of clustering is and why impacts cluster. First, the pressures on deck found for the clusters and single impacts are compared in figure 4.11.

For all tested cases the median pressures found during clusters are larger than the median pressures found during single impacts. For surge cases pressures caused by impacts that occurred during clusters induced on average 61% higher pressures compared to the single impacts. For no-surge cases

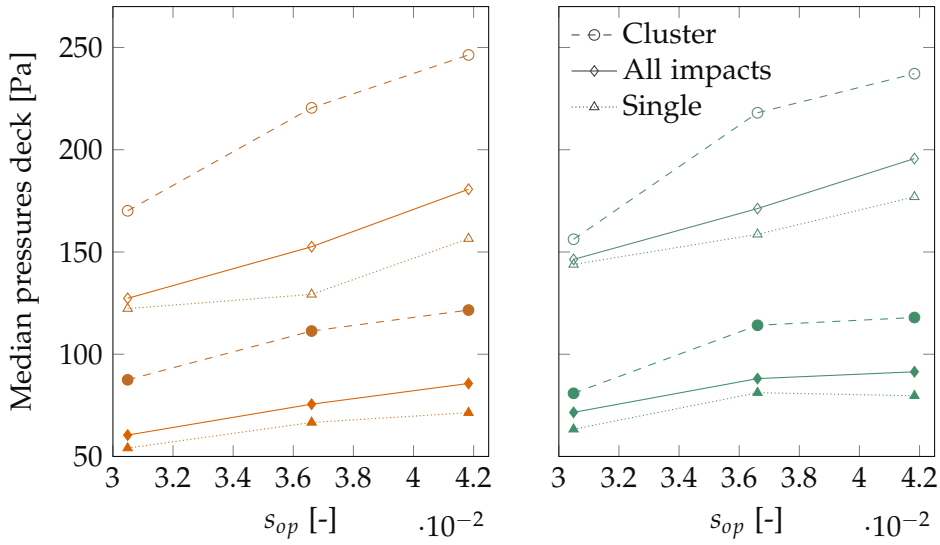

(a) Surge

(b) No surge

Figure 4.11: On average the pressures on deck for green water events in a cluster are larger than the pressures due to single events. The solid markers indicate the median pressures (P_{max}) and the open markers the maximum (p_{max})

impacts in clusters induced 33% higher pressures on average. The overall pressures found for no-surge cases are larger, but the pressures caused by clusters are actually larger for surge cases. The complexity of impacts interacting in clusters combined with surge motion is a possible reason for the larger difference between pressures in clusters and single impacts for surge cases. More research is needed to be able to explain the differences.

Within clusters, impacts occur at intervals around the natural pitch period, as is discussed in the previous section. From looking at footage of clusters during the experiments the hypothesis is developed that clusters are caused by large pitch motions. A pitch motion out of phase with the waves causes an impact, and the theory is that in the built-up to a large pitch or as the large pitch motion damps out, there is a high probability of another impact occurring as the pitch amplitude is still large. Clustering and the probability of impacts correlate in figure 4.10 because if a sea state causes limited pitch motions, the probability of an impact is small, and the probability of a large enough pitch motion to cause multiple impacts is also small. For a sea state that causes large pitch motions the probability of an impact is high and the probability of a pitch motion large enough to cause a cluster is high, resulting in zero-inflation.

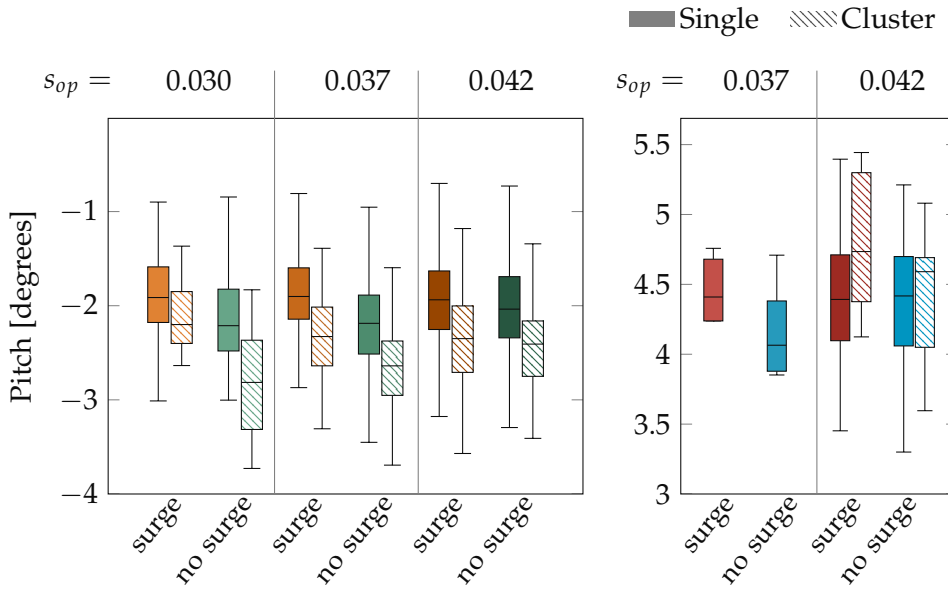

(a) Green water

(b) Slamming

Figure 4.12: The maximum pitch motion during clustered and single events are compared, showing on average larger pitch motions for clustered events than single events

If large pitch motions indeed cause the clustering of impacts we also expect pitch in a cluster to be on average larger than the pitches during single impacts. The pitches for single impacts are compared to the largest pitch in a cluster in figure 4.12. A large pitch is far forward for green water, thus negative, and a large pitch is far backward for slamming, thus positive.

The mean pitch motions in clusters are for both green water and slamming larger than the mean pitch motions during single impacts. The pitch motions in clusters are on average larger, but the spread overlaps. A large pitch motion makes it likely for an impact to occur in the periods before or after the large motion, but for an impact to occur not only the pitch has to be large, the wave also has to be out of phase with the pitch. In an irregular sea the waves can shift phases, causing a pitch motion initially out of phase with the wave to be in phase with the wave, resulting in large pitch motions that could have caused multiple impacts to become single impacts. Impacts can also independently occur together, resulting in clusters without large pitch motions. Overlap of pitch motions for clustered and single impacts is thus expected.

The results in figure 4.12 are in line with the theory that clusters are caused by large pitch motions building up or damping out. To further check the theory, the number of impacts in clusters is analyzed. If clusters indeed occur

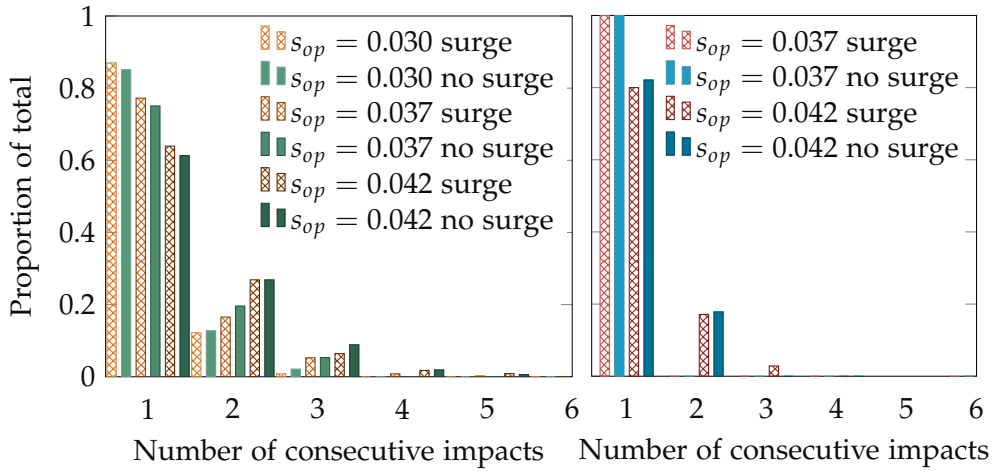

(a) Green water

(b) Slamming

Figure 4.13: Comparing the number of consecutive events for different spectral steepnesses. The average number of events per cluster is lower for a lower spectral steepness, with somewhat larger cluster sizes for test cases where surge was restricted

because of the pitch motions building up or damping out the average size of a cluster is expected to be small, as the amplitude of the pitch will quickly become too small to cause green water or slamming impacts.

Figure 4.13 shows that clusters indeed tend to be small. Only two green water clusters within the 4703 green water impacts are six impacts long. The longest cluster for slamming is only three impacts.

The steepness of the sea state influences the length of the clusters and the number of clusters, as for $s_{op} = 0.042$ about 40% of green water impacts and 20% of slamming impacts are part of a cluster, while for $s_{op} = 0.037$ about 25% of green water impacts and none of the slamming impacts are part of a cluster. A larger spectral steepness leads to larger pitch motions, which take longer to build up or damp, and thus also lead to larger clusters.

Surge also influences the number of clusters. No-surge cases lead to slightly more and longer clusters for green water compared to surge cases. Previously smaller impacts were found for surge cases as energy from the water is transferred to reduce the forward velocity of the ship. Following the same reasoning no-surge cases are expected to lead to larger pitch motions and thus lead to larger clusters, as was indeed found to be the case. It can be concluded that for both green water and slamming clustering of impacts is caused by large pitch motions.

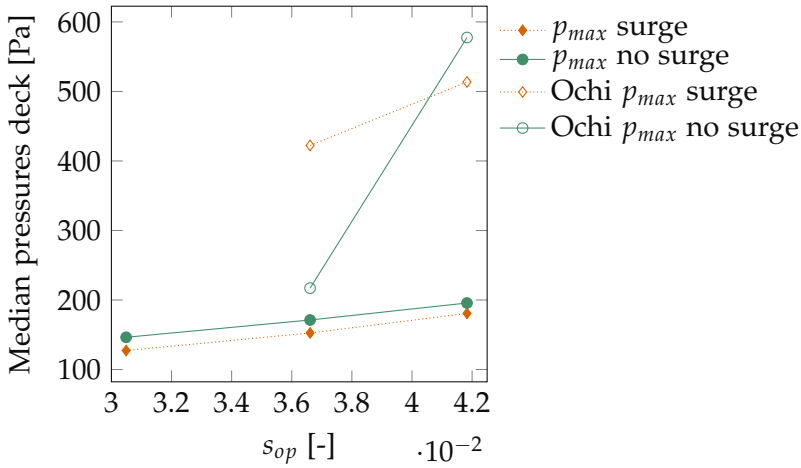

Figure 4.14: Identifying large pressure green water impacts with the Ochi slamming criterion

4.3.4 *Comparing green water and slamming*

All conclusions hold for both green water and slamming: surge has a similar influence on probabilities of green water and slamming and clustering start to occur at certain probabilities. The only difference between green water and slamming is quantitative. The used ship model can be the cause of the quantitative difference, as the freeboard is important for green water, and the draft for slamming. Also, damping of the large pitch motions can happen quicker for green water compared to slamming, as the waves break over deck, leading to a higher threshold for clustering.

Qualitatively, the underlying physics for the occurrence of impacts seems to be the same for green water and slamming. To test this theory the coincidence of green water and slamming is looked at. Slamming always occurred together with green water. For every slamming impact green water occurred within 0.36 seconds of a slamming impact, half of the natural period of pitch.

For every occurrence of slamming a green water event occurred before or after. This coincidence suggests that these two event types, often considered separately, are actually the outcomes of similar wave and ship motions. In the present work slamming has been identified with the Ochi criterion and no pressures have been measured for slamming. The argument could be made that the slamming events discussed in the present work are not actual slamming events but just large backward pitch motions followed by a large relative velocity. To investigate the theory that slamming and green water are similar we use the Ochi criterion to identify green water. The median

pressures on deck of green water events that occur before and after a slam are compared to the median pressures for all green water events, shown in figure 4.14. This comparison tests if the Ochi slamming criterion identifies green water that induces large pressures.

The Ochi criterion, developed for slamming, finds green water events with larger median pressures on deck than the average green water event. The events identified with the Ochi criterion were no larger than the average deck box impacts. Still, a tool designed to identify slamming finds large green water events, indicating that green water and slamming are closely related. Future work can look at how to use the similarity between green water and slamming to apply results from slamming research, which might be considered more developed than green water research, on green water.

4.4 CONCLUSION

The original goal of this research is to find the influence of surge on green water and slamming impacts. Long running experiments for a ship with forward velocity in head waves free to heave and pitch in irregular waves were repeated with and without surge.

The experimental results show that surge increases the probability of green water impacts on deck, but reduces the pressures on deck and the probability of green water impacts impacting the deck box.

While checking the distribution of green water and slamming a larger than expected probability of impacts following each other closely was found: clustering. Clustering of green water and slamming impacts only happens above a certain probability of occurrence. Impacts are found to cluster because of large pitch motions. A large pitch motion out of phase with the waves causes an impact, and as this large pitch motion builds up or damps out additional impacts are likely to occur, creating a cluster of impacts.

The pressures on deck during green water clusters are larger than during non-clustering impacts. For no-surge cases the pressures during clustered impacts are 33% higher than non-clustering impacts, while for surge cases the pressures were 61% higher. Restricting surge also slightly increases the number of green water clusters. The number of clusters and impacts per cluster increases for larger spectral steepness.

5

INFLUENCE OF DRAFT AND FREEBOARD AT BOW ON GREEN WATER

This chapter is based on:

[134] A. D. Boon and P. R. Wellens, 'How draft and freeboard affect green water: A probabilistic analysis of a large experimental dataset', *43th International Conference on Ocean, Offshore and Arctic Engineering*, ASME, 2024. DOI: 10.1115/OMAE2024-123640

5.1 INTRODUCTION

Green water on the bow of a ship is an active field of study as these rare impacts can endanger the ship and those on it. Not only the impacts themselves have been researched but also how different ship designs influence green water. Previous studies have examined the influence of bow shape on green water, with contributions from Buchner who looked at different breakwaters, bow fullness, hull shapes and flare angles [12], [18]. Greco looked at the effect of wave length and steepness, trim angle, bow flare angle and length over breadth ratio's [21]. Others have researched the effect of bow overhang [135], bow flare [14], [136], bow rake angle [137], bow rake angle and angle of entrance [138], bow rake angle of a tumblehome bow [139] and rectangular breakwaters [140]. However, most of these studies have primarily compared bow designs by analyzing the differences for a limited number of green water impacts.

Existing research has revealed mechanisms of green water loading, but falls short in comparing the probabilities of green water as designs are compared based on a limited number of green water impacts. Because of the limited number of green water impacts, the bows cannot be compared based on the tail of the probability distribution: the probability of the rarer but higher pressure impacts. The probability of high pressure impact is, however, a

critical parameter as the probability of a high pressure green water impact should be minimized in the design process.

In this chapter, we compare bow designs based on the probabilities of impacts and probability distributions of impact pressures, rather than focusing on the flow over the bow for a few impacts. This chapter includes variations in draft at the bow and freeboard. The effect of the draft at the bow on green water is a relatively unexplored aspect in existing literature, even though literature has shown that increased draft at the bow results in larger swell-up [141]. The swell-up is the increase in water level at the bow due to the effect of the presence of the ship in the waves and the ship's forward velocity. An increase will increase the relative wave elevation, which is known to correlate with green water occurrences and pressures [12], [27], [91]. Increasing the freeboard is known to reduce the probability of green water [21], [23], [29], [55]. However, it remains unclear whether this reduction affects all green water impacts uniformly or selectively eliminates some green water types while leaving the occurrence of other types unchanged.

This chapter will evaluate the effect of draft and freeboard on green water by considering their probabilities and the distribution of impact pressures. First, the effect of draft and freeboard on the probabilities and pressure are investigated. Secondly, the shape of the probability distributions of impact pressures is analyzed. Lastly, the pressure distributions for different drafts and freeboards are compared while accounting for the difference in probability of green water. The draft and freeboard both change the probability of green water, but the freeboard also changes the pressures. The difference in pressures turns out to not only be caused by the reduced number of green water impacts.

5.2 METHODOLOGY

As in this chapter the bow variations are compared based on the probabilities and probability distributions of impact pressures, a large number of green water impacts has to be collected for each bow. The test facility described in chapter 2 is used. The bows were systematically varied to not only investigate how to compare different designs but also to find the effect of added draft and freeboard. To be able to systematically vary the bows a bow type with a straight stem was used: the axe-bow. The axe-bow was placed on the S175 container ship. To stay true to the axe-bow design the ship length was elongated by 25%.

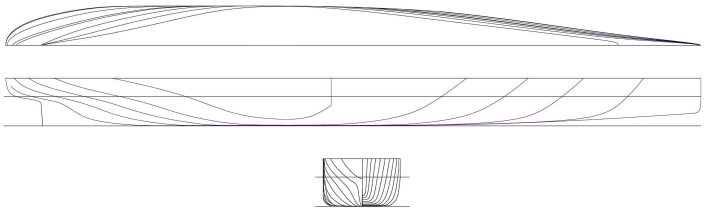

(a) Bow 1 fb-

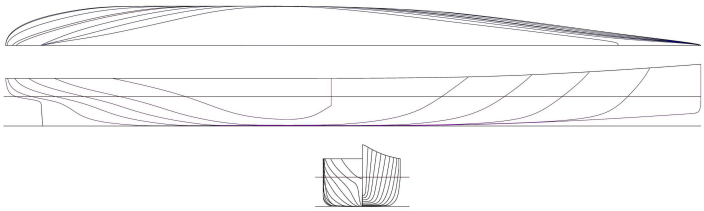

(b) Bow 1 fb+

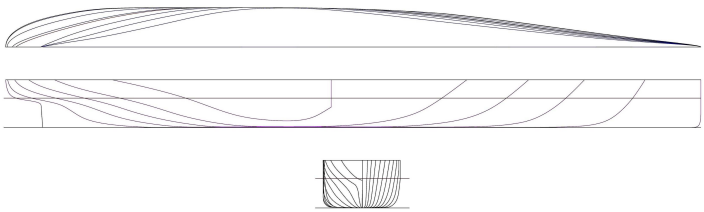

(c) Bow 2 fb-

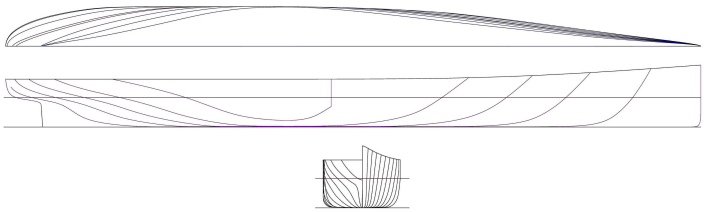

(d) Bow 2 fb+

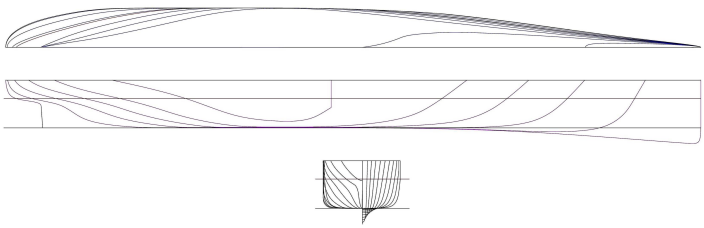

(e) Bow 3 fb-

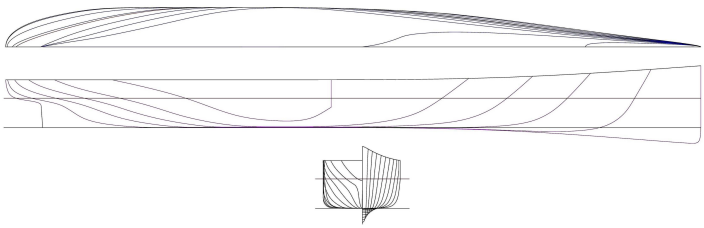

(f) Bow 3 fb+

Figure 5.1: Lines plans of the variations tested

Table 5.1: Parameters of the variations on test scale

	Bow 1		Bow 2		Bow 3	
	fb-	fb+	fb-	fb+	fb-	fb+
Length perpendiculars [m]	1.683		1.683		1.683	
Max. width on waterline [m]	0.195		0.195		0.195	
Depth at midship [m]	0.123		0.123		0.123	
Draft at stem [m]	0.041		0.073		0.105	
Freeboard at stem [m]	0.050	0.085	0.050	0.085	0.050	0.085
Underwater volume [l]	12.9		13.3		13.7	
Mass model+heave rod [kg]	12.9		13.3		13.7	
Mass heave rod [kg]	2.26		2.26		2.26	
Mass surge carriage [kg]	1.14		1.14		1.14	
Centre of bouyancy [m]	0.734		0.759		0.777	
Centre of gravity [m]	0.734		0.759		0.777	
Vertical centre of bouyancy [m]	0.041		0.040		0.038	
Vertical centre of gravity [m]	0.065	0.064	0.066	0.065	0.066	0.066
Water plane area [m^2]	0.220		0.221		0.221	
Centre of floatation [m]	0.718		0.721		0.722	
Pitch radius of gyration [m]	0.438	0.436	0.439	0.437	0.433	0.433

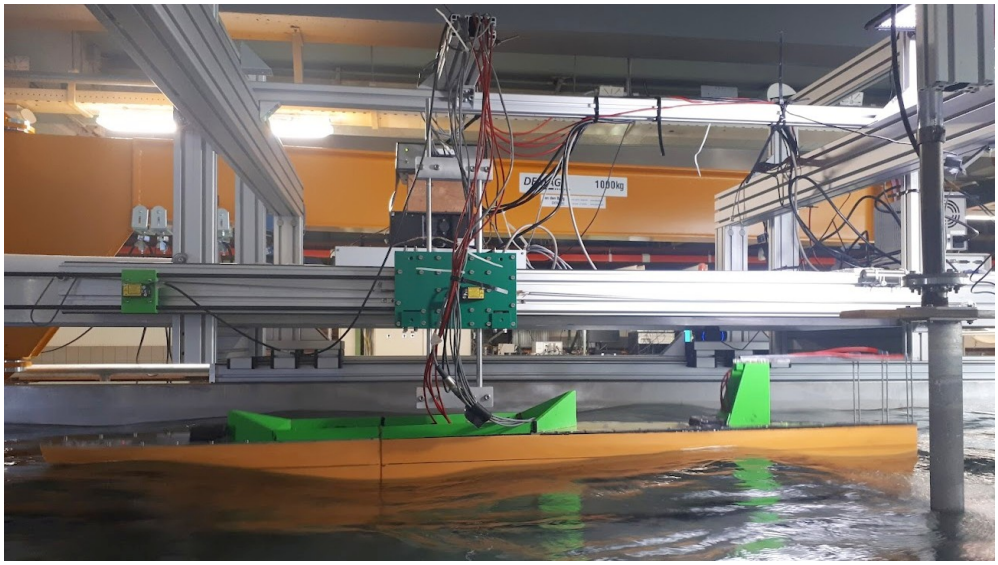

Figure 5.2: Picture of the test setup

5.2.1 *Model design*

As a basis of the model design the S175 ship at a 1:130 scale is used. The draft of the bow is increased systematically. Three draft variations are implemented at the bow and all three were also tested with and without an increased freeboard.

The lines plans of the models are shown in figure 5.1. The models were 3D printed with separate freeboard pieces that could be removed. The parametric description of the models is given in table 5.1. When two numbers are given for a bow the left value is for a freeboard equal to the deck height (fb-) and the right for the extended freeboard (fb+). As the focus of the research is on the geometry of the bow, the radius of gyration, mass and the centre of gravity is kept close to constant for the various bow designs by utilizing ballast weights in the model. As the volume at the bow changes, the centre of bouyancy changes and thus the longitudinal centre of gravity also changes for the different models to keep the trim neutral. The radii of inertia were obtained with swing tests. To model a superstructure a deck box was placed at 0.34 m from the bow with a width and height of 0.06 and 0.12 m respectively.

5.2.2 *Test setup*

The model experiments are conducted in the wave-current tank that allows for continuous testing in irregular waves with modelled forward velocity

discussed in chapter 2. The testing condition is a 5 hour irregular wave spectrum with a significant wave height of 0.062 m and a peak period of 0.97 s. The modelled forward velocity is 0.25 m/s. The full scale equivalent is a 57 hour wave spectrum with a significant wave height of 8.1 m, a peak period of 11.1 s and a modelled forward velocity of 2.85 m/s. This sea state and forward velocity are chosen as they represent realistic sailing conditions within the working range of the test facility.

Data was acquired at 1000 Hz. The same test setup as discussed in chapter 4 and shown in figures 4.1 and 4.2 is used. A picture of the setup used for testing the various bows is shown in figure 5.2. Three resistance type relative wave elevation (RWE) probes are placed 0.06 meters apart with the most forward RWE probe at the stem. The RWE probes are oriented vertically and are attached to the model via the deck box with a plexiglass plate reinforced with carbon fiber. Six GE Druck PDCR 42 type sensors with a range of up to 350 kPa are used to measure the pressure. Two were positioned on the deck box at a height of 0.01 and 0.03 m, and four were positioned on the model's center line on the deck with 0.04 m between them. The third pressure sensor's (0.14 m from the stem) signal was noisy, so the measurements from this sensor were not used. The model was free to heave, pitch and surge as two vertical linear guides, also called heave rods, attached the model to the surge carriage. The surge carriage was attached to the tank via a vertical rail. Two soft springs (3 N/m) restricted the model from moving off the rail. At the center of buoyancy and 0.645 meters behind the centre of bouyancy, Panasonic HG-C1400 laser distance sensors were used to measure the vessel's heave and pitch. Both laser sensors were attached to the surge carriage. The Honeywell 940-R4Y-RD-ICO acoustic sensor, which measures the horizontal location of the surge carriage, was used to measure surge. In order to gauge the resistance, a load-cell was positioned in between the hinge and the heave rod. To measure water on deck, a wetness sensor was positioned 0.005 m in front of the forward most pressure sensor. However, during the experiments, water remained around the sensor after impacts, so the data was not used. At 0.86 meters from the tank's side and 2.79 meters from the wave maker, a resistance-type waveprobe was placed. To remove noise originating from the electrical power grid from all data, a 3rd order low pass filter set to 40 Hz was used. All experiments were recorded using two webcams, one positioned above the setup and the other to the side of it. All information is available on doi.org/10.4121/15f0d739-b84c-48f3-879a-68c08f068ab3 [1], including data, video, 3D print and laser cut files.

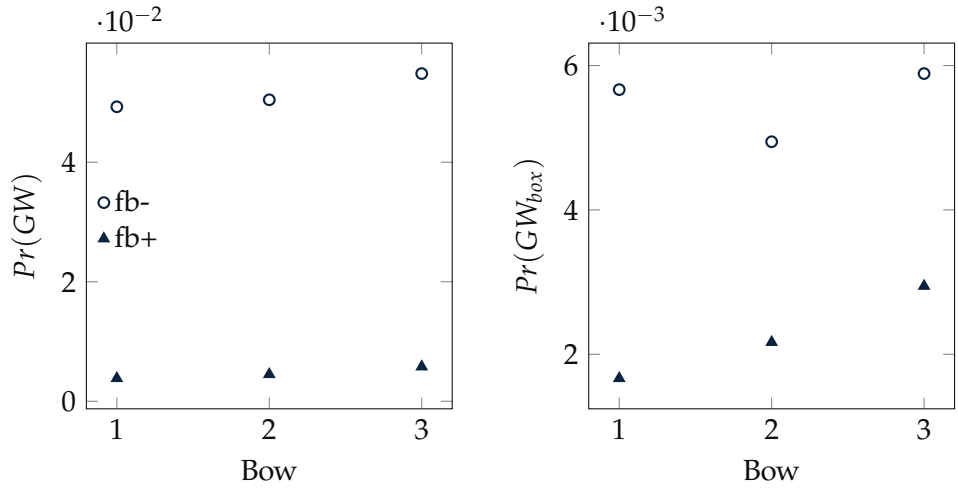

(a) Deck

(b) Deck box

Figure 5.3: Probability of a green water impact causing an impact on the deck or deck box

5.2.3 *Impact identification*

For the initial identification of impacts, the most forward pressure sensor was used. If a pressure higher than 10 Pa is measured on a sensor the impact is marked. Some pressure peaks were caused by noise or previous water on the deck flowing off. To eliminate these impacts from the data set the camera footage was used and each identified pressure peak was visually checked. Only the impacts where water flowed over the bow onto deck towards the deck box, causing the pressure peak were kept. In total 3263 green water impacts were identified. Deck box impacts were identified creating a subset of green water impacts for which a deck box impact pressure of 50 Pa was measured. 472 green water impacts that impacted the deck box were found.

5.3 RESULTS

The experimental data for the 6 different variations are analyzed to gain insight into the effect of draft and freeboard on the statistics of green water.

5.3.1 *Freeboard's effect on probabilities*

The first step of analyzing the green water impacts is to compare the probability of a green water impact for the tested variations. The probabilities of

Table 5.2: Decrease in $Pr(GW)$ caused by increasing freeboard from experiments compared to calculation methods from literature

	fb- $Pr(GW)$	fb+ $Pr(GW)$	Decrease [%]
Experiments Bow 1	0.049	0.0038	1289
Experiments Bow 2	0.050	0.0045	1111
Experiments Bow 3	0.055	0.0058	948
$e^{-\frac{fb^2}{R_{\text{RWE}}}}$ [55]	0.039	$5.34\ e^{-5}$	73034
$e^{-1.19\frac{fb}{H_{m0}}^2}$ [113]	0.456	0.091	501

green water impacts are found by dividing the total number of impacts by the testing time. Figure 5.3 shows the results.

Increasing the freeboard decreases the probability of green water impacts occurring. The decrease in probability due to the freeboard increase is expected. To further investigate if the probabilities found from the experiments correspond to the expectations based on literature, the probabilities are quantitatively compared. To quantify the expected change of $Pr(GW)$ due to the freeboard increase the probability estimation for deck wetness by Price and Bishop [29] and Hamoudi and Varyani [55] is used, shown in equation 1.4. For R_{RWE} the average over all relative wave variations is used. With equation 1.4 the probability of green water is calculated, shown in table 5.2. As the probabilities deviate from the actually found probabilities, an empirical equation from Boon and Wellens [113] is also used to calculate the expected probabilities of occurrence for fb- and fb+. Comparing the results shows that all predictions vary greatly from one another. The prediction from Hamoudi and Varyani [55] overestimates the decrease in probability by increasing the freeboard with a factor 50. The prediction from Boon and Wellens [113] underestimates the decrease in probability by a factor 2 and overestimates $Pr(GW)$ for both cases.

5.3.2 *Draft's effect on probabilities*

Looking back at figure 5.3 we see that the draft at the bow also influences $Pr(GW)$. Especially for bows with an increased freeboard a larger draft correlates with a larger probability of green water. This correlation fits with the hypothesis that for an increased draft the probability of green water increases. The theory is that increased draft increases the swell-up, resulting

in a larger relative wave elevation, and thus results in a larger probability of green water occurrences.

To test the hypothesis the expected difference in probability of green water is calculated. The calculated change in probability following this hypothesis is compared to the actually measured difference in probability. To calculate the hypothesized difference in $Pr(GW)$ due to draft various assumptions are made. The motion response of the vessel to the waves is assumed constant over all bow variations. This assumption was checked for heave and pitch by comparing the standard deviations and the distribution of crest amplitudes. Only in the tail of the crest amplitude distributions some differences were identified. The second assumption is that the probability of green water can be calculated with equation 1.4. The last assumption made is that the swell-up (su) at the bow is constant over time, which is only true for the bow wave created by the forward velocity, not the swell-up created by wave radiation and reflection. As the swell-up is assumed constant over time the change will not be captured in R_{RWE}. A constant increase of swell-up can also be seen as a decrease in effective freeboard, so the swell-up is taken into account with $fb - su$. The swell-up is calculated using the equation proposed by Noblesse et al. [141]:

$$su = \frac{2.2 \cdot U^2/g}{1 + \frac{U}{\sqrt{g \cdot d}}} \frac{\tan(\alpha_E)}{\cos(\alpha_E)} . \tag{5.1}$$

In this equation, U is the forward velocity, g the gravitational acceleration, d the draft at the bow and α_E the entrance angle of the bow. As the motion response is assumed to be constant over all bow variations R_{RWE} should be the same for all bows. As R_{RWE} is assumed constant and we are only interested in the expected change in $Pr(GW)$ we can use

$$R_{\text{RWE}} = -\frac{(fb - su)^2}{\ln(Pr(GW))} \tag{5.2}$$

to find R_{RWE}. Because the difference in $Pr(GW)$ between fb- and fb+ cannot be quantified with equation 1.4 as shown in table 5.2, R_{RWE} is calculated for fb- and fb+ separately. Bow 2 fb- and bow 2 fb+ are used to find R_{RWE}. Next the expected change in $Pr(GW)$ for different draft variations can be calculated with

$$Pr(GW) = e^{-\frac{(fb-su)^2}{R_{\text{RWE}}}} \tag{5.3}$$

where the only varying parameters over the design variations are fb and su. Table 5.3 shows the results. As bow 2 is used to find R_{RWE} only the results of bow 1 and 3 are shown.

Table 5.3 shows that for the fb- cases the difference in probability for the different bows is explained well by the increase in swell-up. For the fb+ cases

Table 5.3: Calculated increase in $Pr(GW)$ following the proposed hypothesis for increased draft leading to increased $Pr(GW)$ compared to actual increase in $Pr(GW)$

	Experiments $Pr(GW)$	Calculated $Pr(GW)$	Difference [%]
Bow 1 fb-	0.0493	0.048	-1.8
Bow 3 fb-	0.0548	0.052	-6.0
Bow 1 fb+	0.0038	0.0043	13
Bow 3 fb+	0.0058	0.0046	-20

the actual increase in $Pr(GW)$ for larger drafts is larger than is expected under the above assumptions. As following the hypothesis with all its assumptions only leads to a maximum error of 20% the increase in swell-up due to the increase in draft is deemed to be the reason for the increase in probability of green water.

5.3.3 *Pressures*

For design purposes it is not only interesting to know what the probability of green water is, but also what pressures to expect. The average pressures on the deck and deck box for the different designs are compared in figure 5.4.

The figures show that additional freeboard increases the average pressures on the deck and deck box. The average pressures increase with an increase in freeboard, indicating that not all impacts are reduced equally when the freeboard is increased. Increasing the freeboard causes the probability distribution of the pressures to be different, resulting in different average pressures. The difference indicates that the distribution of the pressures has to be further analyzed, as to find what design minimizes the probability of high pressure impacts.

As figure 5.4 indicates that the probability distribution of the pressures might be different for fb- and fb+ cases these probability distributions are further analyzed. The probability distributions are analyzed by means of the probability of exceedance. The probability of exceedance is commonly used in green water research, most often for the (relative) wave elevation [27], [28], [77], [81]. The probability of exceedance for the pressures is shown in figure 5.5 with the fitted Fréchet distributions. Based on literature the probability distribution of the pressures is expected to be Fréchet distributed [113]. The

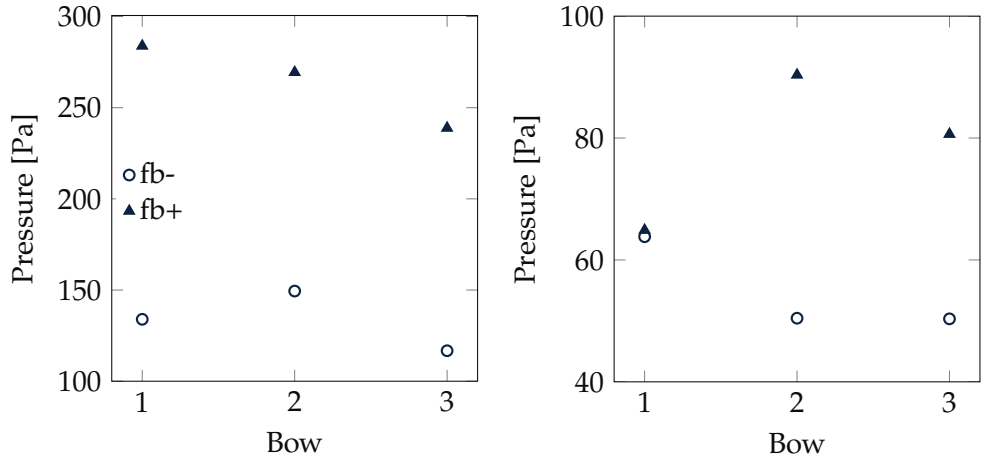

(a) Deck (b) Deck box

Figure 5.4: Average of the maximum measured pressures per impact on the deck or deck box

fitted Fréchet distributions are tested with the Kolmogornov-Smirnov test and all fit with a p-value above 0.05, meaning that the pressure can indeed be Fréchet distributed.

Figures 5.5a, 5.5b, 5.5c and 5.5d show both the experimental and fitted Fréchet distribution. Deck box impacts are rarer than deck impacts so less data has been collected on these impacts. As there is less data the distributions of experimental data in figures 5.5c and 5.5d fluctuate and thus no conclusions are made based on these figures. Figures 5.5a and 5.5b are visually analyzed. The figures show that for the fb- variations the tail of the distribution does not fit with the fitted Fréchet distribution. The tail in the distribution from the actual data is lower than that of the expected distribution for the fb- cases. In other words, the low-probability high-pressure impacts for the fb- cases are somehow different than higher-probability lower-pressure impacts as the larger, rarer impacts do not cause the pressure impacts expected based on the Fréchet distribution. Figure 5.5b does not show this difference between the experimental data and the Fréchet distribution. It is thus concluded that a difference in high and low pressure impacts only occurs for the fb- cases. The analysis in the following section concludes in a possible reason for the difference between fb+ and fb-.

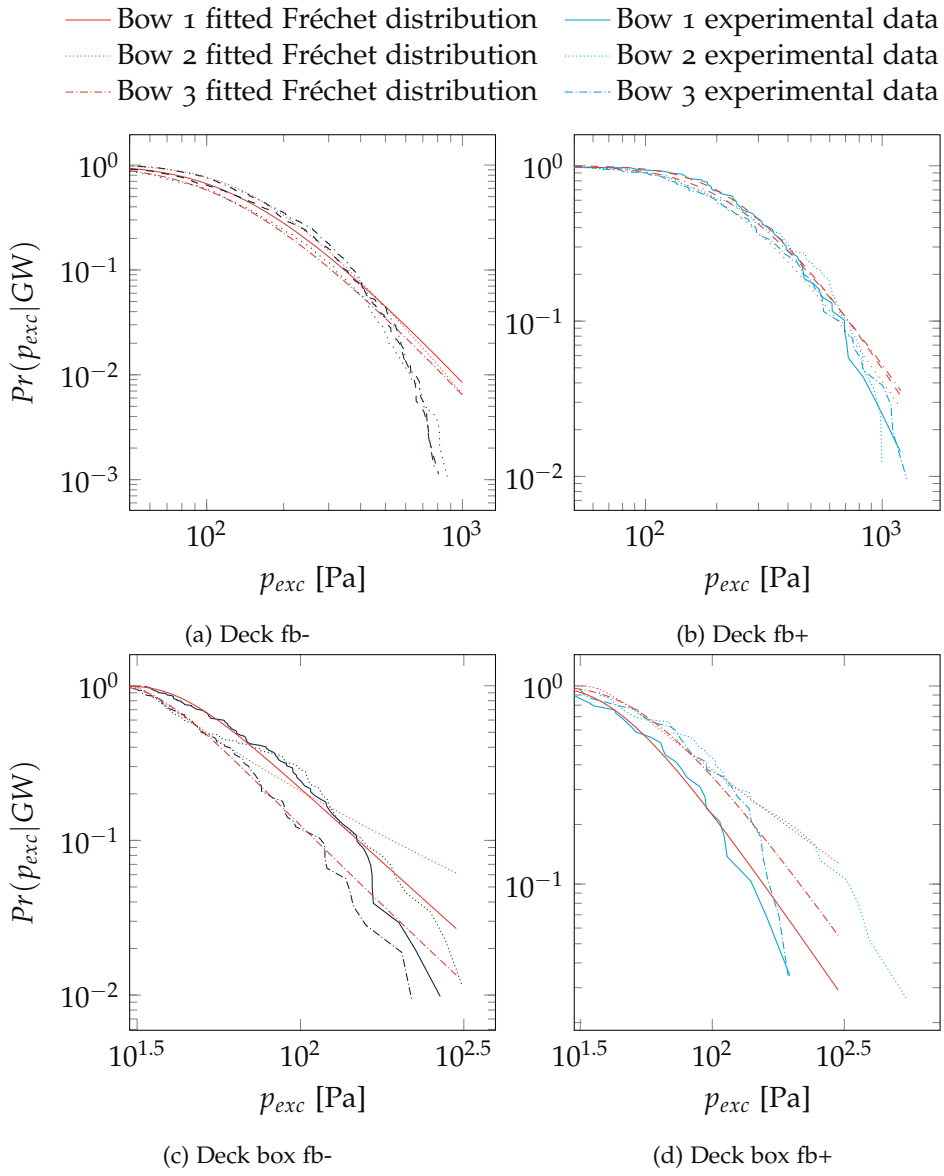

(a) Deck fb-

(b) Deck fb+

(c) Deck box fb-

(d) Deck box fb+

Figure 5.5: Probability of exceedance plot for the pressures with the fitted Fréchet distribution shown in red

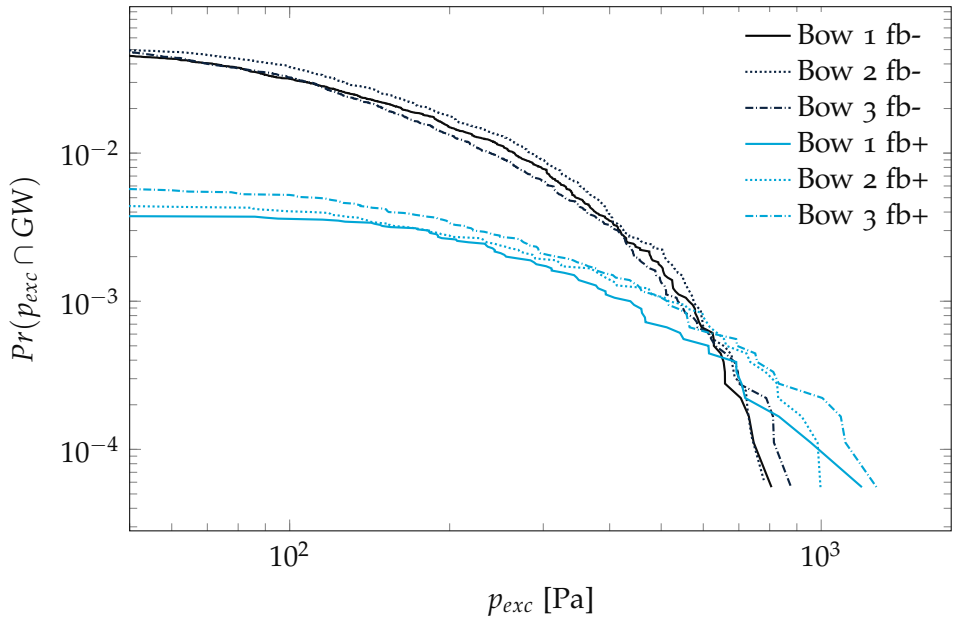

(a) Deck pressures

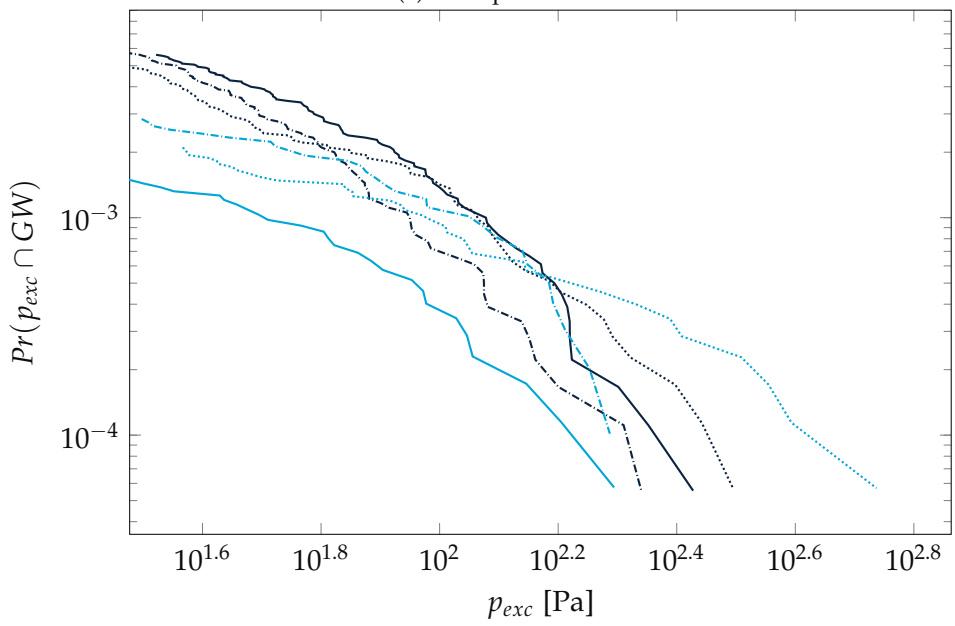

(b) Deck box pressures

Figure 5.6: The joint probability of exceedance for pressures showing that the additional freeboard reduces the probability of low pressure impacts, but increases the probability of high pressure impacts

5.3.4 *Joint probability of impacts and pressures*

When comparing the design variations using the probability of exceedance for pressures, as is done in figure 5.5, the difference in the probability of an impact occurring in the first place is ignored. Ignoring $Pr(GW)$ will result in a skewed comparison. To exemplify this statement we give an example: there are two designs and during testing a similar number of high pressure impacts occurred. But for the first design only high pressure impacts occur while for the second design also a similar number of low pressure impacts occur. The second design will seem preferable when comparing the probability of pressures because for the first design 100% of the impacts caused high pressures, while for the second design only 50% of the impacts caused high pressures. The conclusion of which design minimizes high pressure impacts is wrong because $Pr(GW)$ is not included.

To prevent unequal comparison $Pr(GW)$ has to be included. To combine the probability of pressure exceedance and $Pr(GW)$ the probabilities are joined:

$$Pr(p_{exc} \cap GW) = Pr(p_{exc}|GW) \cdot Pr(GW) \, . \tag{5.4}$$

In this equation, p_{exc} is the pressure exceeded, and $Pr(p_{exc} \cap GW)$ is the probability of a green water impact and the impact pressure exceeding p_{exc}. $Pr(p_{exc} \cap GW)$ is visualized in figure 5.6 for the design variations. The left side of the figures shows that for the minimum p_{exc} the increased freeboard decreases the probability and the increased draft slightly increases the probability, as was also shown in figure 5.3. As every green water impact exceeds the minimum p_{exc} indeed figure 5.3 and the left hand side of figure 5.6 show the same.

Moving to higher p_{exc} for deck impacts, further to the right in figure 5.6a, shows us the probability of higher pressure impacts. The probabilities for the fb- and fb+ move closer together for higher impact pressures exceeded, until a pressure of 600 Pa. For impact pressures above 600 Pa the probability of occurrence is actually larger for the designs with increased freeboard. For bows with additional freeboard green water impacts with a probability of below 10^{-4} go from a maximum impact pressure of 800 Pa for bows without an extended freeboard to an impact pressure above 1000 Pa for bows with an extended freeboard.

Figure 5.6a clearly shows that increasing the freeboard increased the probability of green water with an impact pressure above 600 Pa. For impacts that reached the deck box, in figure 5.6b, first increasing the freeboard reduces the probability of an impact. As p_{exc} increases, the difference between the designs with and without increased freeboard decreases, similar to figure 5.6a. Due to the more limited data set size for deck box impacts the probability curve

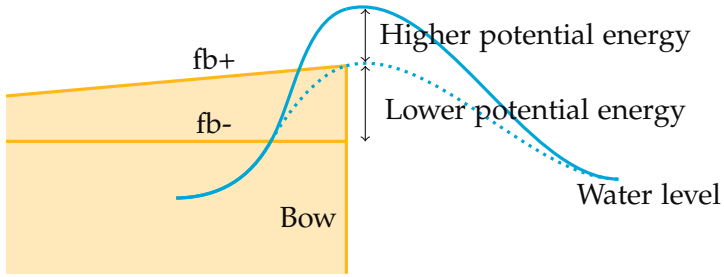

Figure 5.7: Schematic of increased freeboard (fb+) restricting water with lower potential energy from flowing on deck

is shorter and shows more variation, as was already shown in figures 5.5c and 5.5d. The figure does show that the reduction of probability of deck box impacts by increasing the freeboard only occurs for the low impact impacts.

The deck box data shows that a limited number of impacts limits our ability to compare the probability of a higher impact occurring. In figure 5.6a the lower the probabilities (lower on y-axis), the larger the uncertainty interval will become as the line is based on less data points, as less impacts occurred, thus making conclusions less certain at the lower probabilities. However, as for all three fb+ cases the highest pressure impacts are higher than their fb- counterparts and the same trend is found for deck and deck box impacts it is concluded that increasing the freeboard only decreases the probability of low pressure impacts. The probability of a high pressure impact on deck actually increases when the freeboard is increased.

How freeboard decreases the probability of green water has been discussed in 5.3.1, but how increasing the freeboard could cause an increase in high pressure impacts is not discussed. No explanation is found in literature either as no literature is found to discuss the increase of impact pressures due to an increased freeboard.

As no explanation is found a potential cause is hypothesized. As all the bows were tested in the same sea states and their mass and inertia is kept close to constant the probability of a certain wave and motion response are the same for fb+ and fb-. The probability of certain motions and waves that will lead to high pressure impacts is thus also the same. The probabilities staying the same means that the difference in figure 5.6a can only be explained by the same combination of motions and waves leading to higher pressures when the freeboard is increased.

The increased freeboard restricts water flowing onto deck at deck level. For low impacts this restricts the flow entirely. For large relative wave elevations only the water near deck level is restricted, the water that exceeds the extended

freeboard will impact on deck. The difference in impact pressures follows from the difference in the height from where the water flows onto deck. As the deck levels are kept constant for all designs, increasing the freeboard leads to a larger height difference between the deck and water as the water can not flow onto deck at deck level. Only when the water is high enough to overtop the freeboard can it flow onto deck. Even then the water with lower potential energy, closer to deck level, is restricted from flowing onto deck. The added freeboard effectively only allows the part of the water with the largest potential energy to impact. Figure 5.7 shows schematically how the extended freeboard limits the flow of the water with lower potential energy.

If the freeboard restricting low potential energy water from flowing onto deck is indeed the reason for the increase in high pressure impacts, the difference in pressure for fb- and fb+ for low probability impacts should be close to the difference in potential energy between the deck and freeboard level: $\rho \cdot g \cdot h = 343$ Pa. ρ is the water density and h the difference in freeboard height between fb- and fb+. Looking at figure 5.6a the increase in the highest pressures on deck due to increasing the freeboard is about 250 Pa. This theory is also in line with the results found in figure 5.5, where we found that the impact pressures in the tail of the distribution are lower than the theoretical distribution for only the fb- cases. The combination of potential energy calculation as well as the difference in the fit to the theoretical distribution for fb- and fb+ cases both agree with the hypothesis. It is thus concluded that increasing the freeboard restricts water with low potential energy from entering the deck, eliminating low pressure impacts but increasing the pressures of high pressure impacts.

5.4 CONCLUSION

Green water impacts for different bow designs with varying drafts and freeboards are analyzed. Probabilities of the impacts and pressures were used to compare design variations. A large set of green water impacts in irregular waves with forward velocity was obtained experimentally using a continuous testing facility.

The results show that, especially for bow designs with increased freeboards, a larger draft correlates with a higher likelihood of green water impacts. The result supports the hypothesis that a greater draft leads to a larger swell-up, resulting in a reduced effective freeboard and, consequently, an increased probability of green water impacts.

The joint probability of green water occurring and the probability of pressure exceedance was also used to compare the bow designs. The joint prob-

ability shows that increasing the freeboard decreases the probability of low pressure impacts, as expected. But increasing the freeboard increases the probability of high pressure impacts. The surprising result shows the importance of using statistically representative data sets when designing for green water impacts.

6

MOTIONS AND WAVES FOR WHICH GREEN WATER OCCURS

This chapter is based on:

[142] A. D. Boon and P. R. Wellens, 'Kinematics of green water in a large data set of events and a resulting prediction method of probability', *Ocean Engineering*, vol. 311, p. 118776, 2024, ISSN: 0029-8018. DOI: 10.1016/J.OCEANENG.2024.118776

6.1 INTRODUCTION

Green water is an extreme wave impact event and has been defined as a continuous volume of water flowing on deck [16]. Experimental research into green water has looked at the pressure and pressure development during events, finding impulsive and non-impulsive event types and a variety of flows and impacts [19], [44], [80]–[83]. Parameters like freeboard, relative vertical motion, stem angle, surge motions and wave steepness are found to influence green water [18], [22], [55], [127]. Different types of green water events have been identified, like dambreak, plunging or the hammer-fist type [15], [20], [143]. Analytical work on green water often uses the dam-break model [18], [38]–[40], [47]. However, not all green water impacts are dam-break type impacts [16]. Even for the dam-break green water types, the dam-break model deviates from the green water impacts, as green water impacts are three-dimensional dynamic impact types where water flows over a moving deck [17]. Work on simulating green water impacts is also conducted [63]. However, the span of spatial and temporal scales needed to model green water means that numerical techniques are not yet capable of addressing the complexity and computational cost of screening for green water events from long time series of waves [13]. The flow on deck caused by green water poses a risk as large pressures during impacts can damage the structure of the ship. The flow of water on the deck itself also poses a risk to people on deck.

Besides green water events, there are also exceedance events. Exceedance has been defined as a measured relative wave elevation exceeding the deck level, often measured by relative wave probes located at one or more locations at the bow [12], [20], [28], [91]. Exceedance can occur together with spray events, which is when water arrives on deck mostly in the form of a rain of water, not a continuous flow [11], [135]. Exceedance can develop into green water, but it does not always have to [11], [113]. If exceedance does not develop into a flow on deck it does not pose a risk to the ship or those on board. Water exceeding the deck becomes a risk when it develops into green water.

Screening methods have been used for green water to identify the critical events to design for. Previous research has developed methods based on exceedance [12], [27]–[29], [55], [91]. Nonlinearity in the waves and ship response and asymmetry in the relative wave elevation distribution causes deviations from the distribution [12], [14], [27], [28]. Also, these cited prediction methods assume that all instances where water exceeds deck level lead to green water, but, as discussed, not all exceedance events become green water.

Previous research also proposed screening and prediction methods based on events that induce large pressures on deck [144], [145]. These screening methods focus on large impact pressures. Low-pressure impact flows on deck are neglected, even though they can still be a risk to those on board. Veer and Boorsma [89] specifically investigates green water. Their work, however, focuses on the categorization of the green water events and the flow on deck, not the prediction of the probability of green water.

This chapter analyses the motions, waves and swell-up during a large number of green water events and exceedance events that did not develop into green water. From the analysis, differences between the motions during green water and exceedance events are found. Based on the difference, the present paper proposes a novel prediction method of probability for all green water events, excluding exceedance events that do not develop into green water. Limit values for heave, pitch and wave elevations are adopted as part of the method.

6.2 METHODOLOGY

Green water and exceedance events are identified by using the distance of continuous flow onto the deck as an identifier. If the flow on the deck is limited, but water is measured to exceed the deck level the impact is classified as exceedance. A continuous flow of water on the deck from the stem to at least 8% of the ship's length between perpendiculars (L_{pp}) is classified as green water. This limit was chosen based on the green water impacts shown by

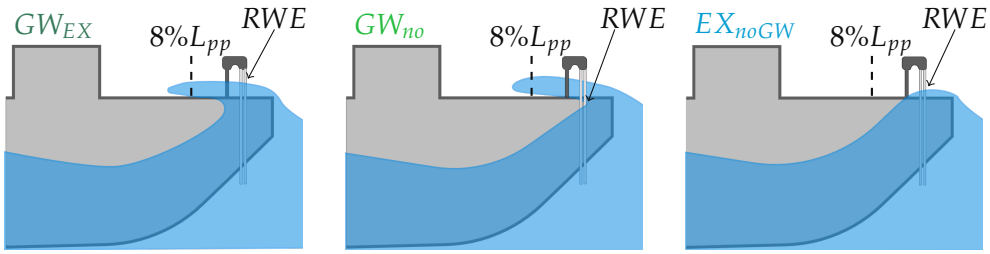

Figure 6.1: Schematic of the different impact types. From left to right green water with exceedance (GW_{EX}), green water without exceedance (GW_{no}) and exceedance without green water (EX_{noGW})

Buchner [12] and Pham and Varyani [93] which all reached over 8% L_{pp}. Green water events for which no exceedance was measured were also identified. During these events water has flowed onto deck, so water exceedance has occurred. No measured exceedance means that the exceedance was local and the location differs from the exceedance measurement location. As the exceedance for GW_{no} events is local, the kinematics possibly differ from GW_{EX} type events. Figure 6.1 shows schematics for the different event types. Data from experiments modelling 1945 full-scale sailing hours at forward speed in irregular head waves is used, available on `doi.org/10.4121/21031981` [146]. The experiments are described in chapter 3. With the data set, a focused investigation is conducted of exceedance and green water impacts and their differences.

Different data sets for exceedance events and green water impacts with and without measured exceedance are created. The set of green water impacts for which exceedance is measured is called GW_{EX}, and the set of exceedance events for which no green water occurred is EX_{noGW}. The green water impacts that do not belong to either group are GW_{no}. The relations between sets are

$$GW_{EX} \cap GW_{no} = \emptyset, \quad GW_{EX} \cup GW_{no} = GW, \tag{6.1}$$

$$GW \cap EX_{noGW} = \emptyset, \quad GW_{EX} \cup EX_{noGW} = \{\text{events} | RWE > fb\} \tag{6.2}$$

In equation 6.2 fb is the still water freeboard.

6.2.1 *Event type identification*

The event types described in the introduction are identified in the data. Wetness sensors are used to initially detect the occurrence of green water impacts. Visual identification was used as water on the deck caused false

positives and negatives. The wetness or pressure sensor, which is 0.012 m behind the stem of the bow and represents 8% of the length of the ship, must be reached for an impact to be considered a green water impact. According to a visual inspection, this criterion excludes spray-like deck wetness impacts. Exceedance events are defined as RWE being at least 0.01 seconds above deck level.

Figure 6.2 shows impacts for different tested cases from both GW and EX_{noGW}. Time traces during a green water and exceedance event are given in figure 6.3. In this figure, z is the heave, θ the pitch and η the wave elevation. For all impact types, the maximum measured relative wave elevation (RWE_m) measured during the impact was used as the time that the event took place (t_e).

6.3 RESULTS

The difference between the impacts, as defined in paragraph 6.2.1, is analyzed. Test cases 1c and 2 were excluded from further analysis as not all event types occurred for these test cases.

The number of each impact type per case is shown in table 6.1. Here n is the number of impacts, with the subscript indicating the data set it belongs to. Pr is the probability of an event occurring per encountered wave. Pr is calculated with

$$Pr = \frac{n}{n_w}. \tag{6.3}$$

The number of encountered waves (n_w) is calculated as $n_w = \frac{t_{test}}{T_{z_e}}$.

$Pr(EX_{noGW})$ and $Pr(GW_{EX})$ increase for larger H_{m0}, as is shown in figure 6.4. The increase in $Pr(EX_{noGW})$ and $Pr(GW_{EX})$ is exponential within the tested range, as was shown to be the case in chapter 3.

All the data sets are of different sizes but the relative number of occurrences of the different event types is somewhat constant. The average relative number of occurrences is $n_{GW} = 0.45 \cdot (n_{EX_{noGW}} + n_{GW_{EX}})$ and $n_{GW_{no}} = 0.17 \cdot n_{GW}$. These results indicate that for over 80% of green water events, water was measured to exceed deck level before the event. Also, over half of all measured exceedance events did not develop into green water. The exceedance was measured at one location, likely increasing the the number of GW_{no} event types compared to experiments with more RWE probes. The values in table 6.1 show that less than half of all exceedance events ($GW_{EX} \cup EX_{noGW}$) are the problematic green water events, while at least a tenth of the green water events are not included when only measured exceedance is considered, as the exceedance for these events occurred away from the measurement location.

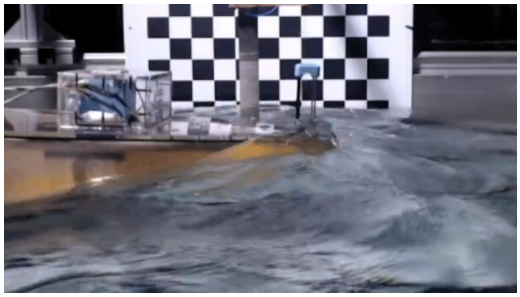

(a) *GW* impact from case 3

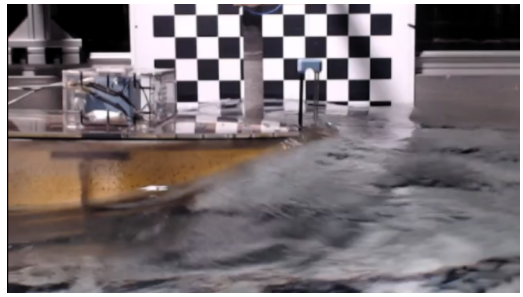

(b) EX_{noGW} event from case 3

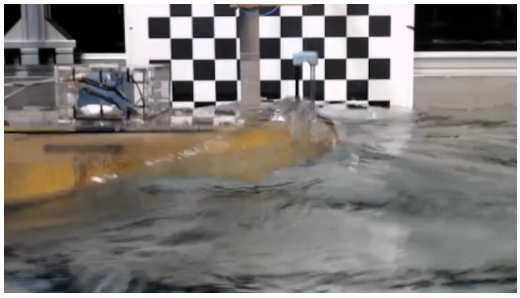

(c) *GW* impact from case 4

(d) EX_{noGW} event from case 4

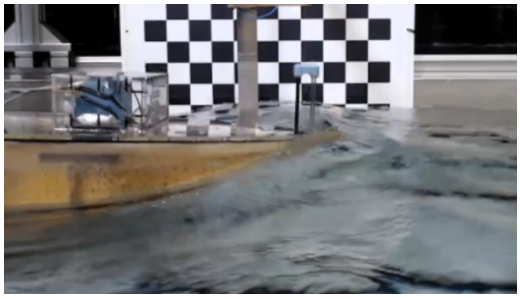

(e) *GW* impact from case 4a

(f) EX_{noGW} event from case 4a

(g) *GW* impact from case 5

(h) EX_{noGW} event from case 5

Figure 6.2: Stills from footage of *GW* and EX_{noGW} events for different cases

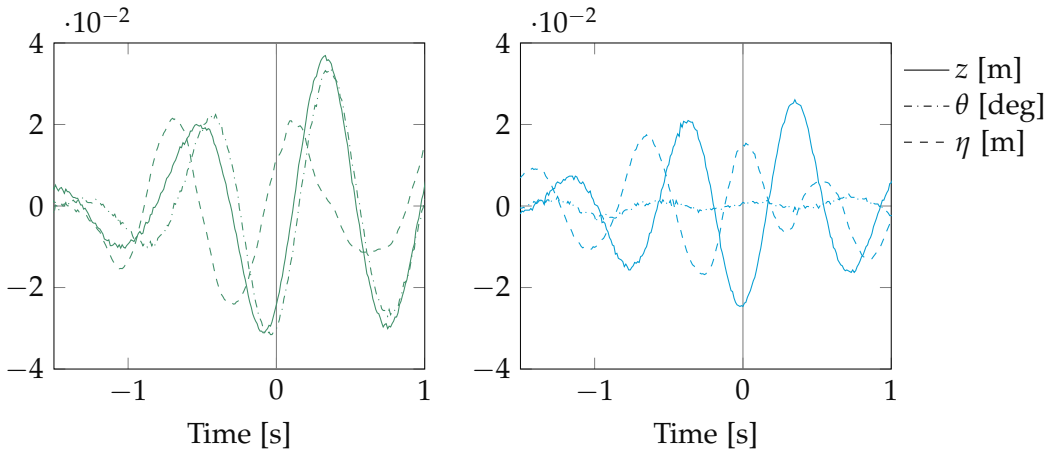

Figure 6.3: Time traces of the measured heave, pitch and wave elevation during a green water impact (left) and exceedance event for which no green water occurred (right) both from case 3. Note that the wave elevation is measured at forward speed of the ship model

Table 6.1: Number of events included in each data set and the probability per event type

	$n_{EX_{noGW}}$	$Pr(EX_{noGW})$	$n_{GW_{EX}}$	$n_{GW_{no}}$	n_{GW}	$Pr(GW)$
Case 1	16	0.00037	8	1	9	0.00021
Case 1a	9	0.00021	6	1	7	0.00016
Case 1b	37	0.00083	15	5	20	0.00045
Case 3	35	0.00017	29	5	34	0.00016
Case 4	221	0.00094	160	39	199	0.00084
Case 4a	20	0.00189	9	0	9	0.00083
Case 5	91	0.00119	81	10	91	0.00181

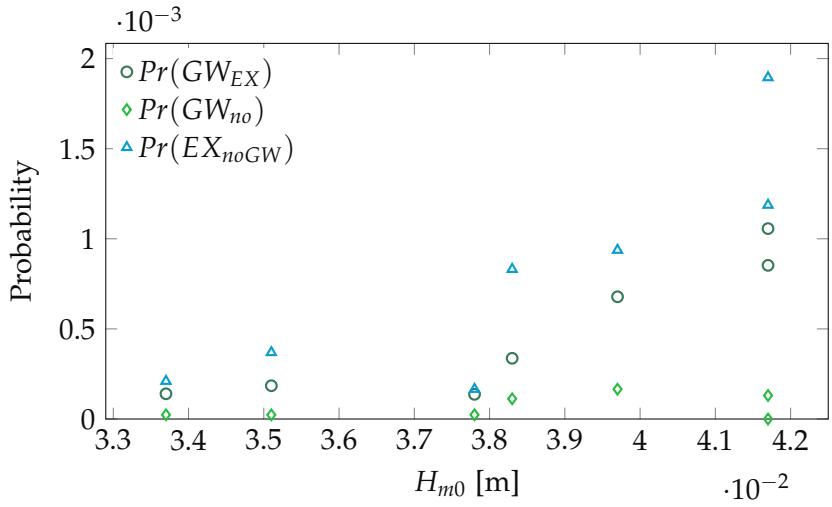

Figure 6.4: Increase of probability of occurrence of $Pr(EX_{noGW})$ and $Pr(GW_{EX})$ over H_{m0} per case. $Pr(GW_{no})$ remains fairly constant

6.3.1 *Relative wave elevation*

Figure 6.5 shows the maximum measured relative wave elevation during events ($RWE_m(t_e)/fb$) as a function of H_{m0} for the different event types. Soares and Pascoal [28] identified an increase in $RWE_m(t_e)$ as a function of H_{m0} for a data set containing all exceedance events ($GW_{EX} \cup EX_{noGW}$ in the present study). The present study found a similar increase in $\mathrm{RWE}_m(t_e)$ for $GW_{EX} \cup EX_{noGW}$ as was found by Soares and Pascoal [28]. The increase in $RWE_m(t_e)$ for $GW_{EX} \cup EX_{noGW}$ is mostly caused by an increase in $RWE_m(t_e)$ for GW_{EX}, as GW_{EX} increases from 107% of the freeboard to 122%, while for EX_{noGW} $RWE_m(t_e)$ only slightly increases from 103% to 106%. Overall, the average $RWE_m(t_e)$ for EX_{noGW} is consistently lower than the average $RWE_m(t_e)$ for GW_{EX}. This difference is notable as the difference in the definition for GW_{EX} and EX_{noGW} events is water flowing on deck, not the relative wave elevation. Apparently, there is a difference between the flows of GW_{EX} and EX_{noGW}, resulting in different relations between $RWE_m(t_e)$ to H_{m0}. To investigate where the differences come from, the different contributions to $RWE_m(t_e)$ are analyzed.

$RWE_m(t_e)$ can be calculated as

$$RWE_m(t_e) = -z(t_e) - tan(\theta(t_e)) \cdot x_{bow} + \eta(t_e) + su(t_e). \tag{6.4}$$

t_e is the time of the maximum relative wave measured during an impact/event. The heave ($z(t_e)$), pitch times the distance from the centre of gravity to the RWE probe ($\tan(\theta(t_e)) \cdot x_{bow}$) and the undisturbed wave elevation ($\eta(t_e)$) are

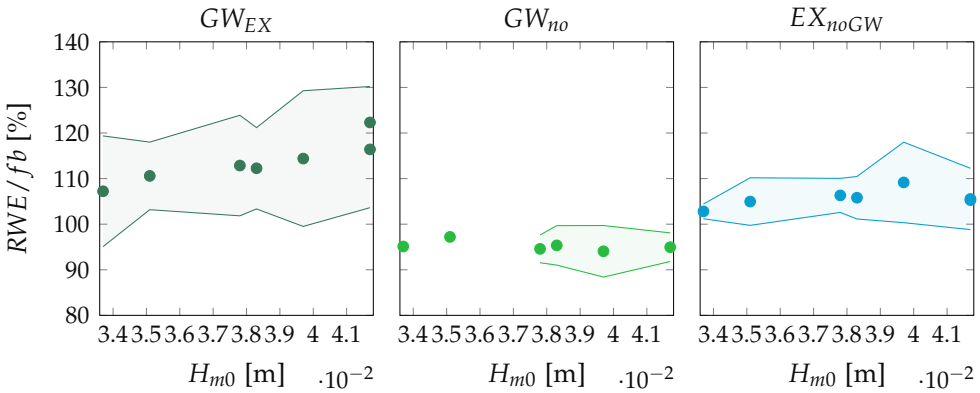

Figure 6.5: Difference in average RWE during events per case for GW_{EX}, GW_{no} and EX_{noGW} shown from left to right. The shaded area indicates the standard deviation of RWE. As for $H_{m0} < 0.036$ m the GW_{no} set has one impact per case no standard deviation is shown

the maximum value during 0.1 seconds before and after an impact. The margin was taken because the wave measurement was taken some distance from the ship model. As section 2.1 shows, the flow profile in the test facility was not completely uniform, and some phase shifts in the measurement could have occurred. The further analysis is of a statistical nature so the variations will average out and should not affect the conclusions. The swell-up ($su(t_e)$) has been determined by subtracting the heave, pitch and wave elevation from $RWE_m(t_e)$. Swell-up consists of radiated and reflected wave components and dynamic swell-up, further discussed in section 6.3.1.1. Figure 6.6 shows for each impact type the average of the different parts per case. The figure shows that on average a negative heave and pitch occur together with a positive wave elevation at the bow, indicating that the phases between the motions and wave are consistently out of phase for all events.

The contribution of heave, pitch, wave elevation and swell-up differ for the different impact types. The average percentages show that the contribution of motions is larger for GW_{EX} compared to EX_{noGW}, while it is close to the same for GW_{no} and GW_{EX}.

The previously identified increase in $RWE_m(t_e)$ for larger H_{m0} is not the same for EX_{noGW} and GW_{EX}, making it likely that the mechanics behind $RWE_m(t_e)$ also differ. Figure 6.6 shows that for EX_{noGW} the increase in $RWE_m(t_e)$ is caused in equal parts by an increase in wave elevation and the swell-up, while the contribution of pitch decreases. For GW_{EX} the increase in $RWE_m(t_e)$ is caused by the increase in the swell-up, while the wave elevation stays about constant above $H_{m0} = 0.034$ m. The heave and the pitch

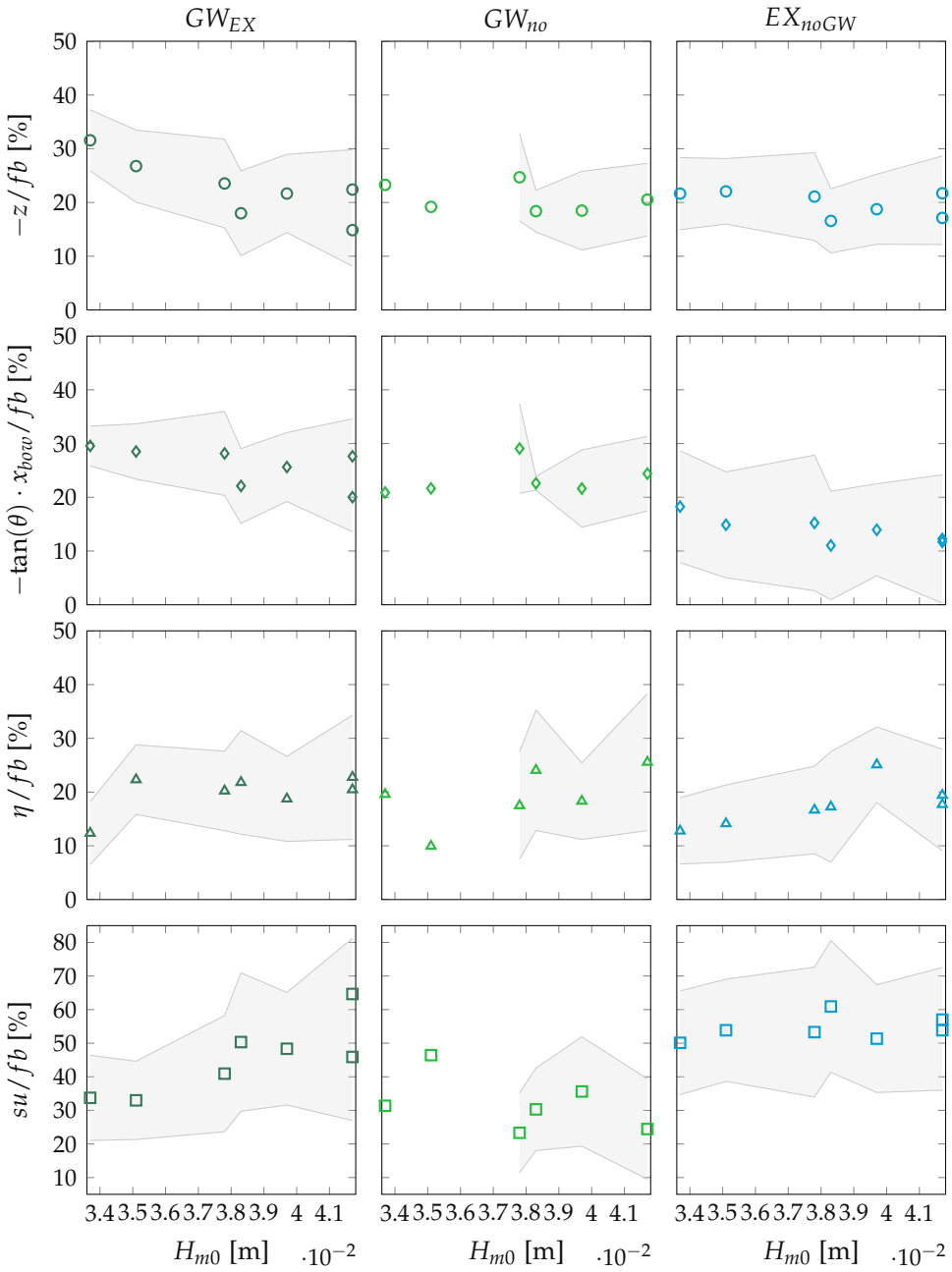

Figure 6.6: Contribution of the motions, waves and swell-up to *RWE* on average per case for GW_{EX}, GW_{no} and EX_{noGW} from left to right. The shaded area indicates the standard deviation. As for $H_{m0} < 0.036$ m the GW_{no} set has one impact per case no standard deviation is shown

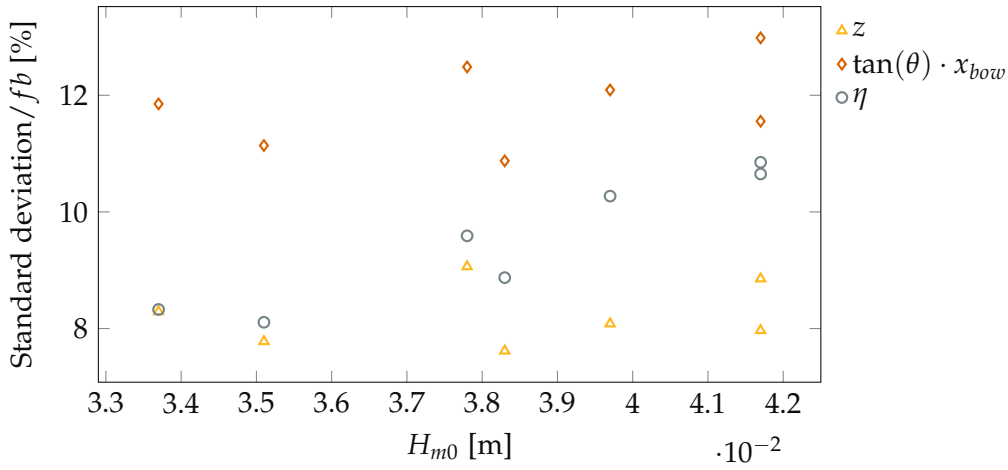

Figure 6.7: The heave, pitch and wave elevation's standard deviations from the overall experiments over H_{m0}

actually decrease for larger H_{m0} for GW_{EX}. This decrease means that the swell-up causes the increase in $RWE_m(t_e)$ for GW_{EX}.

The decrease in the contribution of the ship motions to $RWE_m(t_e)$, shown in figure 6.6, are not in line with the standard deviation of the motions found throughout the experiments shown in figure 6.7. The smaller motions during GW_{EX} impacts for larger H_{m0} should thus be explained on the basis of what happens during the impacts. With the decrease in heave and pitch, also an increase in the standard deviation of the heave and pitch is found for GW_{EX}, as the shaded area becomes wider. This increase in the standard deviation, combined with the larger GW_{EX} data set sizes for larger H_{m0} makes it likely that for larger H_{m0} large swell-ups occur, thus allowing for additional green water impacts to occur at lower heaves and pitches. The GW_{EX} data set is thus extended with impacts with lower heaves and pitches for larger H_{m0}, lowering the average and increasing the data set size and the standard deviation.

The increase in wave elevation and swell-up leading to a decrease in the average heave and pitch contribution is not found for EX_{noGW} impacts. The contribution of the wave elevation does increase, similar to GW_{EX}, but this increase does not lead to the large increase in swell-up found for GW_{EX}. The increase in swell-up is similar to the decrease of the average pitch, but no increase in the standard deviation is found related to the decrease. The pitches are thus overall smaller for EX_{noGW} for larger H_{m0}, instead of the data set being extended by impacts with lower pitches as was the case for GW_{EX}.

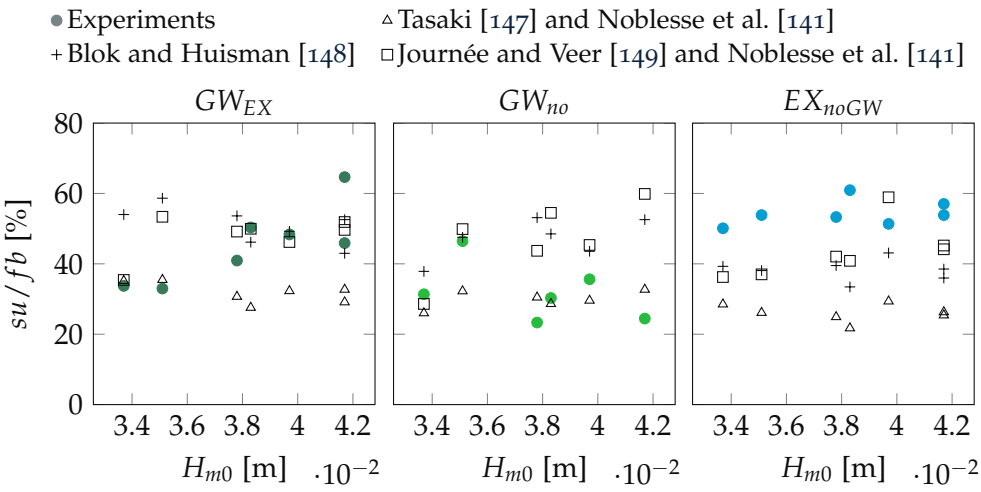

Figure 6.8: Difference between measured swell-up for EX_{noGW}, GW_{EX} and GW_{no} and estimations based on literature [141], [147]–[149]

In summary, the contribution and relations of the heave, pitch, wave elevation and swell-up differ per event type. To further understand the differences between EX_{noGW}, GW_{EX} and GW_{no} the swell-up is analyzed.

6.3.1.1 *Swell-up*

The large values found for the swell-up and the differences in swell-up for the different types of events are motivations for further investigation. The swell-up consists of a wave reflecting from the bow, wave radiation from the damping wave from the ship's motions, and dynamic swell-up from the forward speed [12], [147], [149]. No existing estimation method based on the combination of these effects was found, but a study by Blok and Huisman [148] gives values for separate empirical swell-up coefficients for the heave, pitch and waves, all at forward speed. Tasaki [147] gives the swell-up coefficient for the combination of heave, pitch and waves but does not include forward speed. Noblesse et al. [141] proposes a partially empirical equation for the swell-up for forward speed, and Journée and Veer [149] give a theoretical equation for the swell-up of a radiated wave at forward speed but does not include swell-up caused by this forward speed.

The above methods are used to predict the swell-up during events identified in our data set. The predicted swell-up by Noblesse, Delhommeau, Guilbaud *et al.* [141] is added to the swell-up predictions by Journée and Veer [149] and Tasaki [147] to account for the swell-up caused by forward speed. The predictions resulting from the different estimation methods are compared

to the swell-ups found during the different events in figure 6.8. For the calculations, the heave, pitch, wave elevation and forward speed were inputs, as well as draft, Froude number and waterline entrance angle. The values of the experiments in the present falling within the considered ranges of the above-mentioned studies. As the heave, pitch and wave elevation are irregular the choice was made to use the motions and waves during an event: $h(t_e)$, $\tan(\theta(t_e)) \cdot x_{bow}$ and $\eta(t_e)$.

The measured swell-up is reasonably well predicted by Journée and Veer [149] and Noblesse et al. [141] for GW_{EX}. A discrepancy is shown between the predicted and measured swell-up for EX_{noGW}. Buchner [12] has identified a similar discrepancy and concluded that the discontinuity at the freeboard level is the cause. Even though the same discontinuity at the freeboard level happens for GW_{EX} as for EX_{noGW}, the same underestimations are not found. The difference between GW_{EX} and EX_{noGW} for the prediction accuracy suggests that the underestimation for the swell-up for EX_{noGW} is due to different drivers for the swell-up during these impacts, not the discontinuity at the freeboard level.

For GW_{no} similar swell-ups as for GW_{EX} are predicted from theory. The measured swell-ups are lower, but as the predictions are similar for GW_{EX} and GW_{no} there is no apparent reason for the swell-up for GW_{EX} and GW_{no} to be different. Section 6.3.1 also concludes that these data sets are similar for everything except the swell-up. The only difference between GW_{EX} and GW_{no} impacts is if the swell-up was measured by the RWE probe. In the following analysis GW_{EX} and GW_{no} are thus combined into GW.

6.3.2 *Motions and waves*

The above analysis consistently identified differences between GW and EX_{noGW} for the motions and wave contribution to $RWE_m(t_e)$. Histograms of the heave, pitch, wave elevation and $RWE_m(t_e)$ are shown in figure 6.9 to directly compare the differences. The histograms are density histograms, averaged proportionally over the different test cases.

Figure 6.9 shows that the pitch motions during EX_{noGW} are not the same as the pitch motions during GW. The difference in pitch motion causes a difference in $RWE_m(t_e)$. The pitch for GW is normally distributed and larger than the pitch for EX_{noGW}, which is not normally distributed. The latter has one peak near 0 and a smaller peak near 35%. The spread in data is explained in part by the trend over H_{m0} shown in figure 6.6. Another part of the explanation is that a strict definition for green water is used, causing EX_{noGW} to include impacts similar to green water impacts, explaining the

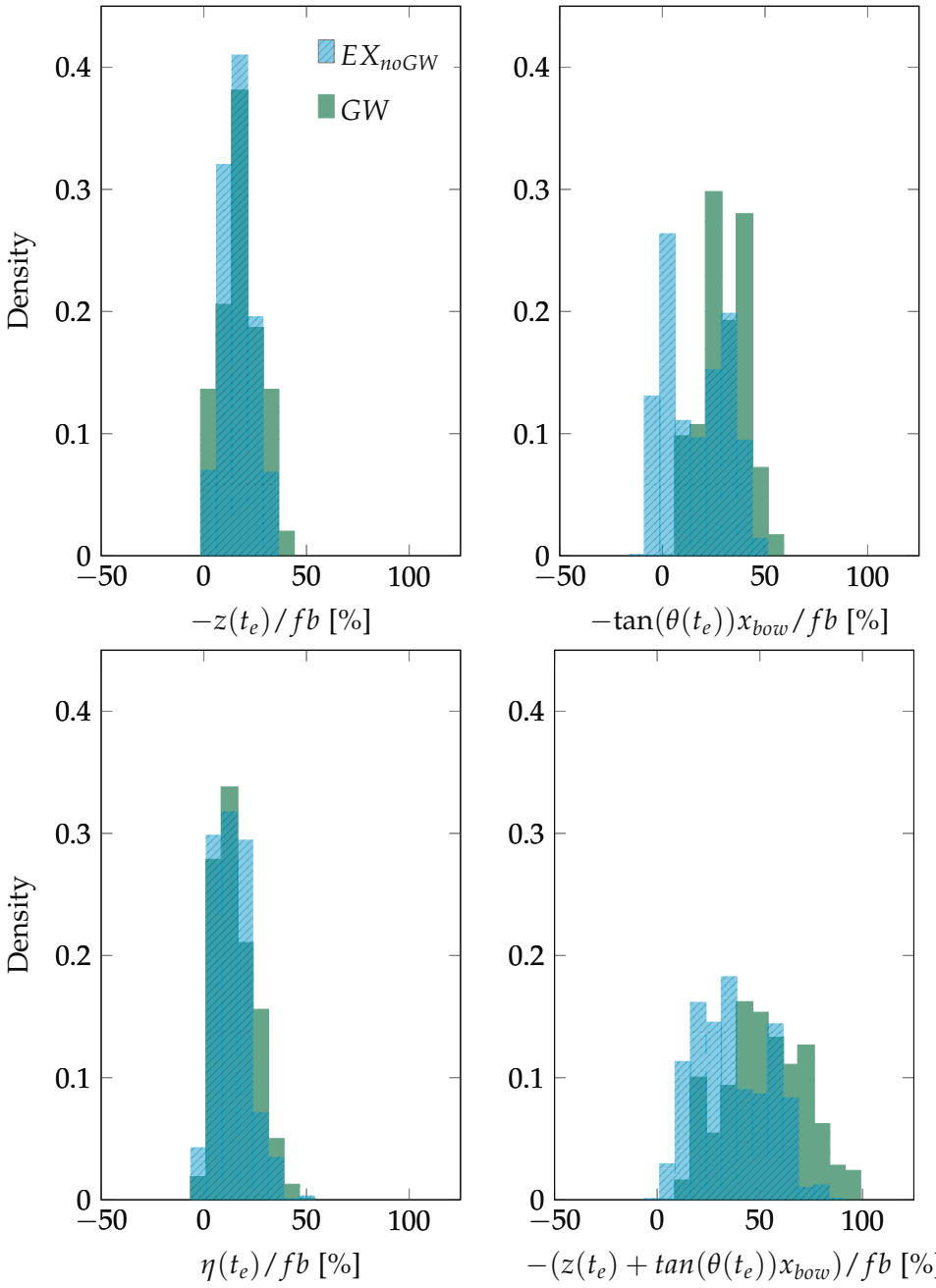

Figure 6.9: Visualizing the differences and similarities between EX_{noGW} and GW with $z(t_e)$, $\eta(t_e)$, $\tan(\theta(t_e)) \cdot x$ and $\eta(t_e)$ as percentage of freeboard in density histograms proportionally averaged over the cases 1, 1a, 1b, 3, 4, 4a, 5

large number of EX_{noGW} impacts with pitches similar to *GW* impacts. The separate peak around a neutral to somewhat forward pitch would then be most representative for EX_{noGW}. A difference in the motions between *GW* and EX_{noGW} also explains the difference in swell-up between EX_{noGW} and *GW* discussed in section 6.8. The main difference between *GW* and EX_{noGW} impacts is thus identified to be the pitch motion during the event.

Comparing the values from the histograms to the standard deviation of the motions and wave elevation found throughout the experiments, figure 6.7 shows that the motions and wave elevations found during *GW* impacts are large. These large motions of forward pitch and downward heave occur while the wave elevation at the bow is positive. The combination of a large downward heave and forward pitch with a positive wave elevation at the bow is unlikely, possibly as unlikely as green water impacts are to occur.

From the above, it is hypothesized that if a low heave and large wave elevation coincide but the pitch is neutral, an event will be an EX_{noGW} event, and thus will pose a limited risk to the ship or people on the ship. When this situation coincides with a large forward pitch, a *GW* event occurs. The reason for this difference is not clear from the present data and further research is needed. A possible explanation is that the swell-up combined with a neutral or somewhat forward pitch results in a large swell-up with mostly vertical velocities, causing exceedance but no flow on deck. A forward pitch motion coinciding with a wave leads to a scooping effect, causing a continuous flow on deck. This explanation is also in line with the difference in prediction accuracy of swell-up for EX_{noGW} and GW_{EX} events, discussed in section 6.3.1.1. The driver for swell-up to be different is pitch.

6.3.3 *Predicting the occurrence of green water*

Differences between *GW* and EX_{noGW} events has been identified above. From the difference, a prediction or screening method can be proposed specifically for *GW* impacts and excluding EX_{noGW} events. The result is a method that focuses on the impacts that pose a risk. The prediction method uses the heave, pitch and wave elevation and is based on the histograms in figure 6.9.

Limit values based on the values found during impacts are used to quantify for which heave, pitch and wave elevation *GW* impacts occur. Figure 6.9 shows that green water impacts mostly occur for certain values of heave, pitch and wave elevation. The combined data of all impacts is used to find the limit values, as otherwise no representative limit value could be determined for

Table 6.2: Limit values above or below which *GW* impacts occur based on the values found during impacts and the percentages of the impacts included by these limit values

	Limit as ratio to fb	**% of GW impacts above limit**
z_{lim}	-0.13	85%
$\tan(\theta_{lim}) \cdot x_{bow}$	-0.25	85%
η_{lim}	0.095	90%
su_{lim}	0.58	75%

cases with few impacts. The limit values should be chosen such that they adhere to the requirement

$$su_{lim} \geq fb + z_{lim} + \tan(\theta_{lim}) \cdot x_{bow} - \eta_{lim}. \tag{6.5}$$

In equation 6.5, the subscripts *lim* indicate limit values. The equation ensures that an upper limit for the expected swell-up is included through the used limit values, as the swell-up depends on the waves and motions on the ship, as discussed in paragraph 6.3.1.1. To ensure a realistic upper limit for the swell-up, su_{lim} is conservatively chosen so that 25% of *GW* impacts were measured to have a larger swell-up than su_{lim}. For the wave crest elevation, a limit is chosen for which 90% of the wave elevations found during *GW* impacts are larger than η_{lim}. The limit values for the heave and pitch are chosen such that they fulfill the condition in equation 6.5. The condition is fulfilled for limits for the heave and pitch where 80% of impacts occurred with larger heaves and pitches. The resulting limit values are shown in table 6.2. The swell-up is implicitly included through the limit values of heave, pitch and wave elevation, as they adhere to the boundary condition in equation 6.5, but also because the swell-up is related to the heave, pitch and wave elevation.

Not only swell-up but also the effect of forward speed is implicitly included through the heave, pitch and wave elevation as the motions are influenced by the forward speed. In previous paragraphs, no need for including the differences in forward speed explicitly in the analysis was found. The influence of the forward speed on the occurrence of green water is thus thought to be indirect as the influence of forward speed influences the motions and swell-up, which in turn influences the probability of green water.

To test the hypothesis that impacts occur when the limit values of the heave, pitch and wave elevation are exceeded, the probability of an impact occurring is calculated with

$$Pr(GW) = Pr(\eta > \eta_{lim}) \cdot Pr(z < z_{lim} | \eta > \eta_{lim}) \cdot Pr(\theta < \theta_{lim} | \eta > \eta_{lim}). \tag{6.6}$$

To find the probability of a limit value being exceeded, needed for equation 6.6, the probability density functions of the wave elevation, heave and pitch are used. Following linear theory, the heave and pitch are assumed to be independent from each other, but to both depend on the wave elevation. The dependent distributions of both the heave and the pitch are found for each case by finding all heave and pitch values coinciding with $\eta > \eta_{lim}$. The probability density functions of η, $z|\eta > \eta_{lim}$ and $\theta|\eta > \eta_{lim}$ were assumed to be normal distributions. This assumption was tested and shown to be correct with the D'Agostino-Pearson test with a p-value limit of 0.05 [150].

Figure 6.10 shows the resulting prediction of the method in equation 6.6 with the results closely following the experiments. The diamonds in the figure show the sensitivity of the prediction to changes in used limit values as the diamonds indicate the difference in predictions for $Pr(GW)$ if z_{lim} and θ_{lim} are chosen so that they include 5% more or fewer impacts. The prediction method in equation 6.6 is sensitive to the limit values used. There could be arguments made for choosing the limit values differently, which would lead to somewhat different results. For cases 1, 1a and 3 the prediction method for $Pr(GW)$ is conservative for the limit values from table 6.2 because the limit values are based on the whole data set. As cases 4 and 5, both with large H_{m0}, dominate the data, the limit values for the motions are underestimated for cases 1, 1a and 3 as it is known from figure 6.6 that for cases with lower H_{m0}, larger motions are found during impacts. For smaller H_{m0} also smaller swell-ups were found, meaning that for cases 1, 1a and 3 the boundary condition in equation 6.5 is not fulfilled, causing an overestimation in the number of impacts. The limit value of η is overestimated for cases with low H_{m0} which reduces the overestimation.

Cox and Scott [27] propose a method based on the relative motion of the bow exceeding the freeboard to calculate the probability of exceedance ($Pr(GW_{EX} \cup EX_{noGW})$). This estimation is compared to $Pr(GW)$ from the experiments and $Pr(GW)$ estimated with equation 6.6. As expected, the method of Cox and Scott [27] for $Pr(GW_{EX} \cup EX_{noGW})$ results in a large over-prediction of $Pr(GW)$ as it uses exceedance as an analogy for green water. Using exceedance is in line with most existing literature on predicting green water events [12], [27]–[29], [55]. As a consequence, no data from previous work could be adopted for further comparison.

Figure 6.10 shows the proposed method gives better predictions than the method proposed by Cox and Scott [27]. The method is based on the same data set it is tested on, resulting in the most optimal results. Still, equation 6.6 being able to predict the number of green water events shows promise, likely because of these improvements:

(1) Equation 6.6 explicitly sets limit values for heave, pitch and wave eleva-

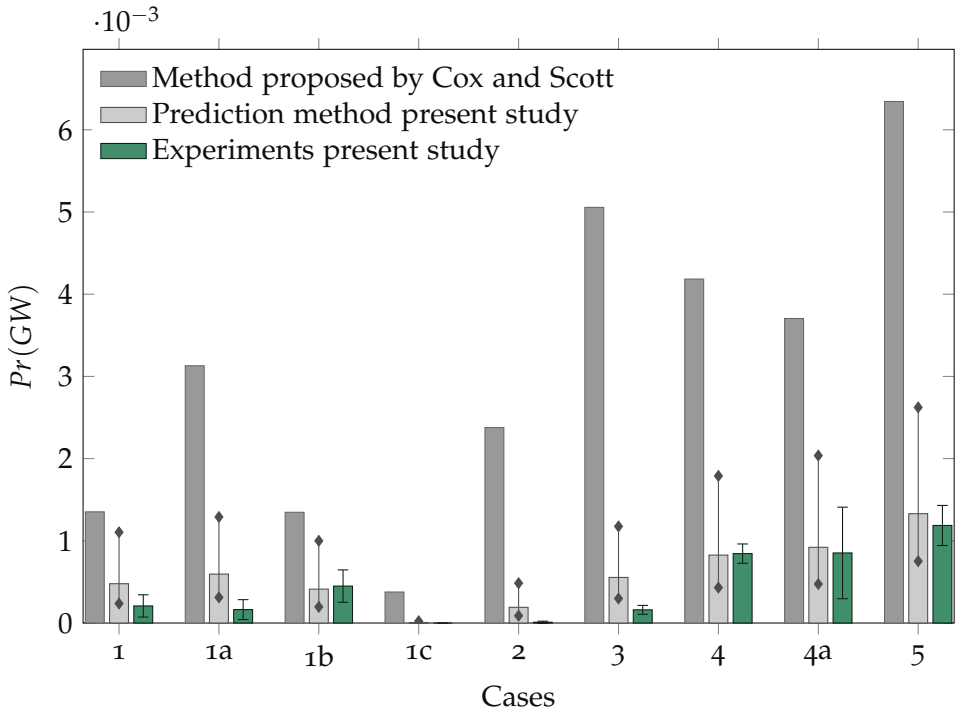

Figure 6.10: The probabilities estimated with the proposed screening method compared to the probabilities found from the experiments and literature. The lines indicate a 95% confidence interval and the diamonds a 5% in- and decrease in the percentage used to determine the limits

tion, instead of using RWE, thus becoming a prediction method for specifically green water as exceedance is not required anymore and events with neutral pitches are excluded.

(2) Because of the use of dependent limit values the phase between the heave and wave and pitch and wave is included

(3) The swell-up is implicitly included through the limit values set as the swell-up depends on heave, pitch and wave elevation

Comparing outcomes of the prediction method to the data gives confidence in the hypothesis that if a certain heave, pitch and wave elevation occur it will lead to a green water event. Future research is to be conducted to include the effect of different ship designs, sea states and forward velocities to improve the choice of limit values.

6.4 CONCLUSION

A large data set from experiments was used to find the difference between heave, pitch and wave elevation for which exceedance events occur and when they develop into the continuous flow on deck associated with green water. Based on the results, a prediction method of probability is proposed that focuses on the high-risk green water events.

The difference between green water events and exceedance events that do not develop into green water is explained by the pitch of the ship. Green water events consistently occurred with large forward pitch motions, while exceedance also occurred when the pitch was neutral. Also, differences in the relative wave elevation during green water and exceedance events were identified. For green water events, the wave elevation above deck increases by 15% for an increase of the significant wave height of 24%. The increased wave elevation is caused by an increase in swell-up. For exceedance events, only a limited increase in relative wave elevation above deck was found, caused by an increase in heave and wave elevation.

Previous work uses exceedance to predict green water. With the newly identified differences between green water and exceedance events, a method is proposed that focusses on green water events. By using the values of heave, pitch and wave height found during green water events and calculating the probability of these limit values all being exceeded at the same time, an improved estimate of the probability of green water can be obtained.

7

MACHINE LEARNING AND LARGE DATA SETS FOR SHIP MOTION MODELS

7.1 INTRODUCTION

Recent results from machine learning combined with 'big data' have been impressive. The developments caused Frické [151] to ask if machine learning and 'big data' might lead to a semi-mechanical way of producing valuable scientific theories. Tolle, Tansley and Hey [152] consider 'big data' to be the fourth scientific paradigm after experiments, theoretical work and simulations. A semi-mechanical method to find the needed scientific insight would be helpful for maritime problems, like extreme wave impacts. Machine learning methods have already been used for marine applications for seakeeping, ship design, route planning and fuel predictions [153]–[159]. Even for extreme wave impacts machine learning has been used, as an artificial neural network is trained to correct peak amplitudes of the relative wave elevations [160].

The identified previous research uses machine learning methods that result in a model that is not straightforward to interpret as the generated models are highly dimensional. The preferable result from the machine learning method is a model that is predictively accurate, descriptively accurate and relevant [161]. To evaluate if the model captured the underlying problem, it must be interpretative. A machine learning method that can result in an interpretative model that represents the physics should thus be used. A method that fits these requirements is SINDy: Sparse Identification of Nonlinear Dynamics [162]. SINDy has been shown to be a promising tool for the identification of system dynamics when trained on analytical or numerical data [163], [164]. In maritime applications SINDy has been incorporated to predict wave excitation forces [165], steps are made to apply SINDy to wake prediction of wind turbines [166], SINDy is used to find a model for the manoeuvring of flapping foils in tandem [167] and SINDy is extended to detect model inconsistencies for autonomous marine surface vessel motions [168].

Previous work has also utilized SINDy in combination with experimental data. Work with experimental biological oscillators investigated why, despite its recent popularity, SINDy has rarely been applied to experimental data [169]. Limitations due to data availability and quality, noise, dimensionality and limited prior knowledge are identified. Work with experimental data from a double pendulum finds that the problem definition is important as ill-conditioned problems lead to inaccurate models [170]. The work advises applying SINDy to optimize parameters within a model instead of identifying the full system dynamics. Work with experimental data from the classical problem of falling objects found that SINDy struggles to identify coherent dynamics, concluding that models produced by SINDy, like other machine learning methods, work best when applied to problems similar to the ones they are trained on [171]. However, the application of SINDy on experimental data of gene expression in bacteria in response to zinc does result in a representative dynamical system, incorporating a novel exchange mechanism [172].

The discussed literature shows the range of applicability of SINDy but also highlights the difficulties of applying SINDy to experimental data. Another point to account for is that for extreme wave impacts the extremes are of interest. The extreme impacts occur less than every 1000 waves, but the increase in the measurement values is orders of magnitude smaller than the rarity. In the optimization, the errors from not representing extremes will thus be only a fraction of the total error and thus the optimization will not prioritize the extremes in the data. The error in the optimization of misrepresenting the extremes has to be increased to compensate for the rarity. An option is to change the optimization in SINDy to an optimization algorithm for extremes by including an extreme loss function. An extreme loss function is a loss function that is designed such that the rarity of impacts is compensated for. Recent work suggests various options like an entropy-based loss function to highlight outliers [173] or increasing the weight on the extreme values by using a higher order loss function [174].

As shown in chapter 6, the ship motions and waves are important in predicting extreme wave impacts. From the ship motions RWE and $R\dot{W}E$ can also be obtained, parameters which are strongly related to extreme wave impacts [12], [23]. Quickly and accurately being able to predict the heave and pitch is thus a relevant step towards predicting extreme wave impacts. The equations for heave and pitch are:

$$F \cdot sin(\omega t + \epsilon_F) = (a(\omega) + m)\ddot{z}(t) + b(\omega)\dot{z}(t) + c(\omega)z(t) \tag{7.1}$$

$$M \cdot sin(\omega t + \epsilon_M) = (a(\omega) + m)\ddot{\theta}(t) + b(\omega)\dot{\theta}(t) + c(\omega)\theta(t) \tag{7.2}$$

In the equations F is the force, M the moments, ϵ is the phase shift, a the added mass, b the damping coefficient and c the spring coefficient. Cummins [175] describes these equations as: *"The "shoe" is [...] the forced representation of the ship response by a system of second order differential equations. The shoe is squeezed on, with no regard for the shape of the foot. The inadequacy of the shoe is evident in the distortions it must take if it is to be worn at all. I am referring, of course, to the frequency dependent coefficients which permit the mathematical model to fit the physical model"*. The common description of ship motions stands with one foot in the frequency domain, and one foot in the time domain. The equations are both time and frequency dependent. An interesting initial exercise is to find a dynamical system in only the time domain.

7.2 METHOD

The chosen problem is to identify the ordinary differential equations (ODE) for heave and pitch in the time domain. SINDy is combined with sea-keeping data to train a model that predicts the accelerations of heave and pitch.

7.2.1 *SINDy*

SINDy obtains a dynamical system, specifically ODEs, through a data-driven algorithm. In its basis, the chosen machine learning method SINDy is a generalized linear regression method [164], [176]. SINDy combined with big data leverages that most physical dynamical systems have only a few terms defining the dynamics [177]. Identifying the governing equations in a sparse nonlinear function space becomes possible [162], [163]. For the implementation, the open-source code is used [178], [179].

SINDy applies sparsity-promoting regression. To perform the regression an optimization is performed. Various optimization schemes have been implemented within SINDy like the STLSQ, SR3 and Lasso [162], [180]. All of these optimizers are sparsity promoting, with STLSQ and SR3 resulting in a sparser solution than Lasso, which can lead to more small valued coefficients. The SR3 optimization provides a more flexible framework than STLSQ [180]. In the present work, the SR3 optimization is chosen.

Within a dynamical system for extreme wave impacts not only the state of the system but also outside forcing determines the dynamics observed. SINDy has been extended with model predictive control (MPC) [164]. With MPC SINDy allows for control parameters $\mathbf{U}$ outside of state $\mathbf{X}$, making it possible to add forcing terms, resulting in a dynamical system of the form

$$\dot{\mathbf{x}} = \mathbf{f}(\mathbf{x}, \mathbf{u}) \, . \tag{7.3}$$

In this system $\mathbf{x}$ is the state and $\mathbf{u}$ is the forcing.

The optimization used for the regression in the present work is

$$\min_{\Xi,\mathbf{W}} \frac{1}{2}|\dot{\mathbf{X}} - \Xi\Theta(\mathbf{X},\mathbf{U})^T|^2 + \kappa R(\mathbf{W}) + \frac{1}{2\nu}|\mathbf{W} - \Xi|^2 \tag{7.4}$$

In this objective function $\frac{1}{2}|\dot{\mathbf{X}} - \Xi\Theta(\mathbf{X},\mathbf{U})^T|^2$ is the loss function, $\kappa R(\mathbf{W})$ the regularization and $\frac{1}{2\nu}|\mathbf{W} - \Xi|^2$ the relaxation. Θ contains the candidate library and $\mathbf{U}$ the candidate parameters. $\mathbf{X}$ is the system's state. Ξ are the coefficients. κ is the threshold that sets the strength of regularizer R that promotes sparsity. ν is the coefficient that determines the relaxation strength and $\mathbf{W}$ the auxiliary coefficients [180].

In the SINDy optimization the strength of the regularization, which promotes sparsity, can be tuned through the threshold value κ. In the regression, there is a trade-off between the quality of fit to the training data and the sparsity, which prevents overfitting of the solution. By choosing an adequate threshold, solutions that sparsely represent the physics can be identified.

The inputs for SINDy are constructed. Since the goal is to identify a time domain-based dynamical system that represents the ship motions, only time domain candidates are to be given. The state matrix $\mathbf{X}$ consists of both the heave and pitch and the velocity of the heave and pitch. The control parameters $\mathbf{U}$ should represent the outside forcing, which in seakeeping are the waves. The candidate control matrix is thus constructed of the wave elevations on the hull, 10 locations equally spaced over the length of the ship. For the candidate library Θ initially only linear functions of $\mathbf{X}$ and $\mathbf{U}$ functions

$$\Theta(\mathbf{X},\mathbf{U}) = [\mathbf{1^T U^T X^T}] \tag{7.5}$$

are allowed. We will expand this to more candidates later.

7.2.2 *Results fictitious data test*

As an initial test of the problem setup, a fictitious data set is generated using linear wave theory. Since later steps are made towards experimental data, the generated data is based on similar parameters as the experimental data. The length, draft and centre of gravity are 1.346, 0.076 and 0.653 m, based on the S175 model used in chapter 4. A JONSWAP wave spectrum with a peak period of 0.9 s, a significant wave height of 0.05 m and a spectral shape of 3.3 is generated with 1150 wave frequencies with random phases. 10 realizations with different random phases are generated. Each realization lasts for 100 seconds, which is equivalent to about 110 wave encounters per realization. Tests with longer realizations indicate that the solutions are converged at 10

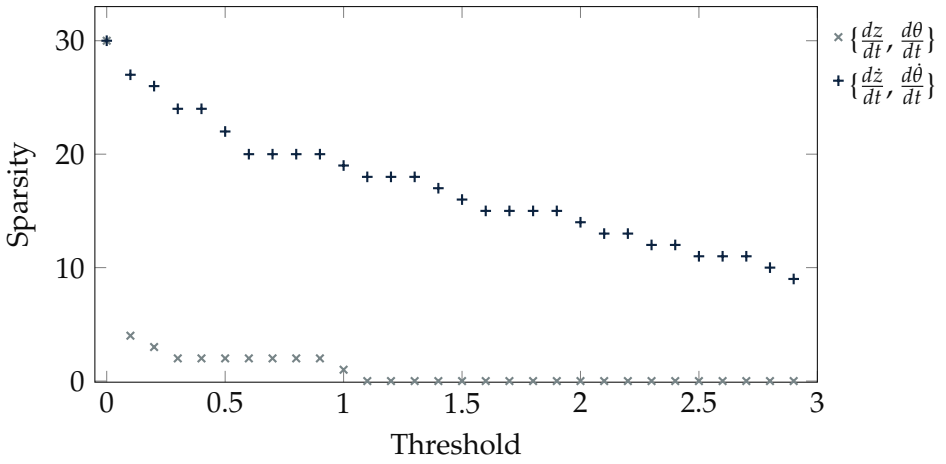

Figure 7.1: The correlation between thresholds and corresponding sparsity. The sparsest solution with a non-zero solution for all functions in the dynamical system is $\kappa = 0.9$

100-second realizations. The wave elevation at the centre of gravity and 10 points along the length of the ship is calculated.

To generate the fictional ship motions, the response amplitude operators (RAO) for the heave and pitch are used. Since the fictitious data is modelled after the experiments that use the S175 RAOs from experiments, given in Hamoudi and Varyani [55], are used to model the data. The heave motion is calculated with

$$z(t) = \sum_{n=0}^{n_{waves}} RAO_{z,n} sin(\omega_n t - \phi_n + \epsilon_{z,n}) \tag{7.6}$$

and the pitch with

$$\theta(t) = \sum_{n=0}^{n_{waves}} RAO_{\theta,n} sin(\omega_n t - \phi_n + \epsilon_{\theta,n}) \tag{7.7}$$

In these equations n_{waves} is the number of wave frequencies, in this case 1150. ω is the wave frequency, ϕ the phase.

The fictitious data is split into a training set and a testing set. The training set consists of 8 of the 10 realizations and the testing set consists of the other 2 realizations. The testing data is used to find the model score. The model score shows the quantification of the quality of fit with the R^2 coefficient. This score shows the proportion of the variation that is predicted, with 0 as minimum and 1 as maximum. A model score of 1 states that the model perfectly predicts the data. The data is not non-dimensionalized as all data is in meters, meters

per second or meter per second^2. Note that for pitch, not the radial value is used but the height difference at the bow due to pitch.

A threshold value is chosen based on figure 7.1. Figure 7.1 visualizes the sparsity (the number of terms in the identified solution) of models identified by SINDy. As $\dot{z} = \frac{dz}{dt}$ and $\frac{d\theta}{dt} = \dot{\theta}$, the sparsity for $\{\frac{dz}{dt}, \frac{d\theta}{dt}\}$ should be two. A threshold of 0.9 is chosen, as this is the highest threshold value for which the correct solution is found for $\{\frac{dz}{dt}, \frac{d\theta}{dt}\}$.

The parameters are set and the data is generated. SINDy is applied to the fictitious data and a model is generated. The model has a model score of 0.998. The dynamical system identified by SINDy is

$$\begin{aligned}
\frac{dz}{dt} &= 1.00\dot{z} \\
\frac{d\theta}{dt} &= 1.00\dot{\theta} \\
\frac{d\dot{z}}{dt} &= -51.25z - 1.41\dot{z} + 2.43\eta_1 + 3.40\eta_2 + 4.41\eta_3 + 4.45\eta_4 \\
&\quad + 4.08\eta_5 + 3.57\eta_6 + 2.76\eta_7 + 1.64\eta_8 + 0.38\eta_9 \\
\frac{d\dot{\theta}}{dt} &= -32.61\theta - 0.86\dot{\theta} - 1.41\dot{z} + 1.88\eta_0 + 2.38\eta_1 + 2.27\eta_2 \\
&\quad + 1.18\eta_3 - 1.78\eta_5 - 1.33\eta_7 - 0.93\eta_8
\end{aligned} \tag{7.8}$$

The subscript for η indicates the location of the wave elevation along the hull with 0 at the front of the model and 9 at the back.

The high model score indicates that the identified dynamical system can accurately predict the ship's motions. Since the solution can be interpreted the descriptive value can be analyzed. A positive indicator of the descriptive value is that $\frac{dz}{dt} = \dot{z}$ and $\frac{d\theta}{dt} = \dot{\theta}$ is identified. For $\frac{d\dot{\theta}}{dt}$ the coupling term $\dot{z}$ is included in the solution. The solution also contains spring and damping terms. The spring terms represent the restoring forces, and the damping terms represent the loss of energy through viscous effects and wave radiation. The theoretic spring term for heave is calculated to be 83.1 N/m with $A \cdot \rho \cdot g$, 1.6 times larger than the spring term found by SINDy. For pitch, the spring term is estimated with $M \cdot g \cdot GM_L$ where GM_L is the longitudinal metacentric height which is 3.57 m for the S175 model. The estimated spring term is 17.5, about 0.53 times the pitch spring coefficient identified by SINDy.

Even though the SR3 optimization is sparsity-promoting, almost all candidate wave elevation parameters are included. To check if the included wave elevation terms represent the forcing, the values of the weights for the terms are plotted. The column number in $\mathbf{U}$ corresponds to the location of the wave elevation over the hull, with 0 near the bow and 9 near the stern. Figure 7.2a shows that the weights follow the contour of the waterline area of the model

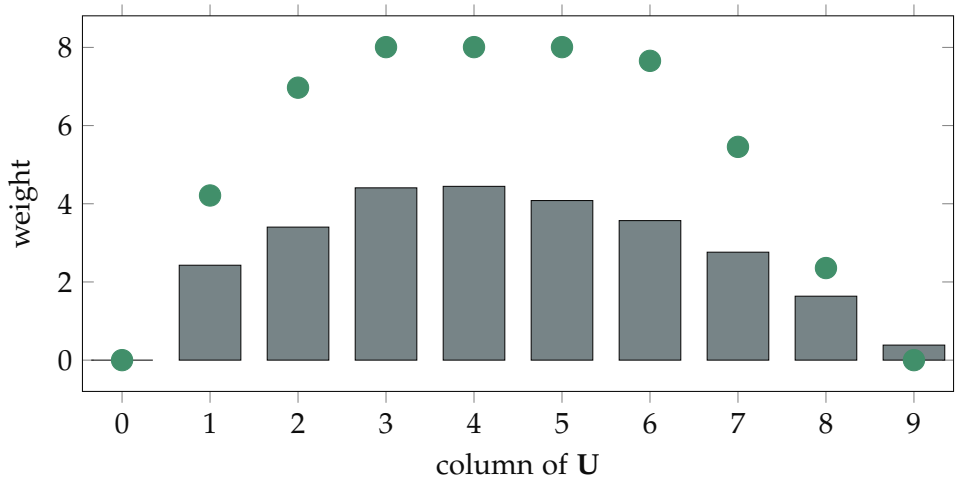

(a) Weights given to candidate parameters in **U** for $\frac{dz}{dt}$

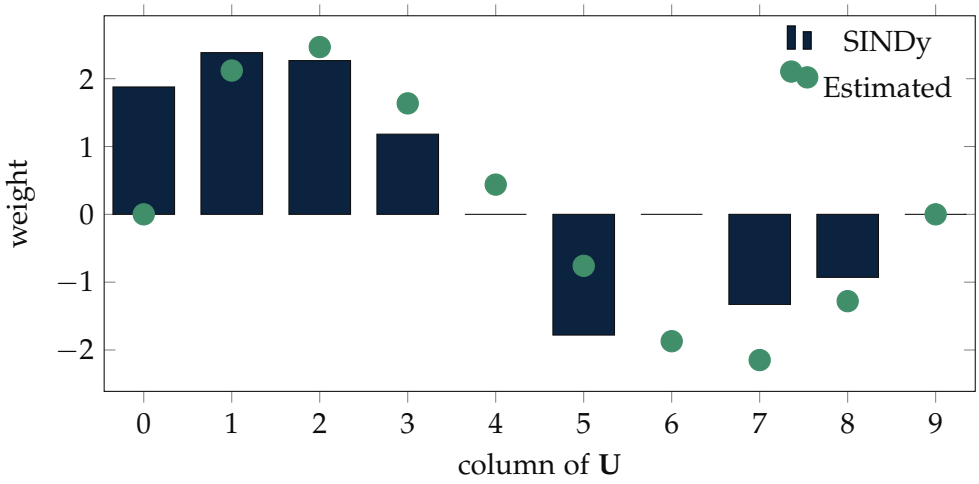

(b) Weights given to candidate parameters in **U** for $\frac{d\theta}{dt}$

Figure 7.2: Weights of the wave elevations over the hull shows that SINDy identifies the forcing as an integration of the wave elevations over the hull and moment as the forces multiplied by the arm

at the location of the wave elevation. The small weight at the front (corresponding to column 0 in **U**) and back (column 9) of the vessel corresponds to the small waterplane area of the vessel at these locations. To quantitatively check the results an estimation of the weights based on Froude-Krylov forces per wave elevation location is made with $A \cdot \rho \cdot g \cdot e^{-k \cdot d}/(M + a)$. A is the area around the wave elevation location at the waterline, k the wave number based on the peak period, M is the models mass (11 kg), and a the added mass, which is estimated to be equal to the model mass. The weights found by SINDy follow the general trend of the estimated weights, but the values of the estimated weights are on average 1.8 times larger. Both the forcing and spring coefficients are underestimated by SINDy. The wave forcing and restoring spring forces are of similar periodicity for heave. The similarity results in unclearity in the source during optimization, causing leakage between the components. Since the forces are opposite and similar, the underestimation of the one will be compensated in the optimization process by reducing the other, causing both to be over- or underestimated.

Figure 7.2b shows that the weights in front of the centre of gravity are positive and after the centre of gravity negative. Additionally, the quantity of the weights is smaller closer to the center of gravity. Combined with the results of figure 7.2a it is concluded that the weights in figure 7.2b correspond to the moment induced by the waves. Indeed the weights follow the estimated weights for the moments, calculated by the estimated forces times the arm to the centre of gravity. Again the weights follow the general trend of the estimated weights. The weights for η_4, η_6 and η_9 are zero. For η_4 and η_9 the zero value is expected. For η_4 the arm to the centre of gravity is small, and for η_9 the waterline area is small. The zero value for η_6 is not as easily physically explained. Most likely η_5 and η_6 are similar and the sparsity promoting optimization resulted in a smaller loss for the case where η_6 was set to zero and an increased weight for η_5 to compensate. In other words, most likely the sparsity-promoting optimization resulted in sparsity being promoted.

The regression performed by SINDy has resulted in the identification of equations that resemble a damped mass-spring system with external forcing and a coupling term. These equations are in line with the physics of the seakeeping problem. Quantitative comparison of the coefficients to estimations shows that the coefficients identified by SINDy deviate from the expected values. The periodicity of the components in the equation is similar, causing leakage between the components. The similarity causes the problem to be ill-conditioned. As a result the model shown in equation 7.8 underestimates both the spring and external forcing for heave and overestimates the spring coefficient for pitch.

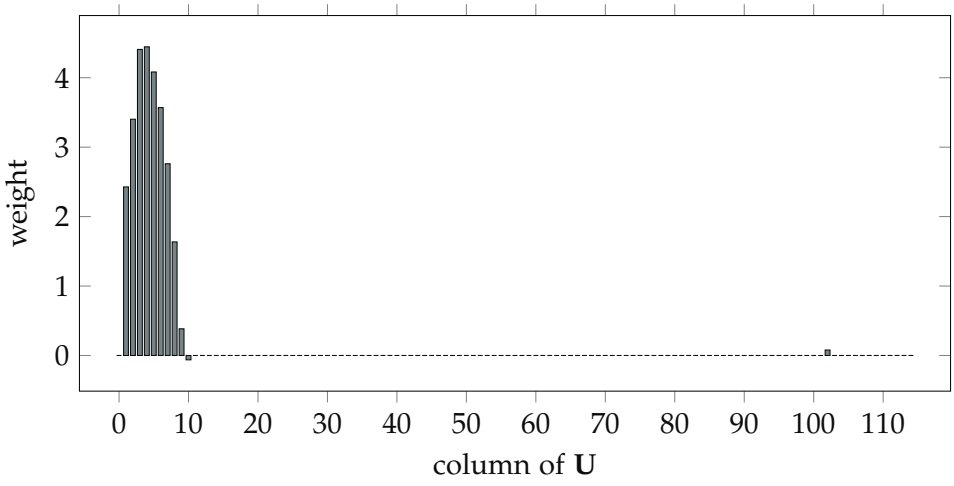

(a) Weights given to candidate parameters in $\mathbf{U}$ for $\frac{d\dot{z}}{dt}$

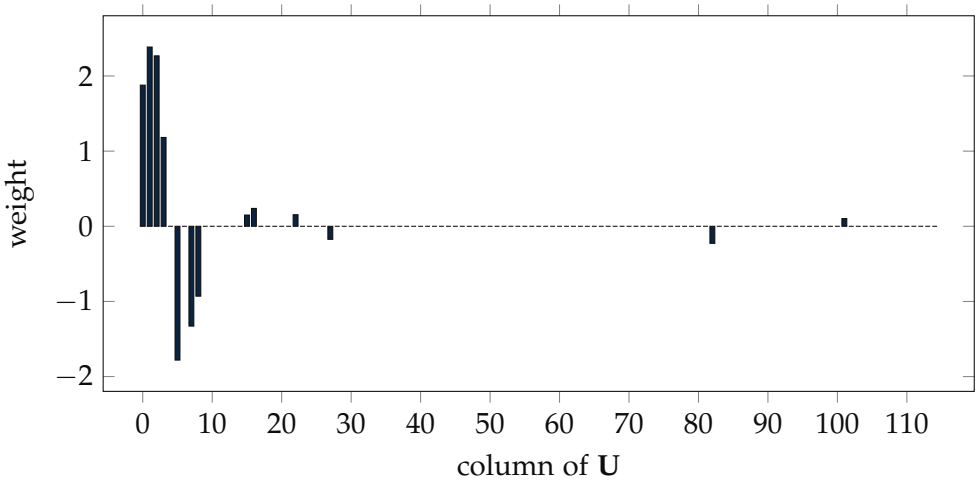

(b) Weights given to candidate parameters in $\mathbf{U}$ for $\frac{d\dot{\theta}}{dt}$

Figure 7.3: Results from applying SINDy with an extended candidate library function including nonlinear terms. The figure shows similar results to those in figure 7.2.

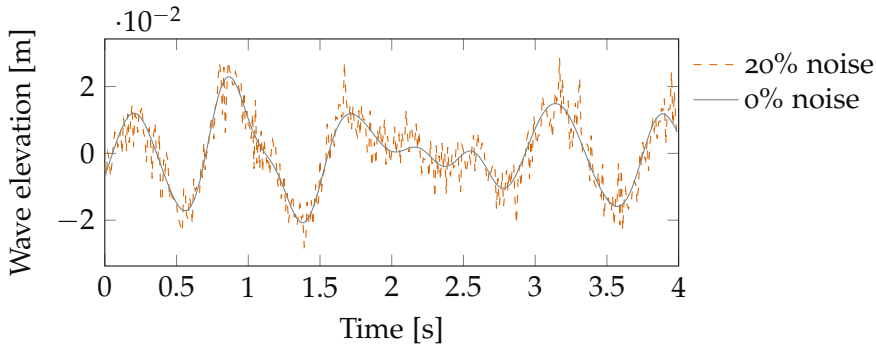

Figure 7.4: Visualization of 20% noise added to the fictitious data

To identify the stability of this solution, the candidate library is extended to include up to quadratic terms.

$$\boldsymbol{\Theta}(\mathbf{X},\mathbf{U}) = [\mathbf{1}^{\mathbf{T}}\mathbf{X}^{\mathbf{T}}\mathbf{U}^{\mathbf{T}}(\mathbf{X}\otimes\mathbf{X})^{\mathbf{T}}(\mathbf{U}\otimes\mathbf{X})^{\mathbf{T}}(\mathbf{U}\otimes\mathbf{U})^{\mathbf{T}}] \tag{7.9}$$

Note that $\mathbf{U}$ consists of 10 candidate parameters. Adding the nonlinear candidate functions thus increases the number of columns in $\boldsymbol{\Theta}(\mathbf{X},\mathbf{U})$ from 15 to 120. The results in figure 7.3 show that even with eight times more candidate parameters in the regression still, only some of the nonlinear terms have a small nonzero weight, as is correct for this linear system.

Noise is added to further check the stability of the results. Normally distributed noise around zero is added to all data. The standard deviation of the noise varies from 0 to 0.01, equal to 0 to 20% of the significant wave amplitude. The level of noise is visualized in figure 7.4. The linear candidate functions are used. Figure 7.5 shows the effect the noise has on the identified solution. For noise with a standard deviation above 8% of the significant wave amplitude the sparsity of $\{\frac{dz}{dt}, \frac{d\theta}{dt}\}$ becomes one, indicating that for either $\frac{dz}{dt}$ or $\frac{d\theta}{dt}$ the solution is zero. The sparsity for $\{\frac{d\dot{z}}{dt}, \frac{d\dot{\theta}}{dt}\}$ changes with the noise. Figure 7.5 shows that as the noise increases, more terms are activated. Figure 7.7 shows the activation of the spring, damping and coupling terms. With the increase of noise overall more terms are activated, but the weight per term decreases. These results are in line with the leakage between terms discussed before. The increased spreading of the weights with increased noise indicates that leakage is aggravated by noise.

To evaluate the effect of random noise on the reconstruction of the force and moment, the weights given to the wave components are visualized in figure 7.6. Figure 7.6a shows that for all levels of noise, the forces are reconstructed to some extent. For increasing noise levels the total weight given to wave elevations decreases, indicating energy leakage from the forcing to other

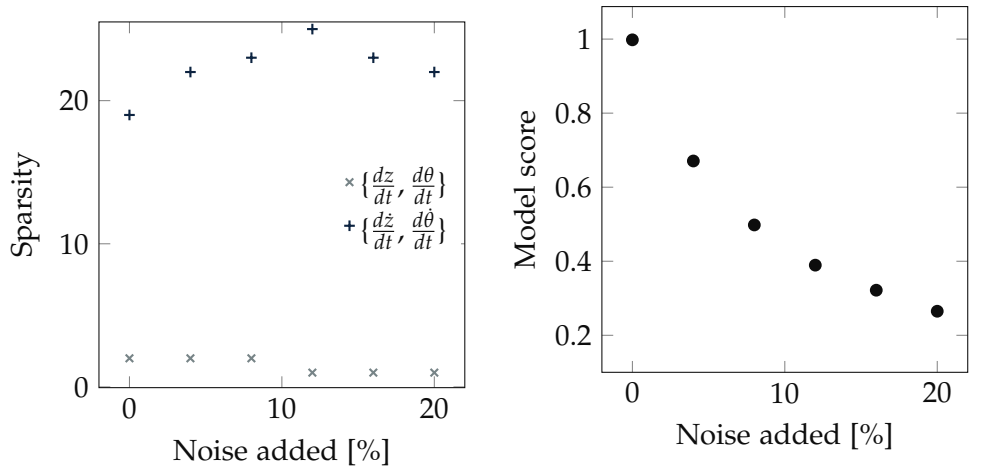

(a) Relation between the sparsity of the solution and random noise added to input data

(b) Relation between model score and random noise added to input data. Note that noise is also added to the testing data, reducing the model score

Figure 7.5: The effect of random noise added to the input data on the solution identified by SINDy. Noise is given as the percentage of the standard deviation of noise to the significant wave amplitude

parameters. The reconstruction of the moments, shown in figure 7.6b is more noise-sensitive. At the lowest noise level of 4%, the moments are no longer identifiable, indicating that the reconstruction of physics is sensitive to noise. SINDy's sensitivity to noise is in line with literature as Hoffmann, Fröhner and Noé [181] and Sandoz, Ducret, Gottwald *et al.* [172] also found that for SINDy increasing noise levels can interfere with successful model discovery. In the seakeeping problem, the periodicity of the inputs are similar, causing leakage. This leakage makes the problem at hand specifically sensitive to noise.

7.2.3 *Projecting wave measurements*

The above shows that the ODE for heave and pitch acceleration with only time domain components can be identified with SINDy for fictitious data. The next step is to test if a physically relevant model can also be obtained from the experimental data discussed in the previous chapters. The measurements within these data sets are, however, not directly suitable for the problem setup considered. The wave elevations were only measured at one location. This measurement location was at the height of the bow but far to the side to measure the undisturbed incoming wave. As the undisturbed wave is only

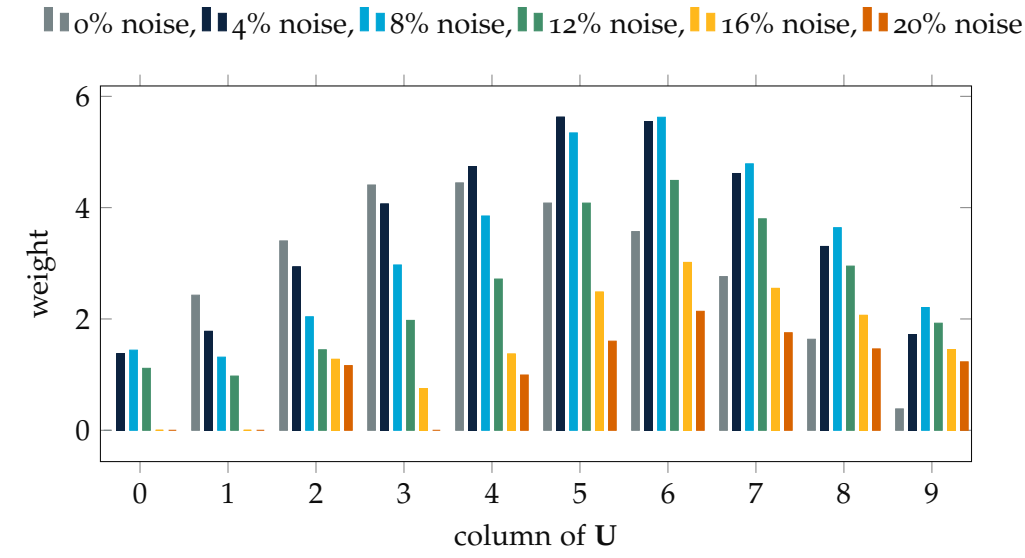

(a) Effect of random noise on the weights given to candidate parameters in $\mathbf{U}$ for $\frac{d\dot{z}}{dt}$

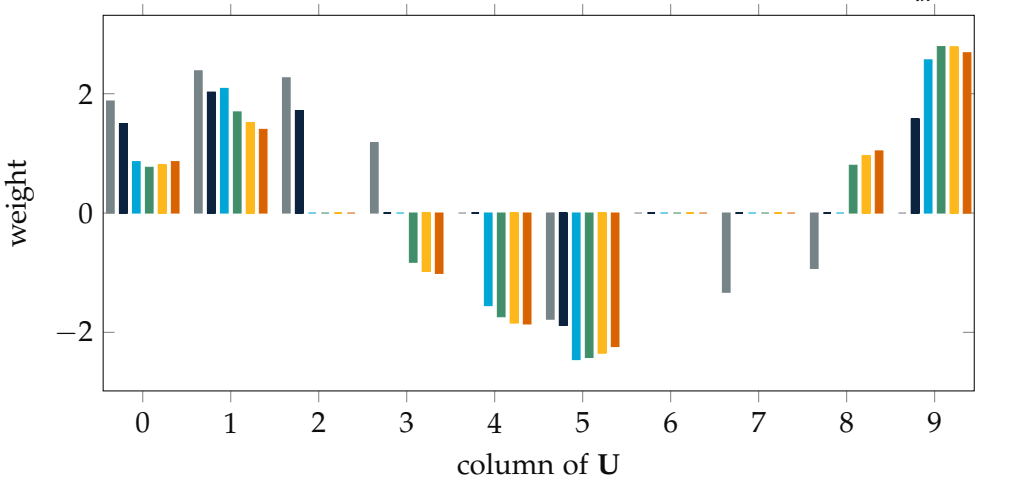

(b) Effect of random noise on the weights given to candidate parameters in $\mathbf{U}$ for $\frac{d\dot{\theta}}{dt}$

Figure 7.6: The reconstruction of forcing and moments through weights of the wave elevations over the hull are sensitive to random noise added to the input data

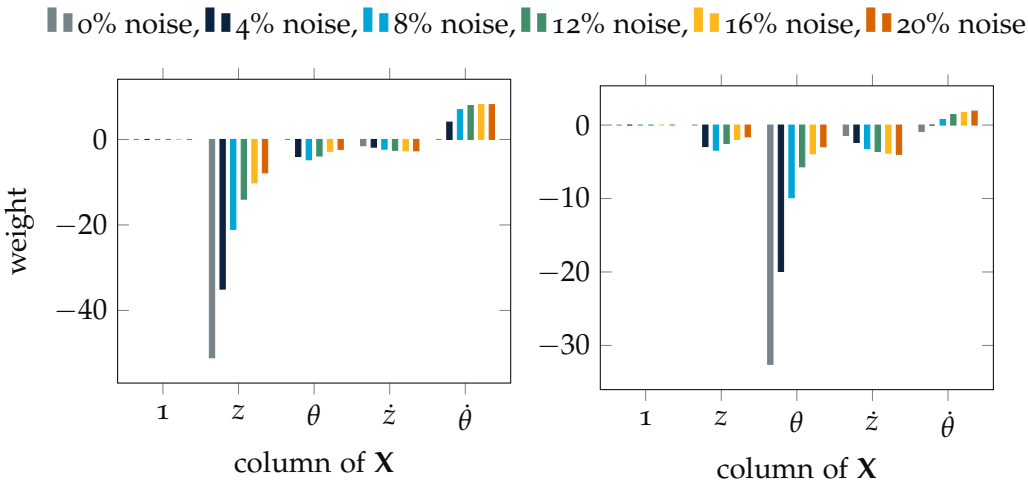

(a) Effect of random noise on the weights given to state parameters in $\mathbf{X}$ for $\frac{d\dot{z}}{dt}$

(b) Effect of random noise on the weights given to state parameters in $\mathbf{X}$ for $\frac{d\dot{\theta}}{dt}$

Figure 7.7: The the spring, damping and coupling terms are sensitive to random noise added to the input data

measured at one location the wave elevations over the other locations on the hull will need to be calculated based on this single measurement location.

From the measurements at a single location the wave elevations at other locations can be calculated. Figure 7.8 shows schematically the setup for projecting the measured waves from the time to the space domain. Assuming linear stable waves, a sea state is a summation of linear waves. By performing Fourier analysis of the wave trace the wave frequencies, amplitudes and phases can be obtained. With this information, the wave elevations at various locations on the ship's hull can be calculated. For the Fourier analysis, the Fast Fourier Transform is used (FFT). The wave measurements were taken with relative forward velocity, so in the projections, the Doppler effect is accounted for.

Theoretically projecting a single wave measurement of perfectly linear, stable waves to various other locations should give the exact same result as the wave realizations on that location from the previous section. There are however some practical limitations. A practical limitation is that a limited frequency resolution is used. A second limitation is that a finite time length is used over irregular waves. For most waves, this will result in not a whole number of wave periods within the time window. With the Fourier analysis, this will cause spectral leakage: energy at a certain frequency will be attributed to neighbouring frequencies, causing changing the amplitudes and phases

found at those frequencies. Applying a window function before the Fourier transform reduces spectral leakage as the difference of the wave component between the start and end of the time signal is reduced. For the reduction of spectral leakage the Tukey window is implemented with a cosine lobe width of 10% of the total length of the signal.

In the experiments, the waves are nonlinear due to shallow water effects and wave-wave interaction. This will cause phase locking of higher frequency components and transfer of energy to different wave frequencies. To allow for nonlinearities in the projecting, local windowed FFT is applied. With local windowed FFT only the Fourier transform of a short time duration is taken instead of the full time signal. By only projecting over a shorter time interval inaccuracies due to time variations and nonlinearity are limited. The local windowed FFT is applied every second, and the identified waves are projected assuming linearity at a frequency of 100 Hz over 10 locations on the ship's hull. The ramp-up of the Tukey window should not overlap with the relevant data, thus a time shift is implemented. The time interval length of 50 seconds is chosen with a 5-second shift, schematically shown in figure 7.8.

Before further steps are taken the errors due to projecting of the waves are quantified. The root mean square error (RMSE) for a 500-second long projection of linear fictitious waves is 0.00219 m. The projection quality for waves in the test facility is also quantified. Measurements in the wave current tank, described in chapter 2, for an irregular wave spectrum of $T_p = 1.17$ s, $H_{m0} = 0.011$ m and $U = 0.25$ m/s are used. The measurement location of the two wave probes is 2.4 m apart. Using the measurements at the most forward wave probe the waves are projected to the second wave probe. The RMSE for a 40-second long projection is 0.0025 m. Figure 7.9 visualizes the quality of the projection for experimental measurements. The local windowed FFT results in accurate wave projections and thus the method is used to project the wave elevations over the ship hull.

7.2.4 *Pre-processing data*

Before the SINDy can be applied to the experimental data, the data has to be prepared. The published experimental data sets are used [1], [146]. In total, these data sets contain over 246 hours of experimental data over 23 different testing conditions and different test setups. Not all the test setups resulted in suitable data. Some test setups allowed for the ship model to surge. Even though the model surged, the wave elevation probe was fixed in place. This results in varying locations of measurements relative to the ship model and thus test cases where the model was free to surge are eliminated. As the

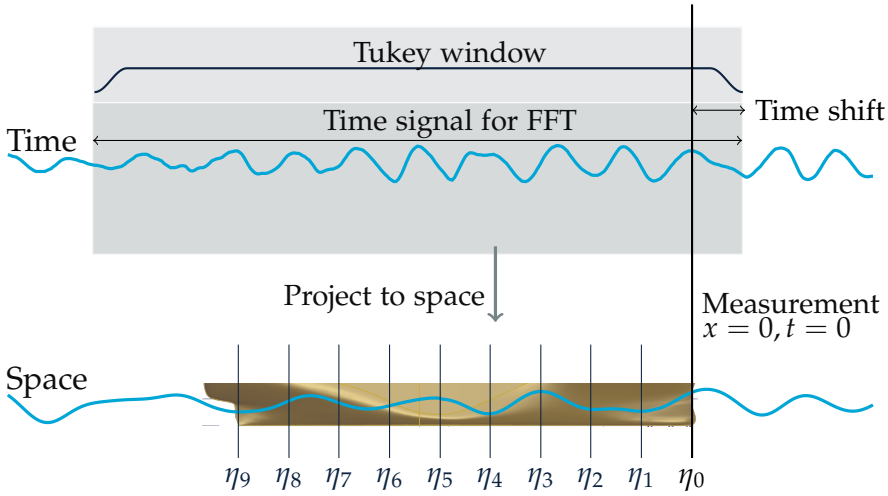

Figure 7.8: Schematic representation of the projection of a time trace of wave elevations at a single location to various locations along the ship using local windowed FFT

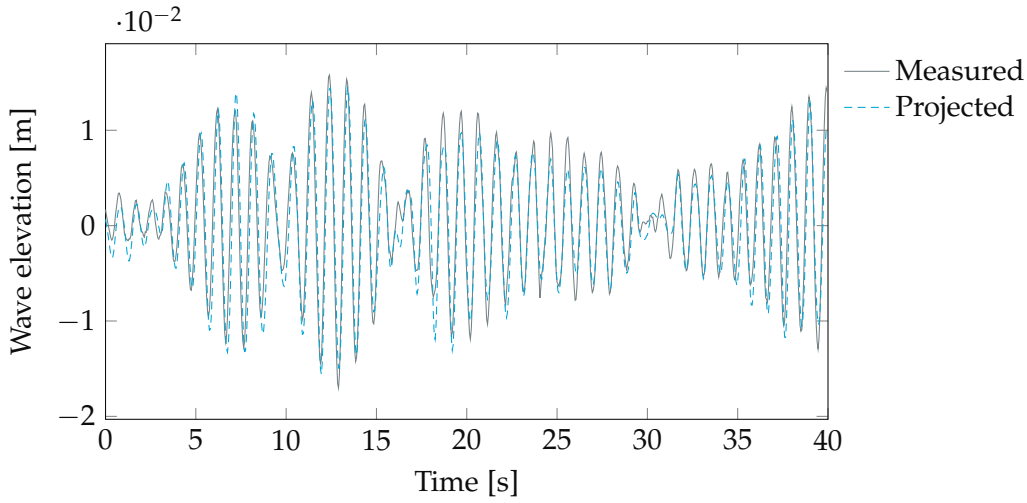

Figure 7.9: Quality of projecting waves with local windowed FFT visualized. Measurements projected to second wave probe compared to actual measurements at wave probe

reconstruction of physics is sensitive to noise, as shown in figure 7.6, all data is filtered with a 2nd order low pass filter at 8 Hz.

To allow for easier use of the data, the data is separated in batches each containing all input parameters, but only part of the measurement time. An appropriate time length should be chosen to store in the batches. The dynamics of the ship depend on the waves and the wave history, but not the full time history of the waves is equally important. With the impulse response function (IRF) the time traces of the waves relevant to the ship's motions are calculated. The function decays to zero as the time since the waves passed increases. The impulse response function for the ship motions is calculated with a damping matrix resulting in the impulse response over the time [175], [182]. 50 seconds into the wave history the impulse response function for both heave and pitch is less than 1% of the impulse response of the instantaneous waves. Using 50 seconds as an indicator for the minimal length of the time traces, a time trace length of 500 seconds for each batch is used.

7.3 RESULTS

With the data prepared the next step is to apply SINDy to the experimental data. Even though the problem setup for the fictitious and experimental data is similar, there are bespoke differences. First of all, the experimental data contains the full physics, with known and unknown non-linearity and coupling. Besides actual physics, the experimental data also contains noise and biases. This noise and biases are for instance introduced through the test setup and sensors. Examples are natural frequencies of the test setup and noise from the electrical net. The experimental data was not obtained with the use of machine learning in mind, and as such not all the necessary parameters were measured. To compensate for the missing parameters the waves are projected and the second derivatives of the heave and pitch motions are used as the accelerations. Both introduce further bias and noise into the data set. The differences between the fictitious and experimental data are expected to affect the quality of the identified models.

To apply SINDy to the experimental data, the data is split into training and testing data sets at random, with 80% of the data becoming training data. The same inputs are used for the state matrix, candidate forcing matrix and candidate library as in the fictitious test case. $\mathbf{X}$ contains the heave and pitch motions and velocities, $\mathbf{U}$ the wave elevations at 10 locations of the hull, and the candidate library is shown in equation 7.5. As the experiments lasted for hours the training data includes at least 10 000 wave encounters per test case. The naming conventions of the previous chapters are used for the test cases.

Table 7.1: Model scores for the models trained with experimental data per test case

Test	Model score
1	0.944
1a	0.961
1b	0.959
1c	0.952
2	0.923
3	0.933
4	0.964
4 D+	0.973
4 D-	0.936
4a	0.455
5	0.946
$s_{op} = 0.030$	0.911
$s_{op} = 0.037$	0.938
$s_{op} = 0.042$	0.941

For each case, models are generated with SINDy. For all test cases the solution $\frac{dz}{dt} = \dot{z}$ and $\frac{d\theta}{dt} = \dot{\theta}$ is found. The model scores are shown in table 7.1. It should be highlighted that the model scores are calculated by substituting the known values of the parameters instead of starting with only initial conditions, limiting accumulative errors. The high model scores are caused by the correct equations identified for the velocities, so the modelling for half of the data is perfect. The score for test 4a thus indicates that the model identified for the accelerations fit poorly for the testing data.

Figure 7.10 shows the weights for the columns of $\mathbf{U}$: the time traces of the wave elevation on 10 locations on the hull. The expectation is that the weights found will show the same trends as the weights in figure 7.2. This is not the case. For test cases 1a, 1b and 1c the weights for the wave elevations forcing heave acceleration seem to be somewhat similar, except that the weight for the wave elevation at the bow, η_0, has become negative. For pitch acceleration, the model for cases 1a, 1b, 1c, and 4 D+ could be argued to follow the expectations, but there is variance and the weights at the centre of gravity are not zero as is expected from the moments. All other test cases result in weights that are not easily explainable.

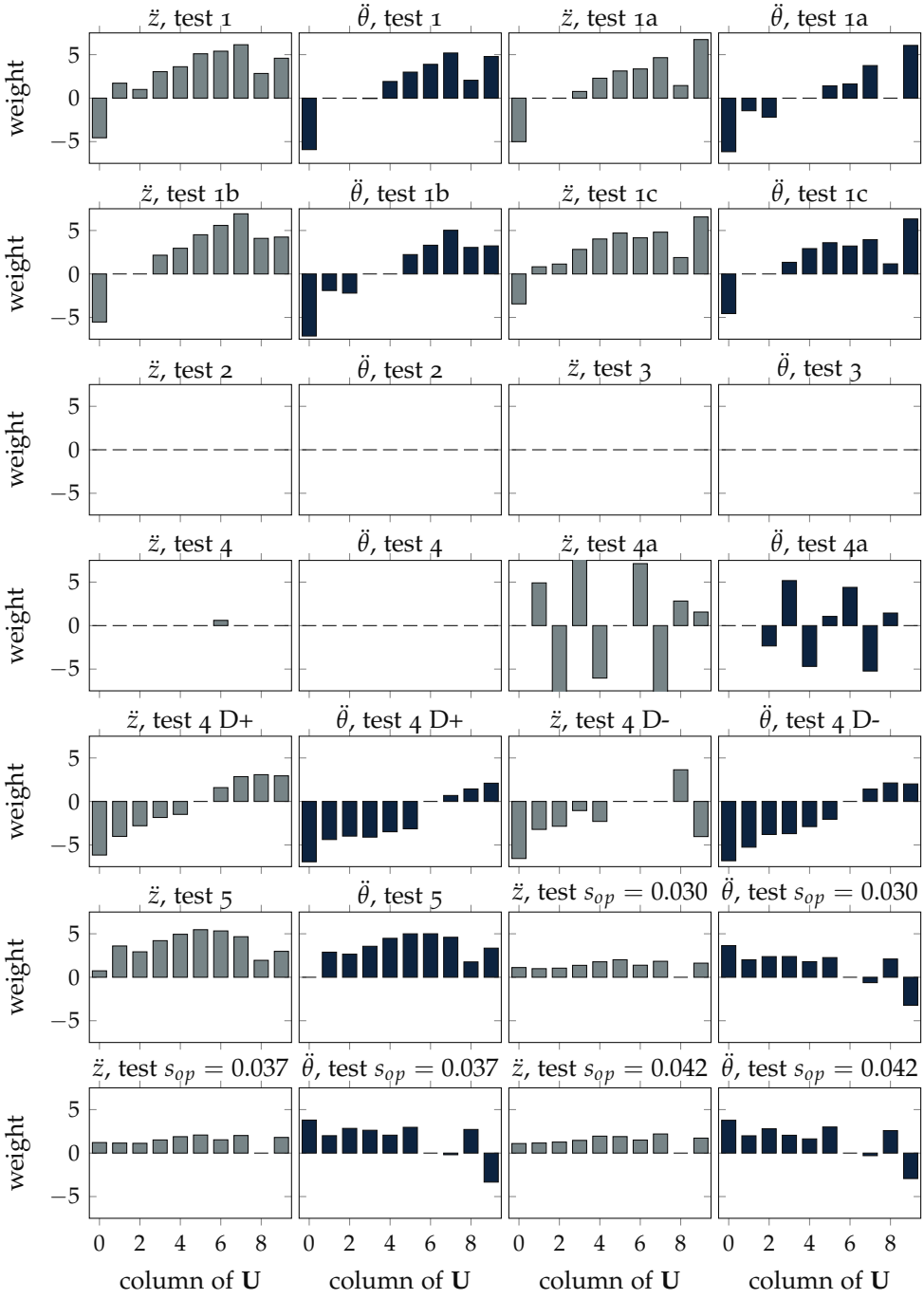

Figure 7.10: Weights of the wave elevations over the hull for experimental data

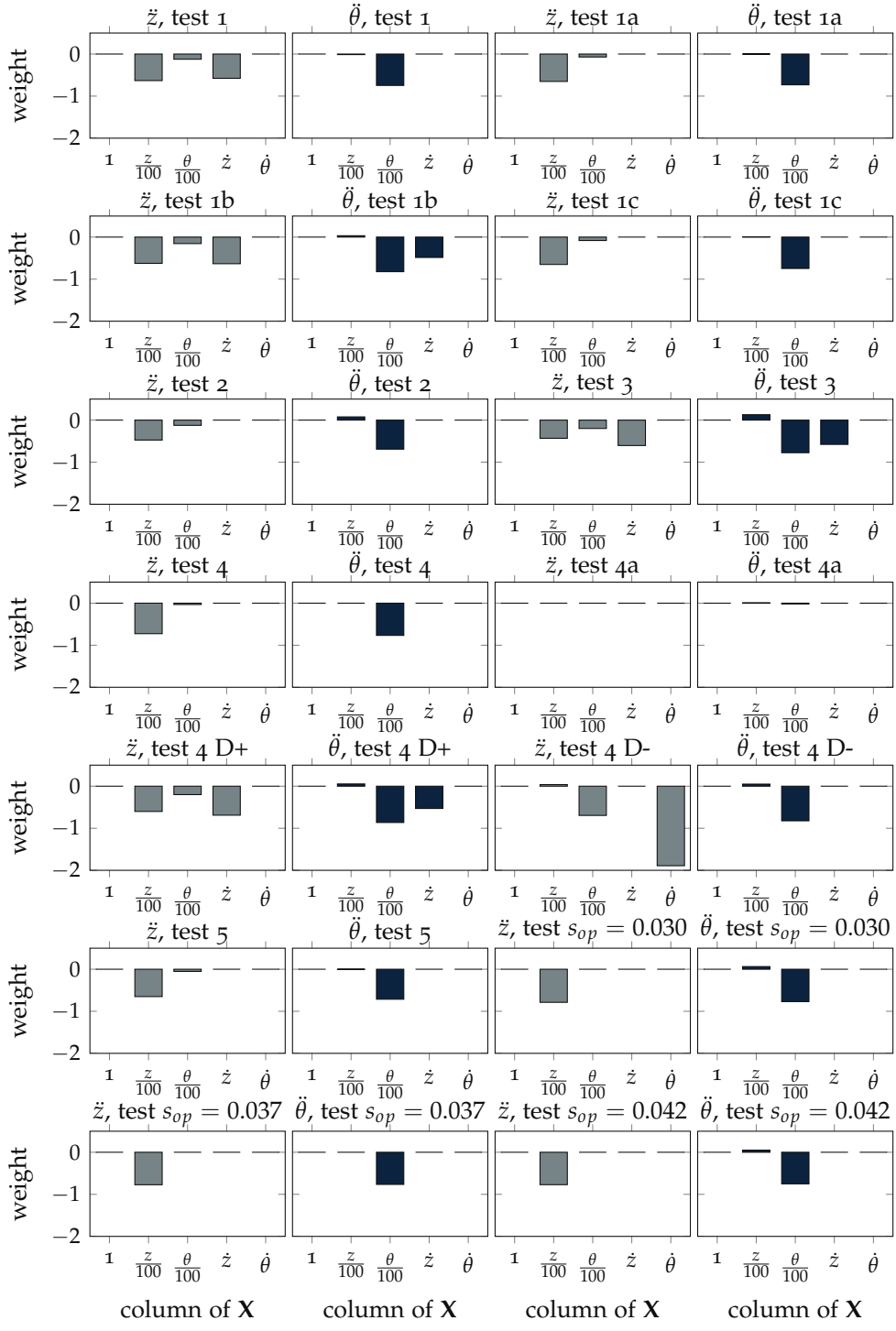

Figure 7.11: Weights of the state parameters indicating activation of the spring, damping and coupling coefficients

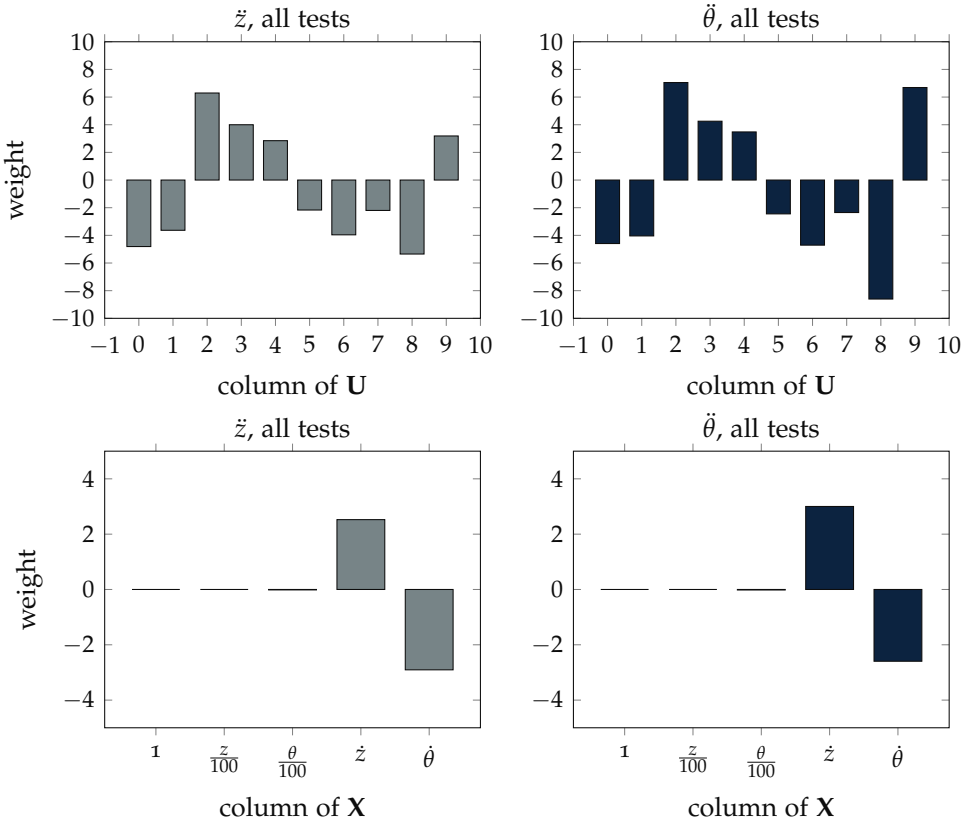

Figure 7.12: Identified coefficients for a model trained on a training set of 110 hours containing data from all tests

Not only the forcing but also the columns of **X** are given weights: the motion and velocity of the heave and pitch. The results are expected to resemble a damped mass-spring system with external forcing. The results are shown in figure 7.11. Due to a difference in value for the motions (z, θ) and velocities $(\dot{z}, \dot{\theta})$ the weights are in different orders of magnitude. For visualization the weights of the motions are divided by 100, the measurement frequency. The weights of the motions correspond to the spring coefficient and the weight of the velocities to the damping coefficient. Both should be identified by SINDy as ships in waves represent a damped mass-spring system with external forcing. However, for the heave acceleration only for tests 1, 1b, 3 and 4 D+ is the expected damping coefficient identified. For the acceleration of the pitch, the damping coefficient is identified for none of the tested cases. The small values for the damping coefficients combined with a sparsity-promoting optimizer and noise in the experimental data can explain why the expected damping coefficient is only identified in 4 out of the 24 equations.

Even though each test case contained a large number of wave encounters, one could argue that more data could improve the quality of the identified models. To be able to train on even more data, the data from all the test cases is combined. A training data set of 110 hours containing over half a million wave encounters is constructed. As was done previously, 20% part of the data was not used for training but used for testing of the model.

The model resulting from training on this large data set is:

$$\begin{aligned}
\frac{dz}{dt} &= 1.02\dot{z} \\
\frac{d\theta}{dt} &= 1.03\dot{\theta} \\
\frac{d\dot{z}}{dt} &= -1.55\theta + 2.53\dot{z} - 2.91\dot{\theta} - 4.81\eta_0 - 3.63\eta_1 + 6.29\eta_2 + 4.00\eta_3 \\
&\quad + 2.85\eta_4 - 2.17\eta_5 - 3.96\eta_6 - 2.20\eta_7 - 5.35\eta_8 + 3.187\eta_9 \\
\frac{d\dot{\theta}}{dt} &= -1.87\theta + 3.00\dot{z} - 2.60\dot{\theta} - 4.59\eta_0 - 4.04\eta_1 + 7.05\eta_2 + 4.25\eta_3 \\
&\quad + 3.48\eta_4 - 2.45\eta_5 - 4.71\eta_6 - 2.35\eta_7 - 8.61\eta_8 + 6.69\eta_9
\end{aligned} \tag{7.10}$$

The model score for the equation is 0.41, indicating that the identified model fits poorly. The equations for the velocities are correctly identified. The equations of interest (the equations for the acceleration of heave and pitch) do contain the expected spring and damping coefficients, as well as coupling. The spring coefficients identified are an order of magnitude smaller than the spring coefficient in the model for the fictitious case. The reconstruction of the force and moment is not identifiable from figure 7.12. The reconstruction of external forcing for the heave and pitch acceleration show again similarities, as is also seen in figure 7.12. The similarity could indicate that the problem is ill-conditioned due to the coupling of the heave and pitch motions.

As shown in figure 7.6, the reconstruction of physics is sensitive to noise. Even though the data is filtered, the experimental data will still contain noise. On top of the noise, experimental data contains biases. Due to the projecting of waves, the method introduces additional bias through the assumption of linearity. The equations identified by SINDy are most likely not representative of the physics of interest.

The noise as a failure point in model discovery by applying SINDy to experimental data is known [169], [180]. Noise is especially challenging for spatio-temporal systems governed by PDEs as noise is amplified by higher order derivatives [176]. In the investigated problem second-order derivatives are used, causing this noise amplification. Work is being conducted to improve the noise robustness of SINDy. Various extensions to the method to improve

robustness are proposed, but these methods require further characterization, exploitation and integration [176], [183], [184].

7.4 CONCLUSION

Large experimental data sets have been combined with a machine learning method: SINDy. The goal was to investigate the possibility of combining this machine learning method with the large experimental data set available. The models are trained to predict the acceleration of heave and pitch with the parameters heave, pitch, velocity of heave and pitch and the wave elevations along the hull.

The defined problem sets out to identify the ODE for the heave and pitch acceleration with only time domain components. Initially, fictitious data is used to train the model. The data is based on empirical response amplitude operators. The SINDy model identifies the relevant terms expected for the damped mass-spring system with external forcing for the fictitious data set, which can be considered to represent perfect experimental measurements. The weights found for the waves over the ship hull reconstruct the forcing and moments expected. Quantitative analysis of the weights does reveal deviations from the physical coefficients. The differences are contributed to the defined problem being ill-conditioned due to the similarity between the components. Tests with random noise added to the fictitious data show that the success of identifying the damped mass-spring system with external forcing is sensitive to noise.

Models have also been trained on the experimental data available. The resulting models fail to identify the damped mass-spring system with external forcing from the experimental data as for most no damping term is included. Also, the external forcing does not show the reconstruction of the force and moment found for the fictitious data. The likely cause for the lack of success in generating physically meaningful models from experimental data is the noise in the experimental data.

8

CONCLUSION

Extreme wave impacts on ships should be minimized to reduce the risks posed by these impacts. Literature review shows that the combined rarity and complexity of impacts have resulted in a limited number of impacts per study in previous research. As a result, there were unanswered questions about probabilities, distributions and ranges in which impacts occur.

The goal of this thesis was to determine the statistics of extreme wave impacts. First, a large experimental data set was collected. Because of the rarity of extreme wave impacts long testing times are needed, so a new testing facility was created by extending an existing recirculating tank. By adding a wave maker to the recirculating tank, water and waves flow past a ship model, allowing for long testing times. Large experimental data sets with a ship with forward velocity in head waves are collected. To limit the research scope, the main focus is on green water impacts, with slamming impacts considered through the Ochi criterion. The collected data is 246 hours of experimental data over 23 test cases, representing over 2766 hours of continuous sailing at full scale. The data is published open access [1], [146].

8.1 INSIGHTS FROM EXPERIMENTAL DATA

From the experimental data statistical distributions of extreme wave impacts and their dependencies are obtained. Green water impact pressures on a ship's deck and superstructure are found to be Fréchet distributed, a type of general extreme value distribution. The Fréchet distribution fits for all tested cases for both maximum and averaged pressures.

The probability distribution for the time between green water impacts was initially identified to be exponentially distributed. The exponential distribution fitting indicates that green water impacts occur independently, a fundamental notion in statistics. However, results from experiments in more severe waves found that the exponential distribution does not fit. In these experiments, green water was found to form clusters of impacts, with mul-

tiple impacts occurring consecutively. Literature has identified clusters of impacts for slamming. However, in the conducted experiments where green water impacts clustered, slamming impacts do not cluster. In these tests, the probability of slamming is low, lower than the probability of slamming in the literature that identified clusters for slamming. By comparing the probability of occurrence and the occurrence of clusters in various studies a threshold for clustering is identified.

The threshold for when impacts form clusters is based on the probability of an impact. Below the threshold impacts occur independently and above the threshold clusters occur. The occurrence of clusters and the probability of impacts are correlated. The correlation stems from shared causation: both clusters and probability of occurrence depend on the pitch motion of the ship. A large pitch motion out of phase with the wave causes an impact. As this large pitch motion builds up or damps out additional impacts are likely to occur, creating a cluster of impacts.

Pitch is not only identified to be related to clustering but a large forward pitch motion is found to be a defining feature of green water. In literature water exceeding deck level is often equated to green water, but not all exceedance events develop into potentially harmful green water impacts. A difference between green water and exceedance is the pitch. During an exceedance event that does not develop into green water, the pitch of the ship is neutral. For green water, a large forward pitch is measured during impacts. This distinction is used to develop a prediction method that only considers green water, instead of all exceedance events.

With the novel test facility also a common way to mitigate green water is tested. Increasing the freeboard at the bow of a ship is an intuitive method for reducing green water, as water has to travel further up before flowing onto the deck. Tests that compared ship models with and without extended freeboard show that increasing freeboard decreases the probability of impacts, as expected. However, increasing freeboard increases the impact pressures of the rarest events. An increased freeboard only allows water with larger potential energy to flow on deck and lead to an impact, as low potential energy water is obstructed by the increased freeboard. As a result, the impact pressures for large impacts are increased by increasing the freeboard. These results show the importance of considering statistical distributions.

The large data sets have also been used in combination with machine learning. Sparse Identification of Nonlinear Dynamics (SINDy) has been used to work towards a model to predict the acceleration of the heave and pitch based on the parameters heave, pitch, velocity of heave and pitch and the wave elevations along the hull. SINDy has been able to reconstruct the damped mass-spring system with external forcing when trained on fictitious data

without noise. Random noise has been added to the fictitious input data. If the physics are successfully captured by the model is sensitive to noise. Models are also trained on experimental data, and the resulting models did not represent a damped mass-spring system with external forcing. The likely cause is the noise in the experimental data. These result shows that the combination of machine learning and large data sets can be a powerful tool, but for machine learning to be applicable special care should be taken during the conducting of experiments to ensure the needed data quality is reached. Further work on improving the noise robustness in the algorithms for model identification can ease the burden on experiments in the future.

8.2 FUTURE OUTLOOK

In experimental extreme wave impact research, most experiments are conducted at model scale. Scaling effects are scarcely mentioned, as the effect of scaling is not clear. Experiments for extreme wave impacts are Froude scaled. By applying Froude scaling an assumption is made that gravity and inertia are the main physics at play during an impact. For the occurrence of extreme wave impacts this assumption is valid, as ship motions and waves lead to an occurrence. However, during the flow dynamics of an extreme wave impact, air entrainment will affect the density ratio and compressibility, cavitation can occur and surface tension and viscosity come into play during flow and impact. The effect of scaling on the flow and pressures of impacts is not clear, and the complexity and variety of extreme wave impacts make it plausible that the effects can never be accounted for.

The scaling problem means that the applicability of experimental results is limited, as either scaling is applied or, as is the case for full scale, the environmental conditions are not accurately measured. The complexity and rarity of extreme wave impacts also limit the applicability of analytical and numerical methods. With all the scientific paradigms deemed inadequate, the only path forward is to combine analytical, numerical and experimental methods with, for example, multi-fidelity methods. By combining methods, the weaknesses of each method can be compensated for by the strength of another method. By combining analytical, numerical and experimental methods minimizing extreme wave impacts could become possible.

BIBLIOGRAPHY

[1] A. Boon and P. Wellens, 'Large experimental data set for extreme wave impacts on s175 ship with and without surge and with various bow drafts and freeboards', *4TU.ResearchData*, 2024. DOI: 10.4121/15f0d739-b84c-48f3-879a-68c08f068ab3. [Online]. Available: https://doi.org/10.4121/15f0d739-b84c-48f3-879a-68c08f068ab3.

[2] G. Brown, *Verhalen over scheveningen, scheveningers vertellen de mooiste verhalen*. [Online]. Available: https://www.allesoverscheveningen.nl/verhalen/view-subverhaal.php?sel=sub&verhaal_id=8666&subverhaal_id=270..

[3] M. Fernandez, *Cruise ship passengers recount deadly waves*, 2010. [Online]. Available: https://www.nbcnews.com/id/wbna35706695.

[4] D. Ricciardi, *Warning Light*. Penguin, 2018, ISBN: 0399585745.

[5] *Zeilen*, 2019. [Online]. Available: https://nl.scoutwiki.org/Zeilen.

[6] *Nautical advice for waves while sailing in croatia*, 2022. [Online]. Available: https://www.angelina.hr/en/blog/nautical-advice-for-waves-while-sailing-in-croatia.

[7] D. Marine, *Marinekommando jahresbericht 2022*, 2022. [Online]. Available: https://www.bundeswehr.de/de/organisation/marine/aktuelles/jahresbericht-marinekommando-2022-5511912.

[8] L. M. Millefiori, P. Braca, D. Zissis *et al.*, 'Covid-19 impact on global maritime mobility', *Scientific Reports*, vol. 11, 1 2021, ISSN: 20452322. DOI: 10.1038/s41598-021-97461-7.

[9] E. Didenkulova, 'Catalogue of rogue waves occurred in the world ocean from 2011 to 2018 reported by mass media sources', *Ocean and Coastal Management*, vol. 188, 2020, ISSN: 09645691. DOI: 10.1016/j.ocecoaman.2019.105076.

[10] G. P. Filip, W. Xu and K. J. Maki, 'Prediction of extreme wave slamming loads on a fixed platform', *Proceedings of the International Conference on Offshore Mechanics and Arctic Engineering - OMAE*, vol. 2, p. 2018, 2018. DOI: 10.1115/OMAE2018-78179.

[11] W.-L. Chuang, K.-A. Chang and R. Mercier, *Review of Experimental Modeling of Green Water in Laboratories*. 2019, ISBN: 9781880653852. [Online]. Available: www.isope.org.

[12] B. Buchner, 'Green water on ship-type offshore structures', 2002. [Online]. Available: https://repository.tudelft.nl/islandora/object/uuid%3Af0c0bd67-d52a-4b79-8451-1279629a5b80.

[13] F. Dias and J. M. Ghidaglia, 'Slamming: Recent progress in the evaluation of impact pressures', *Annual Review of Fluid Mechanics*, vol. 50, pp. 243–273, 2018, ISSN: 00664189. DOI: 10.1146/annurev-fluid-010816-060121.

[14] I. Watanabe, M. Ueno and H. Sawada, 'Effects of bow flare shape to the wave loads of a container ship', *1989*, ISSN: 0514-8499.

[15] M. Greco, G. Colicchio and O. M. Faltinsen, 'Shipping of water on a two-dimensional structure. part 2', *Journal of Fluid Mechanics*, vol. 581, pp. 309–332, 2007, ISSN: 00221120. DOI: 10.1017/S0022112004002691.

[16] J. V. Hernández-Fontes, E. Mendoza, I. D. Hernández *et al.*, 'A detailed description of flow-deck interaction in consecutive green water events', *Journal of Offshore Mechanics and Arctic Engineering*, vol. 143, 4 2021, ISSN: 1528896X. DOI: 10.1115/1.4049121.

[17] R. B. Kudupudi, R. Datta and C. G. Soares, 'Modelling green water loads on ships using coupled impulse response function and cfd solution', *Ocean Engineering*, vol. 281, p. 114 918, 2023, ISSN: 0029-8018. DOI: 10.1016/J.OCEANENG.2023.114918.

[18] B Buchner, 'The impact of green water on fpso design', Offshore technology conference, 1995. DOI: 10.4043/7698-MS.

[19] K. Ariyarathne, K. A. Chang and R. Mercier, 'Green water impact pressure on a three-dimensional model structure', *Experiments in Fluids*, vol. 53, pp. 1879–1894, 6 2012, ISSN: 07234864. DOI: 10.1007/s00348-012-1399-9. [Online]. Available: https://link.springer.com/article/10.1007/s00348-012-1399-9.

[20] M. Greco, M. Landrini and O. M. Faltinsen, 'Impact flows and loads on ship-deck structures', *Journal of Fluids and Structures*, vol. 19, pp. 251–275, 3 2004, ISSN: 08899746. DOI: 10.1016/j.jfluidstructs.2003.12.009.

[21] M. Greco, 'A two-dimensional study of green-water loading', *PhD Thesis, Department of Marine Hydrodynamics, Norwegian University of Science and Technology*, p. 163, 1305 2001.

[22] M. Greco, B. Bouscasse and C. Lugni, '3-d seakeeping analysis with water on deck and slamming. part 2: Experiments and physical investigation', *Journal of Fluids and Structures*, vol. 33, pp. 148–179, 2012, ISSN: 08899746. DOI: 10.1016/j.jfluidstructs.2012.05.009.

[23] M. K. Ochi and L. E. Motter, 'Prediction of slamming characteristics and hull responses for ship design', *David Taylor Model Basin, Naval Ship Research and Development Center, Washington D.C., USA, Paper 4 of the Annual Meeting of the Society of Naval Architects and Marine Engineers, SNAME Transactions 1973, Paper: T1973-1 Transactions.*, 1973. [Online]. Available: https://repository.tudelft.nl/islandora/object/uuid%3Acdebae32-2637-4d78-85b0-2ed4e76a22bb.

[24] O. M. Faltinsen, 'Hydroelastic slamming', *Journal of Marine Science and Technology*, vol. 5, pp. 49–65, 2 2000, ISSN: 09484280. DOI: 10.1007/S007730070011.

[25] D. Dessi and E. Ciappi, 'Slamming clustering on fast ships: From impact dynamics to global response analysis', *Ocean Engineering*, vol. 62, pp. 110–122, 2013, ISSN: 0029-8018. DOI: 10.1016/J.OCEANENG.2012.12.051.

[26] G. K. Kapsenberg, 'Slamming of ships: Where are we now?', *Philosophical Transactions of the Royal Society A: Mathematical, Physical and Engineering Sciences*, vol. 369, pp. 2892–2919, 1947 2011, ISSN: 1364503X. DOI: 10.1098/RSTA.2011.0118. [Online]. Available: https://royalsocietypublishing.org/doi/10.1098/rsta.2011.0118.

[27] D. T. Cox and C. P. Scott, 'Exceedance probability for wave overtopping on a fixed deck', *Ocean Engineering*, vol. 28, pp. 707–721, 6 2001, ISSN: 00298018. DOI: 10.1016/S0029-8018(00)00022-6.

[28] C. G. Soares and R. Pascoal, 'Experimental study of the probability distributions of green water on the bow of floating production platforms', *Journal of Offshore Mechanics and Arctic Engineering*, vol. 127, pp. 234–242, 3 2005, ISSN: 08927219. DOI: 10.1115/1.1951773.

[29] W. G. Price and R. E. D. Bishop, *Probabilistic theory of ship dynamics*. Chapman and Hall, 1974, ISBN: 0470697334.

[30] J. J. Jensen and M. Dogliani, 'Wave-induced ship hull vibrations in stochastic seaways', *Marine Structures*, vol. 9, pp. 353–387, 3-4 SPEC. ISS. 1996, ISSN: 09518339. DOI: 10.1016/0951-8339(95)00031-3.

[31] M. Klein, S. Wang, G. Clauss *et al.*, 'Experimental study on the effect of extreme waves on a lng carrier', *Journal of Marine Science and Application*, vol. 22, pp. 52–74, 1 2023, ISSN: 19935048. DOI: 10.1007/S11804-023-00321-1.

[32] O. A. Hermundstad and T. Moan, 'Numerical and experimental analysis of bow flare slamming on a ro-ro vessel in regular oblique waves', *Journal of Marine Science and Technology*, vol. 10, pp. 105–122, 3 2005, ISSN: 09484280. DOI: 10.1007/S00773-005-0192-3.

[33] G. Wang, S. Tang and Y. Shin, 'A direct calculation approach for designing a ship-shaped fpso's bow against wave slamming load', *Proceedings of the International Offshore and Polar Engineering Conference*, vol. 12, 2002, pp. 163–168, ISBN: 1-880653-58-3.

[34] G. Jacobi, G. Thomas, M. R. Davis *et al.*, 'An insight into the slamming behaviour of large high-speed catamarans through full-scale measurements', *Journal of Marine Science and Technology*, vol. 19, pp. 15–32, 1 2014, ISSN: 0948-4280. DOI: 10.1007/s00773-013-0229-y.

[35] N. M. G. Zakaria, *Effect of ship size, forward speed and wave direction on relative wave height of container ships in rough seas*, 2007. [Online]. Available: http://dspace.unimap.edu.my/123456789/13688.

[36] J. Kvalsvold and O. M. Faltinsen, 'Hydroelastic modeling of wet deck slamming on multihull vessels', *Journal of Ship Research*, vol. 39, pp. 225–239, 3 1995, ISSN: 15420604. DOI: 10.5957/JSR.1995.39.3.225.

[37] J. J. Stoker, *Water Waves, the Mathematical Theory with Applications*. John Wiley and Sons, 1957, vol. 36, ISBN: 978-0-471-57034-9.

[38] N. Fonseca and C. G. Soares, 'Experimental investigation of the nonlinear effects on the vertical motions and loads of a containership in regular waves', *Journal of Ship Research*, vol. 48, pp. 118–147, 2 2004, ISSN: 00224502. DOI: 10.5957/jsr.2004.48.2.118.

[39] S. Rajendran, N. Fonseca and C. G. Soares, 'Simplified body nonlinear time domain calculation of vertical ship motions and wave loads in large amplitude waves', *Ocean Engineering*, vol. 107, pp. 157–177, 2015, ISSN: 00298018. DOI: 10.1016/J.OCEANENG.2015.07.050.

[40] K. Goda and T. Miyamoto, 'A study of shipping water pressure on deck by two-dimensional ship model tests', *Journal of the Society of Naval Architects of Japan*, vol. 1976, pp. 16–22, 140 1976, ISSN: 1884-2070. DOI: 10.2534/jjasnaoe1968.1976.140_16. [Online]. Available: http://joi.jlc.jst.go.jp/JST.Journalarchive/jjasnaoe1968/1976.140_16?from=CrossRef.

[41] G. N. Lee, K. H. Jung, S. B. Suh *et al.*, 'Experimental study on variations in behavior of green water and flow kinematics on deck with various flare angles', *Journal of Ocean Engineering and Technology*, vol. 32, pp. 77–83, 2 2018, ISSN: 1225-0767. DOI: 10.26748/ksoe.2018.4.32.2.077.

[42] J. V. Hernández-Fontes, P. de Tarso T. Esperança, J. F. Graniel *et al.*, 'Green water on a fixed structure due to incident bores: Guidelines and database for model validations regarding flow evolution', *Water 2019, Vol. 11, Page 2584*, vol. 11, p. 2584, 12 2019, ISSN: 2073-4441. DOI: 10.3390/W11122584. [Online]. Available: https://www.mdpi.com/2073-4441/11/12/2584/htmhttps://www.mdpi.com/2073-4441/11/12/2584.

[43] J. V. Hernández-Fontes, I. D. Hernández, E. Mendoza *et al.*, 'On the evolution of different types of green water events', *Water*, vol. 13, 9 2021, ISSN: 2073-4441. DOI: 10.3390/W13091148. [Online]. Available: https://www.mdpi.com/2073-4441/13/9/1148/htmhttps://www.mdpi.com/2073-4441/13/9/1148.

[44] J. V. Hernández-Fontes, I. D. Hernández, E. Mendoza *et al.*, 'Green water evolution on a fixed structure induced by incoming wave trains', *Mechanics Based Design of Structures and Machines*, 2020, ISSN: 15397742. DOI: 10.1080/15397734.2020.1791179.

[45] J. V. Hernández-Fontes, L. Torres, E. Mendoza *et al.*, 'Identification of the advection-diffusion equation for predicting green water propagation', *Ocean Engineering*, vol. 214, 2020, ISSN: 00298018. DOI: 10.1016/j.oceaneng.2020.107658.

[46] W. L. Chuang, K. A. Chang and R. Mercier, 'Kinematics and dynamics of green water on a fixed platform in a large wave basin in focusing wave and random wave conditions', *Experiments in Fluids*, vol. 59, p. 100, 6 2018, ISSN: 07234864. DOI: 10.1007/s00348-018-2554-8. [Online]. Available: https://doi.org/10.1007/s00348-018-2554-8.

[47] W. L. Chuang, T. C. Lin and Y. J. Wang, 'Greenwater due to plunging breaking wave impingement on a deck structure. part 1: Experimental investigation on fluid kinematics', *Ocean Engineering*, vol. 287, p. 115 859, 2023, ISSN: 00298018. DOI: 10.1016/j.oceaneng.2023.115859.

[48] H. Wagner, 'Uber stoss- und gleitvorgange an der oberflache von flussigkeiten', *ZAMM - Journal of Applied Mathematics and Mechanics / Zeitschrift fur Angewandte Mathematik und Mechanik*, vol. 12, pp. 193–215, 4 1932. DOI: 10.1002/ZAMM.19320120402.

[49] Z. N. Dobrovol'skaya, 'On some problems of similarity flow of fluid with a free surface', vol. 4, pp. 805–829, 1969. [Online]. Available: https://www.cambridge.org/core/journals/journal-of-fluid-mechanics/article/abs/on-some-problems-of-similarity-flow-of-fluid-with-a-free-surface/8952AC2E20454C9A6540B9ACB94AA0A6.

[50] A. Korobkin, 'Analytical models of water impact', *Journal of Applied Mathematics*, vol. 15, pp. 821–838, 2004. DOI: 10.1017/S0956792504005765. [Online]. Available: https://doi.org/10.1017/S0956792504005765.

[51] Y.-M Scolan, 'Hydroelastic behaviour of a conical shell impacting on a quiescent-free surface of an incompressible liquid', *Journal of Sound and Vibration*, vol. 277, pp. 163–203, 2004. DOI: 10.1016/j.jsv.2003.08.051. [Online]. Available: www.elsevier.com/locate/jsvi.

[52] I. Stenius, A. Rosén, M. Battley *et al.*, 'Experimental hydroelastic characterization of slamming loaded marine panels', *Ocean Engineering*, vol. 74, pp. 1–15, 2013, ISSN: 00298018. DOI: 10.1016/J.OCEANENG.2013.09.007.

[53] A. E. Mansour and J. Lozow, 'Stochastic theory of the slamming response of marine vehicles in random seas', *Journal of Ship Research*, vol. 26, pp. 276–285, 04 1982, ISSN: 0022-4502. DOI: 10.5957/JSR.1982.26.4.276. [Online]. Available: https://onepetro.org/JSR/article/26/04/276/175599/Stochastic-Theory-of-the-Slamming-Response-of.

[54] S. Guth and T. P. Sapsis, 'Machine learning predictors of extreme events occurring in complex dynamical systems', *Entropy*, vol. 21, 10 2019, ISSN: 10994300. DOI: 10.3390/e21100925.

[55] B Hamoudi and K. S. Varyani, 'Significant load and green water on deck of offshore units/vessels', *Ocean Engineering*, vol. 25, pp. 715–731, 8 1998.

[56] C. T. Stansberg and S. I. Karlsen, 'Green sea and water impact on fpso in steep random waves', *Practical Design of Ships and Other Floating Structures*, Elsevier Science Ltd, 2001, pp. 593–601. DOI: 10.1016/B978-008043950-1/50075-2.

[57] R. C. Leibowitz, 'Comparison of theory and experiment for slamming of a dutch destroyer', *David W. Taylor Naval Ship Research and Development Center, Bethesda, Md, USA, Navy Department, Structural Mechanics Laboratory, Research and Development Report 1511*, 1962. [Online]. Available: https://repository.tudelft.nl/islandora/object/uuid%3A2cac1a23-8de0-4d2f-ac50-c7d32a1a6870.

[58] J. W. Wheaton, *Further analysis of slamming data from the s.s. wolverine state*, 1976. [Online]. Available: http://resolver.tudelft.nl/uuid:69cc8e94-b4e4-4f75-825a-34d9067aca91.

[59] P. F. Hansen, 'On combination of slamming-and wave-induced responses', *Journal of Ship Research*, vol. 38, pp. 104–114, 02 1994, ISSN: 0022-4502. DOI: 10.5957/JSR.1994.38.2.104. [Online]. Available: https://onepetro.org/JSR/article/38/02/104/174754/On-Combination-of-Slamming-and-Wave-Induced.

[60] G. Jiao, 'Probabilistic prediction of extreme stress and fatigue damage for ships in slamming conditions', *Marine Structures*, vol. 9, pp. 759–785, 8 1996, ISSN: 0951-8339. DOI: 10.1016/0951-8339(95)00027-5.

[61] E Nikolaidis and P Kaplan, 'Combination of slamming and wave induced motion: A simulation study', *11th International Conference on Offshore Mechanics and Arctic Engineering*, 1992.

[62] T. C. Fu, A. M. Fullerton, E Terrill *et al.*, 'Measurement and modeling of the motions of a high-speed catamaran in waves', *28th International Conference on Ocean, Offshore and Arctic Engineering*, OMAE2009, 2009. DOI: 10.1115/OMAE2009-79810.

[63] P. Temarel, W. Bai, A. Bruns *et al.*, 'Prediction of wave-induced loads on ships: Progress and challenges', *Ocean Engineering*, vol. 119, pp. 274–308, 2016, ISSN: 00298018. DOI: 10.1016/j.oceaneng.2016.03.030.

[64] K. H. Kim, J. S. Bang, J. H. Kim *et al.*, 'Fully coupled bem-fem analysis for ship hydroelasticity in waves', *Marine Structures*, vol. 33, pp. 71–99, 2013, ISSN: 09518339. DOI: 10.1016/j.marstruc.2013.04.004.

[65] R. B. Kudupudi, S. K. Pal and R. Datta, 'A three-step hybrid method to study the influence of green water impact on a large containership in time domain', *Journal of Offshore Mechanics and Arctic Engineering*, vol. 141, 5 2019, ISSN: 0892-7219. DOI: 10.1115/1.4043416. [Online]. Available: https://asmedigitalcollection.asme.org/offshoremechanics/article/doi/10.1115/1.4043416/727415/A-ThreeStep-Hybrid-Method-to-Study-the-Influence.

[66] S. Huang, J. Jiao and C. Chen, 'Numerical prediction of ship motion and slamming load characteristics in cross wave', *Journal of Marine Science and Technology (Japan)*, vol. 27, pp. 104–124, 1 2022, ISSN: 09484280. DOI: 10.1007/S00773-021-00818-W.

[67] K. R. Babu, S. V. K. R. Nelli, A. Bhattacharyya *et al.*, 'Experimental and numerical investigation of green water occurrence for kriso container ship', *Journal of Ship Research*, vol. 66, pp. 54–72, 01 2022, ISSN: 0022-4502. DOI: 10.5957/JOSR.08200049.

[68] C. Pakozdi, D. F. D. C. E. Silva, A. Östman *et al.*, 'Green water on fpso analyzed by a coupled potential-flow - ns-vof method', *Proceedings of the International Conference on Offshore Mechanics and Arctic Engineering - OMAE*, vol. 8B, American Society of Mechanical Engineers (ASME), 2014, ISBN: 9780791845516. DOI: 10.1115/OMAE2014-23913.

[69] H. Yu, H. Ren, Y. Xu *et al.*, 'On the nonlinear vibrational responses of a large vessel with a broad bow flare under wave excitation: Theory and experiment', *Shock and Vibration*, vol. 2018, 2018, ISSN: 10709622. DOI: 10.1155/2018/7054768.

[70] R. V. Schiller, C. Pâkozdi, C. T. Stansberg *et al.*, 'Green water on fpso predicted by a practical engineering method and validated against model test data for irregular waves', *Proceedings of the International Conference on Offshore Mechanics and Arctic Engineering - OMAE*, vol. 8B, American Society of Mechanical Engineers (ASME), 2014, ISBN: 9780791845516. DOI: 10.1115/OMAE2014-24084.

[71] M. van der Eijk and P. Wellens, 'Two-phase free-surface flow interaction with moving bodies using a consistent, momentum preserving method', *Journal of Computational Physics*, vol. 474, p. 111 796, 2023, ISSN: 0021-9991. DOI: 10.1016/J.JCP.2022.111796.

[72] H. Sun, Z. Sun, S. Liang *et al.*, 'Numerical study of air compressibility effects in breaking wave impacts using a cip-based model', *Ocean Engineering*, vol. 174, pp. 159–168, 2019, ISSN: 00298018. DOI: 10.1016/j.oceaneng.2019.01.050.

[73] C. Hu and M. Sueyoshi, 'Numerical simulation and experiment on dam break problem', *Journal of Marine Science and Application*, vol. 9, pp. 109–114, 2 2010, ISSN: 16719433. DOI: 10.1007/s11804-010-9075-z.

[74] J. Jiao, S. Huang and C. G. Soares, 'Viscous fluid–flexible structure interaction analysis on ship springing and whipping responses in regular waves', *Journal of Fluids and Structures*, vol. 106, p. 103 354, 2021. DOI: 10.1016/J.JFLUIDSTRUCTS.2021.103354.

[75] T. P. Sapsis, 'Statistics of extreme events in fluid flows and waves', *Annual Review of Fluid Mechanics*, vol. 53, pp. 85–111, 2021, ISSN: 00664189. DOI: 10.1146/annurev-fluid-030420-032810.

[76] Z. Y. Wan, P. Vlachas, P. Koumoutsakos *et al.*, 'Data-assisted reduced-order modeling of extreme events in complex dynamical systems', *PLoS ONE*, vol. 13, 5 2018, ISSN: 19326203. DOI: 10.1371/journal.pone.0197704.

[77] S. van Essen and H. C. Seyffert, 'Finding dangerous waves – review of methods to obtain wave impact design loads for marine structures', *Journal of Offshore Mechanics and Arctic Engineering*, pp. 1–22, 2023, ISSN: 0892-7219. DOI: 10.1115/1.4056888. [Online]. Available: https://asmedigitalcollection.asme.org/offshoremechanics/article/doi/10.1115/1.4056888/1157525/Finding-dangerous-waves-Review-of-methods-to.

[78] W. Xu, G. Filip and K. J. Maki, 'A method for the prediction of extreme ship responses using design–event theory and computational fluid dynamics', *Journal of Ship Research*, vol. 64, pp. 48–60, 1 2020, ISSN: 15420604. DOI: 10.5957/jsr.2020.64.1.48.

[79] C Berhault and P Guerin, 'Experimental and numerical investigations on the green water effects on fpsos', *Proceedings of the Eighth*, 1998. [Online]. Available: http://onepetro.org/ISOPEIOPEC/proceedings-pdf/ISOPE98/All-ISOPE98/ISOPE-I-98-043/1933373/isope-i-98-043.pdf/1.

[80] O. M. Faltinsen, M. Greco and M. Landrini, 'Green water loading on a fpso', *Journal of Offshore Mechanics and Arctic Engineering*, vol. 124, pp. 97–103, 2 2002, ISSN: 08927219. DOI: 10.1115/1.1464128.

[81] N. Mori and D. T. Cox, 'Dynamic properties of green water event in the overtopping of extreme waves on a fixed dock', *Ocean Engineering*, vol. 30, pp. 2021–2052, 16 2003, ISSN: 00298018. DOI: 10.1016/S0029-8018(03)00073-8.

[82] H. H. Lee, H. J. Lim and S. H. Rhee, 'Experimental investigation of green water on deck for a cfd validation database', *Ocean Engineering*, vol. 42, pp. 47–60, 2012, ISSN: 00298018. DOI: 10.1016/j.oceaneng.2011.12.026.

[83] Y. K. Song, K. A. Chang, K. Ariyarathne *et al.*, 'Surface velocity and impact pressure of green water flow on a fixed model structure in a large wave basin', *Ocean Engineering*, vol. 104, pp. 40–51, 2015, ISSN: 00298018. DOI: 10.1016/j.oceaneng.2015.04.085.

[84] N. Abdussamie, Y. Drobyshevski, R. Ojeda *et al.*, 'Experimental investigation of wave-in-deck impact events on a tlp model', *Ocean Engineering*, vol. 142, pp. 541–562, 2017. DOI: 10.1016/J.OCEANENG.2017.07.037.

[85] J. Scharnke, R. Lindeboom and B. Duz, 'Wave-in-deck impact loads in relation with wave kinematics', *36th International Conference on Ocean, Offshore and Arctic Engineering*, 2017. DOI: 10.1115/omae2017-61406.

[86] G. N. Lee, K. H. Jung, S. Malenica *et al.*, 'Experimental study on flow kinematics and pressure distribution of green water on a rectangular structure', *Ocean Engineering*, vol. 195, 2020, ISSN: 00298018. DOI: 10.1016/j.oceaneng.2019.106649.

[87] F. Ruggeri, R. A. Watai, P. C. de Mello *et al.*, 'Fundamental green water study for head, beam and quartering seas for a simplified fpso geosim using a mixed experimental and numerical approach', *Marine Systems and Ocean Technology*, vol. 10, pp. 71–90, 2 2015, ISSN: 21994749. DOI: 10.1007/S40868-015-0007-2/FIGURES/46. [Online]. Available: https://link-springer-com.tudelft.idm.oclc.org/article/10.1007/s40868-015-0007-2.

[88] Y.-J. Ha, K.-H. Kim, B. W. Nam *et al.*, 'Experimental study of characteristics of sidewall green water event for a ship-type fpso under irregular wave conditions', *Ocean Engineering*, vol. 296, p. 116876, 2024, ISSN: 00298018. DOI: 10.1016/j.oceaneng.2024.116876. [Online]. Available: https://linkinghub.elsevier.com/retrieve/pii/S0029801824002130.

[89] R. van 't Veer and A. Boorsma, 'Towards an improved understanding of green water exceedance at the bow of an fpso', *35th International Conference on Ocean, Offshore and Arctic Engineering*, 2016. DOI: 10.1115/OMAE2016-54651.

[90] Y. Ogawa, H. Taguchi, I. Watanabe *et al.*, 'Long term prediction method of shipping water load for assessment of the bow height', *Proceedings of the Eighth International Symposium on Practical Design of Ships and Other Floating Structures*, 2001, pp. 603–610. DOI: 10.1016/B978-008043950-1/50076-4.

[91] Y. Ogawa, 'Long-term prediction method for the green water load and volume for an assessment of the load line', *Journal of Marine Science and Technology*, vol. 7, pp. 137–144, 3 2003, ISSN: 09484280. DOI: 10.1007/s007730300004. [Online]. Available: https://link-springer-com.tudelft.idm.oclc.org/article/10.1007/s007730300004.

[92] N. Fonseca and C. G. Soares, 'Experimental investigation of the shipping of water on the bow of a containership', *Journal of Offshore Mechanics and Arctic Engineering*, vol. 127, pp. 322–330, 4 2005, ISSN: 0892-7219. DOI: 10.1115/1.2087527. [Online]. Available: https://asmedigitalcollection.asme.org/offshoremechanics/article/127/4/322/446825/Experimental-Investigation-of-the-Shipping-of.

[93] X. P. Pham and K. S. Varyani, 'Evaluation of green water loads on high-speed containership using cfd', *Ocean Engineering*, vol. 32, pp. 571–585, 5-6 2005, ISSN: 0029-8018. DOI: 10.1016/J.OCEANENG.2004.10.009.

[94] D. A. Liut, K. M. Weems and T.-G. Yen, 'A quasi-three-dimensional finite-volume shallow water model for green water on deck', vol. 57, pp. 125–140, 3 2013. DOI: 10.5957/jsr.2013.57.3.125.

[95] B. Peseux, L. Gornet and B. Donguy, 'Hydrodynamic impact: Numerical and experimental investigations', *Journal of Fluids and Structures*, vol. 21, pp. 277–303, 3 SPEC. ISS. 2005, ISSN: 10958622. DOI: 10.1016/J.JFLUIDSTRUCTS.2005.04.011.

[96] R. Panciroli, S. Abrate, G. Minak *et al.*, 'Hydroelasticity in water-entry problems: Comparison between experimental and sph results', *Composite Structures*, vol. 94, pp. 532–539, 2 2012, ISSN: 02638223. DOI: 10.1016/J.COMPSTRUCT.2011.08.016.

[97] H. Luo, H. Wang and C. G. Soares, 'Numerical and experimental study of hydrodynamic impact and elastic response of one free-drop wedge with stiffened panels', *Ocean Engineering*, vol. 40, pp. 1–14, 2012, ISSN: 00298018. DOI: 10.1016/J.OCEANENG.2011.11.004.

[98] J. Wang, C. Lugni and O. M. Faltinsen, 'Experimental and numerical investigation of a freefall wedge vertically entering the water surface', *Applied Ocean Research*, vol. 51, pp. 181–203, 2015, ISSN: 01411187. DOI: 10.1016/J.APOR.2015.04.003.

[99] C. Chen, X. Q. Chen, F. Ma *et al.*, 'A knowledge-free path planning approach for smart ships based on reinforcement learning', *Ocean Engineering*, vol. 189, 2019, ISSN: 00298018. DOI: 10.1016/j.oceaneng.2019.106299.

[100] J. H. Kim, Y. Kim, R. H. Yuck *et al.*, 'Comparison of slamming and whipping loads by fully coupled hydroelastic analysis and experimental measurement', *Journal of Fluids and Structures*, vol. 52, pp. 145–165, 2015, ISSN: 10958622. DOI: 10.1016/J.JFLUIDSTRUCTS.2014.10.011.

[101] J. Lavroff, M. R. Davis, D. S. Holloway *et al.*, 'Wave slamming loads on wave-piercer catamarans operating at high-speed determined by hydro-elastic segmented model experiments', *Marine Structures*, vol. 33, pp. 120–142, 2013, ISSN: 09518339. DOI: 10.1016/J.MARSTRUC.2013.05.001.

[102] P. A. Blackmore and P. J. Hewson, 'Experiments on full-scale wave impact pressures', *Coastal Engineering*, vol. 8, pp. 331–346, 4 1984, ISSN: 03783839. DOI: 10.1016/0378-3839(84)90029-2.

[103] N. Jones, 'Slamming damage.', *Journal of Ship Research*, vol. 17, pp. 80–86, 2 1973, ISSN: 00224502. DOI: 10.5957/jsr.1973.17.2.80.

[104] G. A. Thomas, M. R. Davis, D. S. Holloway *et al.*, 'Slamming response of a large high-speed wave-piercer catamaran', *Marine Technology and SNAME News*, vol. 40, pp. 126–140, 2 2003, ISSN: 19453582. DOI: 10.5957/mt1.2003.40.2.126.

[105] J. Scharnke, 'Elementary loading processes and scale effects involved in wave-in-deck type of loading: A summary of the breakin jip', *38th International Conference on Ocean, Offshore and Arctic Engineering*, vol. 3, 2019, pp. 1–11, ISBN: 978-0-7918-5878-3.

[106] G. Ferro and A. E. Mansour, 'Probabilistic analysis of the combined slamming and wave-induced responses', *Journal of Ship Research*, vol. 29, pp. 170–188, 03 1985, ISSN: 0022-4502. DOI: 10.5957/JSR.1985.29.3.170. [Online]. Available: https://onepetro.org/JSR/article/29/03/170/174543/Probabilistic-Analysis-of-the-Combined-Slamming.

[107] O. S. Madsen, 'Waves generated by a piston- type wavemaker', *Coastal Engineering Proceedings*, vol. 1, 1970, pp. 589–607. DOI: 10.9753/icce.v12.36.

[108] Y.-C. Wu, 'Plunger-type wavemaker theory', *Journal of Hydraulic Research*, vol. 26, 4 1988. DOI: 10.1080/00221688809499206.

[109] S. Lowell and R. A. Irani, 'Sensitivity analysis of plunger-type wavemakers with water current', *Global Oceans 2020: Singapore – U.S. Gulf Coast*, 2020, pp. 1–9, ISBN: 9781728154466. DOI: 10.1109/IEEECONF38699.2020.9389447.

[110] V. Chegini, 'Design of upright perforated energy dissipators for use in wave basins', 1994. [Online]. Available: https://unsworks.unsw.edu.au/bitstreams/177341de-b8bd-41fc-a8e1-12f64d6c0ee8/download.

[111] Y. Ouellet and I. Datta, 'A survey of wave absorbers', *Journal of Hydraulic Research*, vol. 24, pp. 265–280, 4 1986, ISSN: 00221686. DOI: 10.1080/00221688609499305.

[112] S. M. R. Hodaei, M. R. Chamani, M. N. Moghim *et al.*, 'Experimental study on reflection coefficient of curved perforated plate', *Journal of Marine Science and Application*, vol. 15, pp. 382–387, 4 2016, ISSN: 16719433. DOI: 10.1007/s11804-016-1383-5.

[113] A. D. Boon and P. R. Wellens, 'Probability and distribution of green water events and pressures', *Ocean Engineering*, 2022. DOI: 10.1016/j.oceaneng.2022.112429.

[114] F. of American Scientists, *Lpd 4 austin class - navy ships*, 1999. [Online]. Available: https://man.fas.org/dod-101/sys/ship/lpd-4.htm.

[115] D. H. Peregrine, 'Water-wave impact on walls', *Annual Review of Fluid Mechanics*, vol. 35, pp. 23–43, 2003, ISSN: 00664189. DOI: 10.1146/annurev.fluid.35.101101.161153.

[116] G. Cuomo, W. Allsop, T. Bruce *et al.*, 'Breaking wave loads at vertical seawalls and breakwaters', *Coastal Engineering*, vol. 57, pp. 424–439, 4 2010, ISSN: 03783839. DOI: 10.1016/J.COASTALENG.2009.11.005.

[117] M. Hattori, A. Arami and T. Yui, 'Wave impact pressure on vertical walls under breaking waves of various types', *Coastal Engineering*, vol. 22, pp. 79–114, 1994, ISSN: 03783839. DOI: 10.1016/0378-3839(94)90049-3.

[118] M. S. Kirkgoz, 'An experimental investigation of a vertical wall response to breaking wave impact', *Ocean Engineering*, vol. 17, pp. 379–391, 4 1990. DOI: 10.1016/0029-8018(90)90030-A.

[119] M. B. Wilk and R Gnanadesikan, 'Probability plotting methods for the analysis of data', *Biometrika*, vol. 55, p. 1, 1 1968. [Online]. Available: http://biomet.oxfordjournals.org/.

[120] F. J. Massey, 'The kolmogorov-smirnov test for goodness of fit', *Journal of the American Statistical Association*, vol. 46, pp. 68–78, 253 1951. DOI: 10.2307/2280095.

[121] L. de Haan and A. Ferreira, *Extreme value theory: An Introduction*. Springer, 2000, pp. 3–60. [Online]. Available: https://link-springer-com.tudelft.idm.oclc.org/content/pdf/10.1007%2F0-387-34471-3.pdf.

[122] S. M. Ross, 'Confidence interval of the mean of the exponential distribution', 6th ed. Elsevier Academic Press, 2020, pp. 267–282, ISBN: 9780128177471. [Online]. Available: https://books.google.nl/books?id=mXP_UEiUo9wC&pg=PA267&redir_esc=y#v=onepage&q&f=false.

[123] V. Guerriero, 'Power law distribution: Method of multi-scale inferential statistics', *Journal of Modern Mathematics Frontier*, vol. 1, pp. 21–28, 1 2012. [Online]. Available: www.sjmmf.org.

[124] A. Koosheh, A. Etemad-Shahidi, N. Cartwright *et al.*, 'Individual wave overtopping at coastal structures: A critical review and the existing challenges', *Applied Ocean Research*, vol. 106, 2021, ISSN: 01411187. DOI: 10.1016/J.APOR.2020.102476.

[125] L. Franco, M. de Gerloni and J. W. van der Meer, 'Wave overtopping on vertical and composite breakwaters', *Proceedings of the Coastal Engineering Conference*, vol. 1, pp. 1030–1044, 1995, ISSN: 08938717. DOI: 10.1061/9780784400890.076.

[126] P. Besley, *Wave overtopping of seawalls design and assessment manual*, 1999. [Online]. Available: http://www.overtopping-manual.com/assets/downloads/EA_Overtopping_Manual_w178.pdf.

[127] A. D. Boon and P. R. Wellens, 'The effect of surge on extreme wave impacts and an insight into clustering', *Journal of Ship Research*, 2024. DOI: 10.5957/JOSR.07230022.

[128] I. Drummen, G. Storhaug and T. Moan, 'Experimental and numerical investigation of fatigue damage due to wave-induced vibrations in a containership in head seas', *Journal of Marine Science and Technology*, vol. 13, pp. 428–445, 4 2008, ISSN: 09484280. DOI: 10.1007/S00773-008-0006-5.

[129] S. Wang and C. G. Soares, 'Experimental and numerical study of the slamming load on the bow of a chemical tanker in irregular waves', *Ocean Engineering*, vol. 111, pp. 369–383, 2016, ISSN: 00298018. DOI: 10.1016/J.OCEANENG.2015.11.012.

[130] G. Ersdal and A. Kvitrud, 'Green water on norwegian production ships', *Proceedings of the International Offshore and Polar Engineering Conference*, vol. 4, pp. 211–218, July 2000. [Online]. Available: https://www.researchgate.net/publication/242424048.

[131] D. Mendes and T. C. Oliveira, 'Deep-water spectral wave steepness offshore mainland portugal', *Ocean Engineering*, vol. 236, p. 109 548, 2021, ISSN: 0029-8018. DOI: 10.1016/J.OCEANENG.2021.109548.

[132] S. S. Dhavalikar and A. Negi, *Algorithm for finding extreme motions of forward speed vessels*, 2009. [Online]. Available: https://www.researchgate.net/publication/275634882.

[133] J. M. Lachin, *Biostatistical Methods: The Assessment of Relative Risks*. John Wiley and Sons, Ltd, 2000, vol. 1, ISBN: 978-0470508220. [Online]. Available: https://onlinelibrary-wiley-com.tudelft.idm.oclc.org/doi/10.1002/sim.1167.

[134] A. D. Boon and P. R. Wellens, 'How draft and freeboard affect green water: A probabilistic analysis of a large experimental dataset', *43th International Conference on Ocean, Offshore and Arctic Engineering*, ASME, 2024. DOI: 10.1115/OMAE2024-123640.

[135] A. Benmansour, B. Hamoudi and L. Adjlout, 'Effect of ship bow overhang on water shipping for ship advancing in regular head waves', *Journal of Marine Science and Application*, vol. 15, pp. 33–40, 1 2016, ISSN: 16719433. DOI: 10.1007/s11804-016-1345-y.

[136] S. Zhang, G. Shi, Z. Liu *et al.*, 'Data-driven based automatic maritime routing from massive ais trajectories in the face of disparity', *Ocean Engineering*, vol. 155, pp. 240–250, 2018. DOI: 10.1016/J.OCEANENG.2018.02.060.

[137] R. B. Kudupudi, A. Bhattacharyya and R. Datta, 'A parametric study of green water impact on a container ship', *Ships and Offshore Structures*, vol. 15, pp. 318–324, 3 2020, ISSN: 17445302. DOI: 10.1080/17445302.2019.1615728.

[138] C. Bellezi, L.-Y. Cheng and K. Nishimoto, *A numerical study of the effects of bow shape on green water phenomenon*. International Society of Offshore and Polar Engineers, 2013, ISBN: 9781880653999.

[139] K. Hu, H. Zhou and L. Mao, 'Investigation on the effect of bow configuration on motion and green water for tumblehome vessels based on cartesian grid finite difference method', *Ocean Engineering*, vol. 271, 2023, ISSN: 00298018. DOI: 10.1016/j.oceaneng.2023.113703.

[140] X. P. Pham, 'Green water and loading on high speed containerships', 2008. [Online]. Available: https://theses.gla.ac.uk/249/1/2008PhamPhD.pdf.

[141] F. Noblesse, G. Delhommeau, M. Guilbaud *et al.*, 'Simple analytical relations for ship bow waves', *Journal of Fluid Mechanics*, vol. 600, pp. 105–132, 2008. DOI: 10.1017/S0022112008000220. [Online]. Available: https://doi.org/10.1017/S0022112008000220.

[142] A. D. Boon and P. R. Wellens, 'Kinematics of green water in a large data set of events and a resulting prediction method of probability', *Ocean Engineering*, vol. 311, p. 118 776, 2024, ISSN: 0029-8018. DOI: 10.1016/J.OCEANENG.2024.118776.

[143] M. Greco, O. M. Faltinsen and M. Landrini, 'Shipping of water on a two-dimensional structure', *Journal of Fluid Mechanics*, vol. 525, pp. 309–332, 2005, ISSN: 00221120. DOI: 10.1017/S0022112004002691.

[144] C. T. Stansberg, 'A wave impact parameter', *27th International Conference on Offshore Mechanics and Arctic Engineering*, ASME, 2008. DOI: 10.1115/OMAE2008-57801.

[145] S. M. van Essen, C. Monroy, Z. Shen *et al.*, 'Screening wave conditions for the occurrence of green water events on sailing ships', *Ocean Engineering*, vol. 234, p. 109 218, 2021, ISSN: 00298018. DOI: 10.1016/j.oceaneng.2021.109218. [Online]. Available: https://doi.org/10.1016/j.oceaneng.2021.109218.

[146] A. Boon and P. Wellens, 'Data from long-running green water experiments in various sea states at model scale', *4TU.ResearchData*, 2022. DOI: 10.4121/21031981.v1. [Online]. Available: https://data.4tu.nl/articles/dataset/Data_from_long-running_green_water_experiments_in_various_sea_states_at_model_scale/21031981.

[147] R. Tasaki, 'On the shipping water in head waves', *Journal of the Society of Naval Architects ofJapan*, vol. 107, pp. 2–10, 1960. DOI: 10.2534/jjasnaoe1952.1960.107_47.

[148] J. J. Blok and J. Huisman, *Relative motions and swell-up for a frigate bow*, 1983.

[149] J. Journée and A. van 't Veer, 'First order wave loads in beam waves', *International Ocean and Polar Engineering Conference*, 1995. [Online]. Available: https://onepetro.org/ISOPEIOPEC/proceedings-abstract/ISOPE95/All-ISOPE95/ISOPE-I-95-220/23285.

[150] R. B. D'Agistino, A. Belanger and J. R. B. D'Agistino, 'A suggestion for using powerful and informative tests of normality', *The american statistician*, vol. 40, pp. 316–321, 4 1990. DOI: 10.2307/2684359.

[151] M. Frické, 'Big data and its epistemology', *Journal of the Association for Information Science and Technology*, vol. 66, pp. 651–661, 4 2015, ISSN: 2330-1643. DOI: 10.1002/ASI.23212. [Online]. Available: https://onlinelibrary.wiley.com/doi/full/10.1002/asi.23212https://onlinelibrary.wiley.com/doi/abs/10.1002/asi.23212https://asistdl.onlinelibrary.wiley.com/doi/10.1002/asi.23212.

[152] K. M. Tolle, D. S. W. Tansley and A. J. Hey, *The fourth Paradigm: Data-intensive scientific discovery*. 2011, vol. 99, pp. 1334–1337, ISBN: 9780982544204. DOI: 10.1109/JPROC.2011.2155130.

[153] M. Zhang, C. Liu, P. Kujala *et al.*, 'Comparison and evaluation of learning capabilities of deep learning methods for predicting ship motions', *15th International Marine Design Conference (IMDC-2024)*, 2024. DOI: 10.59490/imdc.2024.838.

[154] J. C. Yin, Z. J. Zou, F. Xu *et al.*, 'Online ship roll motion prediction based on grey sequential extreme learning machine', *Neurocomputing*, vol. 129, pp. 168–174, 2014, ISSN: 09252312. DOI: 10.1016/j.neucom.2013.09.043.

[155] C. Gkerekos, I. Lazakis and G. Theotokatos, 'Machine learning models for predicting ship main engine fuel oil consumption: A comparative study', *Ocean Engineering*, vol. 188, 2019, ISSN: 00298018. DOI: 10.1016/j.oceaneng.2019.106282.

[156] L. Bui-Duy and N. Vu-Thi-Minh, 'Utilization of a deep learning-based fuel consumption model in choosing a liner shipping route for container ships in asia', *Asian Journal of Shipping and Logistics*, 2020, ISSN: 20925212. DOI: 10.1016/j.ajsl.2020.04.003.

[157] T. Berghout, L. H. Mouss, T. Bentrcia *et al.*, 'A deep supervised learning approach for condition-based maintenance of naval propulsion systems', *Ocean Engineering*, vol. 221, 2021, ISSN: 00298018. DOI: 10.1016/j.oceaneng.2020.108525.

[158] H. Cui, O. Turan and P. Sayer, 'Learning-based ship design optimization approach', *CAD Computer Aided Design*, vol. 44, pp. 186–195, 3 2012, ISSN: 00104485. DOI: 10.1016/j.cad.2011.06.011.

[159] S. Guth and T. P. Sapsis, 'Wave episode based gaussian process regression for extreme event statistics in ship dynamics: Between the scylla of karhunen–loève convergence and the charybdis of transient features', *Ocean Engineering*, vol. 266, 2022, ISSN: 00298018. DOI: 10.1016/j.oceaneng.2022.112633.

[160] H. J. Park, J. S. Kim, B. W. Nam *et al.*, 'Ann-based prediction models for green water events around a fpso in irregular waves', *Ocean Engineering*, vol. 291, p. 116 408, 2024, ISSN: 0029-8018. DOI: 10.1016/J.OCEANENG.2023.116408.

[161] W. J. Murdoch, C. Singh, K. Kumbier *et al.*, 'Interpretable machine learning: Definitions, methods, and applications', 2019. DOI: 10.1073/pnas.1900654116. [Online]. Available: http://arxiv.org/abs/1901.04592http://dx.doi.org/10.1073/pnas.1900654116.

[162] S. L. Brunton, J. L. Proctor, J. N. Kutz *et al.*, 'Discovering governing equations from data by sparse identification of nonlinear dynamical systems', *Proceedings of the National Academy of Sciences of the United States of America*, vol. 113, pp. 3932–3937, 15 2016, ISSN: 10916490. DOI: 10.1073/pnas.1517384113.

[163] K. Fukami, T. Murata, K. Zhang *et al.*, 'Sparse identification of nonlinear dynamics with low-dimensionalized flow representations', *Journal of Fluid Mechanics*, vol. 926, 2021, ISSN: 14697645. DOI: 10.1017/jfm.2021.697.

[164] E. Kaiser, J. N. Kutz and S. L. Brunton, 'Sparse identification of nonlinear dynamics for model predictive control in the low-data limit', *Proceedings of the Royal Society A: Mathematical, Physical and Engineering Sciences*, vol. 474, p. 20 180 335, 2219 2018, ISSN: 1364-5021. DOI: 10.1098/rspa.2018.0335. [Online]. Available: https://royalsocietypublishing.org/doi/10.1098/rspa.2018.0335.

[165] S. Shi, R. J. Patton and Y. Liu, 'Robust data-driven estimation of wave excitation force for wave energy converters', *IFAC-PapersOnLine*, vol. 53, Elsevier B.V., 2020, pp. 12 346–12 351. DOI: 10.1016/j.ifacol.2020.12.1231.

[166] S. C. Barhate, O. Siram and N. Sahoo, 'Wake modelling of horizontal-axis wind turbines using sparse identification of non-linear dynamics (sindy)', *Lecture Notes in Mechanical Engineering*, pp. 69–82, 2024, ISSN: 21954364. DOI: 10.1007/978-981-97-0418-7_7/FIGURES/5. [Online]. Available: https://link.springer.com/chapter/10.1007/978-981-97-0418-7_7.

[167] R. Vilumbrales-Garcia, G. D. Weymouth and B. Ganapathisubramani, 'Physics-based and machine learning predictions of maneuvering forces in unsteady inflow conditions marine 2021', *ISo7 - Machine Learning and Artificial Intelligence in Marine Engineering*, 2021. DOI: 10.2218/marine2021.6832.

[168] X. Jiang, X. Wei, F. Jin *et al.*, 'Machine learning based model re-identification of complex dynamical systems on autonomous marine surface vehicle', *International Conference on Ocean Studies*, IEEE, 2023, ISBN: 9798350382457. DOI: 10.1109/ICOS60708.2023.10425492.

[169] B. Prokop and L. Gelens, 'From biological data to oscillator models using sindy', *iScience*, vol. 27, 4 2024, ISSN: 25890042. DOI: 10.1016/j.isci.2024.109316.

[170] K. Kaheman, E. Kaiser, B. Strom *et al.*, 'Learning discrepancy models from experimental data', 2019. [Online]. Available: http://arxiv.org/abs/1909.08574.

[171] B. M. de Silva, D. M. Higdon, S. L. Brunton *et al.*, 'Discovery of physics from data: Universal laws and discrepancies', *Frontiers in Artificial Intelligence*, vol. 3, 2020, ISSN: 26248212. DOI: 10.3389/frai.2020.00025.

[172] A. Sandoz, V. Ducret, G. A. Gottwald *et al.*, 'Sindy for delay-differential equations: Application to model bacterial zinc response', *Proceedings of the Royal Society A: Mathematical, Physical and Engineering Sciences*, vol. 479, 2269 2023, ISSN: 14712946. DOI: 10.1098/rspa.2022.0556.

[173] S. H. Rudy and T. P. Sapsis, 'Output-weighted and relative entropy loss functions for deep learning precursors of extreme events', *Physica D: Nonlinear Phenomena*, vol. 443, 2023, ISSN: 01672789. DOI: 10.1016/j.physd.2022.133570.

[174] A. Chang, M. Wang and G. I. Allen, 'Sparse regression for extreme values', *Electronic Journal of Statistics*, vol. 15, pp. 5995–6035, 2 2021, ISSN: 19357524. DOI: 10.1214/21-EJS1937.

[175] W. Cummins, 'The impulse response function and ship motions', *Symposium on Ship Theory*, 1962. [Online]. Available: https://dome.mit.edu/bitstream/handle/1721.3/49049/DTMB_1962_1661.pdf.

[176] U. Fasel, J. N. Kutz, B. W. Brunton *et al.*, 'Ensemble-sindy: Robust sparse model discovery in the low-data, high-noise limit, with active learning and control', *Proceedings of the Royal Society A: Mathematical, Physical and Engineering Sciences*, vol. 478, 2260 2022, ISSN: 14712946. DOI: 10.1098/rspa.2021.0904.

[177] E. Kaiser, J. N. Kutz and S. L. Brunton, 'Data-driven discovery of koopman eigenfunctions for control', *Machine Learning: Science and Technology*, vol. 2, 3 2021, ISSN: 26322153. DOI: 10.1088/2632-2153/ABF0F5.

[178] B. de Silva, K. Champion, M. Quade *et al.*, 'Pysindy: A python package for the sparse identification of nonlinear dynamical systems from data', *Journal of Open Source Software*, vol. 5, p. 2104, 49 2020, ISSN: 2475-9066. DOI: 10.21105/joss.02104.

[179] A. Kaptanoglu, B. de Silva, U. Fasel *et al.*, 'Pysindy: A comprehensive python package for robust sparse system identification', *Journal of Open Source Software*, vol. 7, p. 3994, 69 2022, ISSN: 2475-9066. DOI: 10.21105/joss.03994.

[180] K. Champion, P. Zheng, A. Y. Aravkin *et al.*, 'A unified sparse optimization framework to learn parsimonious physics-informed models from data', *IEEE Access*, vol. 8, pp. 169 259–169 271, 2020, ISSN: 21693536. DOI: 10.1109/ACCESS.2020.3023625.

[181] M. Hoffmann, C. Fröhner and F. Noé, 'Reactive sindy: Discovering governing reactions from concentration data', *Journal of Chemical Physics*, vol. 150, 2 2019, ISSN: 00219606. DOI: 10.1063/1.5066099.

[182] OrcaFlex, *Vessel theory: Impulse response and convolution*, 2024. [Online]. Available: https://www.orcina.com/webhelp/OrcaFlex/Content/html/Vesseltheory,Impulseresponseandconvolution.htm.

[183] J. A. Lemus and B. Herrmann, 'Multi-objective sindy for parameterized model discovery from single transient trajectory data', 2024. [Online]. Available: http://arxiv.org/abs/2405.08771.

[184] C. B. Delahunt and J. N. Kutz, 'A toolkit for data-driven discovery of governing equations in high-noise regimes', *IEEE Access*, vol. 10, pp. 31 210–31 234, 2022, ISSN: 21693536. DOI: 10.1109/ACCESS.2022.3159335.

CURRICULUM VITAE

Anna Boon was born in Haarlem on November 29, 1995. She attended Oakfield school (England), Crayenester basisschool and Stedelijk Gymnasium Haarlem (the Netherlands) from 1998 - 2014. In 2014 she started studying at Delft University of Technology. During the Bachelors she went on exchange to the University of Waterloo (Canada), worked a year as an engineer in the TU Delft Solar Boat Team, did a two month internship at Allseas working on a river plastic solution and she worked as a student assistant at TU Delft. While studying she was also part of various committees. She obtained her Bachelor and Master of Science in Marine Technology at Delft University of Technology in 2018 and 2020 respectively. Her master thesis was on vertical surface piercing cylinders in waves and current.
From 2020 to 2024 she performed her PhD research at Delft University of Technology on the statistics of extreme wave impacts using large experimental data sets. During the PhD she was also a member of the Maritime and Transport Young Professionals (MTYP) board and active in the PhD council of the faculty ME.

ACKNOWLEDGMENTS

With the publication and defence of this book my PhD journey has come to an end. Even though only my name is on the front of this book, this work could not have existed without the people around me.

First I want to thank the one who convinced me to start this journey and who helped me reach the end: Peter. Thank you, Peter, for giving me freedom and guidance within this project.

I also want to thank Gabe for joining my project. Your passion for research is inspiring, and your help and sharing of knowledge helped me stay afloat in the waves (pun intended).

Frits, Jasper, Jennifer, Pascal, Peter and Sebastian, I want to thank you for all the help with the experiments. Without you this project would not have been possible. But also: thank you for staying realistic, in both the ups and downs.

I want to thank those working on the NWO project with me, especially Sanne and Nicole, for all the meetings on and off topic, and your support throughout.

To the master students I got to work with: thank you for your enthusiasm and allowing me to join your interesting projects. I hope you learned as much from me as I got to learn from you.

Thank you to all my amazing colleagues for the great tips and help in the research. And thank you for making the PhD fun with all the discussions on everything and nothing during our many breaks.

To the members of the MTYP board and PhD council and those I worked with through the board and council: I found it a pleasure to strive for a better work environment with such capable and enjoyable people.

To my friends and family: your support and guidance is what made my PhD journey possible. I truly appreciate you.

And lastly of course, my rock, my helpdesk, my Maarten: thank you.

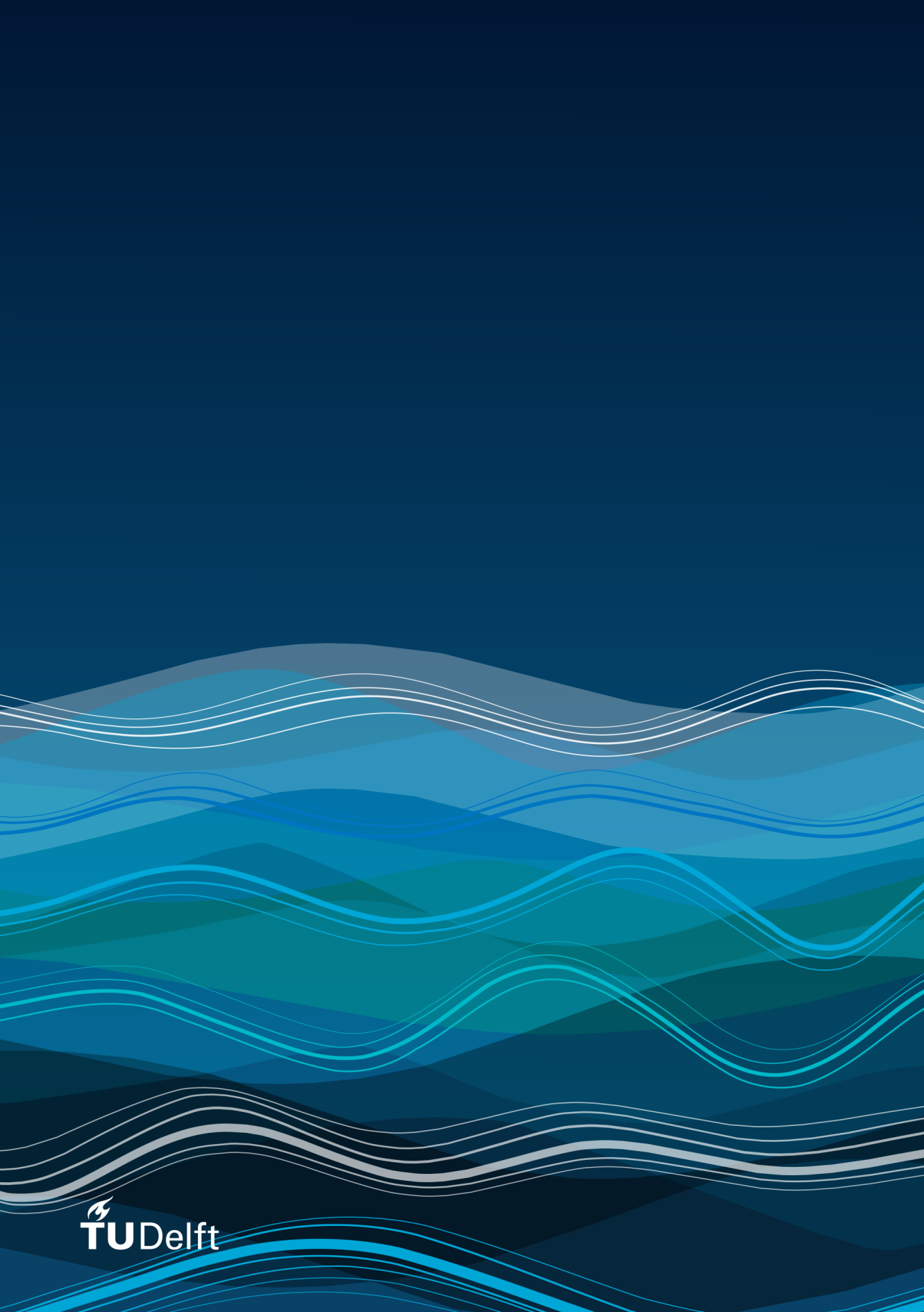
TUDelft